

 or my children



Former LSWR signalbox, Dunbridge. Carmel

The Effects of Solvents on Reactivities,
Kinetics and Charge Transfer Spectra
of some
Transition Metal Diimine Complexes

A Thesis Submitted by

TIMOTHY DIGMAN

for the Degree of

Doctor of Philosophy

in the

Faculty of Science

of the

University of Leicester

Department of Chemistry

The University

Leicester LE1 7RH

May 1984

UMI Number: U344349

All rights reserved

INFORMATION TO ALL USERS

The quality of this reproduction is dependent upon the quality of the copy submitted.

In the unlikely event that the author did not send a complete manuscript and there are missing pages, these will be noted. Also, if material had to be removed, a note will indicate the deletion.



UMI U344349

Published by ProQuest LLC 2015. Copyright in the Dissertation held by the Author.
Microform Edition © ProQuest LLC.

All rights reserved. This work is protected against
unauthorized copying under Title 17, United States Code.



ProQuest LLC
789 East Eisenhower Parkway
P.O. Box 1346
Ann Arbor, MI 48106-1346



Thesis
8.11.84

X75 0 03640X

Statement

This thesis submitted for the degree of Doctor of Philosophy, entitled

"The effects of solvents on reactivities, kinetics, and charge transfer spectra of some transition metal diimine complexes."

is based on work conducted by the author in the Department of Chemistry of the University of Leicester mainly during the period between October 1980 and April 1983.

All the work recorded in this thesis is original unless otherwise acknowledged in the text or by references.

None of the work has been submitted for another degree in this or any other university.

May 1984

ACKNOWLEDGEMENTS

I would like to thank my supervisors, Dr. Mike Blandamer and Dr. John Burgess, for their continual help and guidance during my research.

My thanks are also due to my many colleagues at Leicester who have given invaluable practical and technical advice.

Many thanks go to my wife, Carmel, and her sister Gemma Curry, for typing this thesis.

I would like to express my deepest gratitude to my wife who not only typed, but also drew all the diagrams, as well as attending to the domestic chores.

I acknowledge the receipt of an SERC award.

Finally I would like to thank my daughter, Catherine, who provided so much pleasurable distraction, that this thesis was completed somewhat later than scheduled.

Ligand Abbreviations

bipy	2,2'-bipyridine
bipym	2,2'-bipyrimidine
box	2,2'-bi-4,5-dihydrooxazine
btz	2,2'-bi-4,5-dihydrothiazine, bithiazine
dt	1,3-dithiane
EDTA	ethylenediaminetetraacetic acid
en	ethylene diamine
mba	dimethylbutadiimine
mppm	4-methyl-N-phenyl(2 pyridyl)methylene
2Mephen	2-methyl-1,10-phenanthroline
2,9Me ₂ phen	2,9-dimethyl-1,10-phenanthroline
5NO ₂ phen	5-nitro-1,10-phenanthroline
ox	oxalate anion
phen	1,10-phenanthroline
pip	piperidine
pada	pyridine-2-azo-p-dimethylaniline

Other Abbreviations

DMF	N,N-dimethylformamide
DMIA	dimethylindoaniline
DMSO	dimethylsulphoxide
es	excited state
gs	ground state
is	initial state
m.e.	microemulsion
PNA	p-Nitroanisole
SbT	antimonyl tartate anion, $\text{Sb}_2\text{C}_8\text{H}_4\text{O}_{12}^{2-}$
ts	transition state
G	Gibb's FREE ENERGY
H	ENTHALPY

CONTENTS

CHAPTER ONE	1
Introduction. Kinetics. Analysis of solvent effects. Structure of water. Classification of binary aqueous mixtures. Solvent polarity.	
CHAPTER TWO	22
Initial state-transition state analysis for the reactions $\text{Fe}(\text{phen})_3^{2+} + \text{Nu}$ ($\text{Nu} = \text{OH}^-$, CN^-) in aqueous methanol mixtures.	
CHAPTER THREE	42
Initial state-transition state analysis for the racemisation of $(-)\text{Fe}(\text{phen})_3^{2+}$ in aqueous methanol mixtures. Initial state-transition state analysis for the racemisation of $(-)\text{Fe}(\text{phen})_3^{2+}$ in aqueous DMSO mixtures. Initial state-transition state analysis for the dissociation of $\text{Fe}(\text{phen})_3^{2+}$ in aqueous methanol and aqueous DMSO mixtures. The resolution of $\text{Fe}(\text{mppm})_3^{2+}$. The resolution of $\text{Fe}(\text{5NO}_2\text{phen})_3^{2+}$ and $\text{Ru}(\text{5NO}_2\text{phen})_3^{2+}$. The attempted resolution of $\text{Fe}(\text{btz})_3^{2+}$ and $\text{Ru}(\text{btz})_3^{2+}$. The preparation of d-2'-methoxy-2-nitro-6-carboxydiphenyl.	
CHAPTER FOUR	82
The reactions between $\text{Fe}(\text{btz})_3^{2+}$ and R ($\text{R} = \text{OH}^-$, H^+ , Hg^{2+} , Cd^{2+} , Ag^+ , $\text{S}_2\text{O}_8^{2-}$, phen, bipy). The stability constants of $\text{Fe}(\text{btz})_3^{2+}$, Agbtz^+ , Cdbtz^{2+} , Hgbtz^{2+} . The molar extinction coefficients of $\text{Fe}(\text{btz})_3^{2+}$ and $\text{Fe}(\text{btz})_2(\text{CN})_2$. Attempted preparation of $\text{Fe}(\text{bipym})_2(\text{CN})_2$. The reaction between $\text{Fe}(\text{btz})_2(\text{CN})_2$ and Hg^{2+} . The solvatochromism of $\text{Fe}(\text{btz})_2(\text{CN})_2$. The reactions between $\text{Mo}(\text{CO})_4(\text{pip})_2$ and FeL_3^{2+} ($\text{L} = \text{btz}$, bipym). Attempted preparation of polymerised " $\text{Fe}(\text{bipym})_2$ ". The reactions of $\text{Fe}(\text{mba})_3^{2+}$.	

The preparation of $\text{Mo}(\text{CO})_4\text{bipym}$ and $\text{Mo}(\text{CO})_4\text{btz}$.
The structure of $\text{Mo}(\text{CO})_4\text{btz}$. Initial state-transition
state analysis for the solvolysis of $\text{Mo}(\text{CO})_4\text{btz}$.
Ground state-excited state analysis for the
solvatochromism of $\text{Mo}(\text{CO})_4\text{btz}$, DMIA, PNA. The
effect of temperature on the uv/vis spectrum of
 $\text{Mo}(\text{CO})_4\text{btz}$. The effect of pressure on the uv/vis
spectrum of $\text{Mo}(\text{CO})_4\text{btz}$.

The reactions between $\text{Mo}(\text{CO})_4\text{btz}$ and L (L = HgCl_2 ,
 Hg^{2+} , In^{3+} , Cd^{2+} , $\text{Mo}(\text{CO})_4(\text{pip})_2$, PtCl_4^{2-} , PtCl_2 , MeI,
 PPh_3 , $\text{P}(\text{OPh})_3$, bipy). The reactions between
 $\text{Mo}(\text{CO})_4(\text{pip})_2$ and R (R = btz, dt, (btz + phen),
 PtCl_2btz). The reaction between $\text{Mo}(\text{CO})_4(\text{PPh}_3)_2$ and
btz. The preparation of PtCl_2btz . The reaction
between $\text{Mo}(\text{CO})_4\text{dt}$ and btz.

CHAPTER ONE:

Introduction. Kinetics. Analysis of solvent effects. Structure of water. Classification of binary aqueous mixtures. Solvent polarity.

Introduction

This thesis discusses transition metal complexes of 2,2'-bi-4,5-dihydro-thiazine(bithiazine,btz) and compares their properties with the analogous 1,10-phenanthroline and 2,2'-bipyridyl complexes. The kinetics are described of nucleophilic attack, aquation and racemisation of iron phenanthroline and iron bithiazine complexes. The effects of solvents upon the charge transfer band of $\text{Mo}(\text{CO})_4\text{btz}$ are analysed in terms of ground state and excited state contributions. It is of interest to compare the results with the initial state-transition state analysis for solvolysis of the same complex. In each case the initial (ground) states are the same but the transition and electronic excited states are significantly different i.e. a comparison of a Boltzman transition state with a Franck-Condon excited state. The final part of the present work discusses the kinetics of the formation of $\text{Mo}(\text{CO})_4(\text{bithiazine})$, and the attempted preparations of some multinuclear bithiazine complexes.

Kinetics

The general expression for a first order reaction is given by

$$[A]_t = [A]_0 \exp(-kt) \quad 1$$

Where $[A]_t$ is the concentration of the reactant at time t , $[A]_0$ is the initial concentration of the reactant, k is the first order rate constant and t is the time the reaction has proceeded.

For the experiments described in Chapters 2, 4 and 5 concentrations of solutions were determined spectrophotometrically using either a Pye-Unicam SP8-100 or Pye-Unicam SP1800 spectrophotometer; in the experiments described in Chapter 3 concentrations were determined polarimetrically using a Perkin Elmer 140 polarimeter.

Second order rate constants were determined by the method of "flooding"¹. Chapters 3 and 4 describe reactions involving reversible first order reactions. The general equation for the dependence of concentration with time is given by

$$\ln \left\{ \frac{[A]_t - [A]_\infty}{[A]_0 - [A]_\infty} \right\} = -(k_1 + k_{-1})t \quad 2$$

Where $[A]_t$ is the concentration of the reactant at time t , $[A]_\infty$ is the final concentration of the reactant, $[A]_0$ is the initial concentration of the reactant, k_1 is the rate constant for the forward reaction, k_{-1} is the rate constant for the reverse reaction and t is the time the reaction has proceeded.

Kinetics: experimental

From absorbances or optical rotation first-order rate constants were calculated from standard semi-log plots. All calculations were performed using either programmable calculators or a computer. The majority of calculations used a standard linear regression program.

In a number of studies kinetic data were obtained using a computer controlled (HP9285) Pye-Unicam SP1800 spectrophotometer². The latter automatically records

absorbances and calculates first order rate constants; this is achieved using a non linear regression analysis developed by Moore³.

Analysis of Solvent Effects

Chapters 2,3 and 5 are concerned with the effect of solvent composition upon a variety of reactions. To quantify observed solvent effects one method uses the medium operator, $\delta_m X$.

The medium operator is defined as

$$\delta_m X = X_2^\ominus - X_1^\ominus \quad 3$$

Where X is a standard thermodynamic parameter of a solute in solution, and the subscripts refer to the different solvents. X_1^\ominus refers to the property in a reference solvent, typically water, and X_2^\ominus in a new solvent. For example, at fixed T and p

$$\delta_m \Delta G^\ddagger = \Delta G_2^\ddagger - \Delta G_1^\ddagger \quad 4$$

ΔG^\ddagger represents the difference between the chemical potential of the transition state and the and the chemical potential of the reactants:

$$\Delta G^\ddagger = \mu^\ddagger - \sum \mu^\ominus(\text{reactants}) \quad 5$$

Thus the effect of solvent composition upon ΔG^\ddagger can be written in terms of the medium operator

$$\delta_m \Delta G^\ddagger = \delta_m \mu^\ddagger - \sum \delta_m \mu^\ominus(\text{reactants}) \quad 6$$

From Transition State Theory⁴ the rate of reaction is given by

$$k(r) = kT/h \exp(-\Delta G^\ddagger/RT) c^{\ominus(1-m)} \quad 7$$

Where $k(r)$ is the rate constant reduced to standard state,

k is Boltzman's constant, T is the temperature, h is Plank's constant, R is the gas constant, c^\ominus is the concentration in the standard state to which the thermodynamic parameters are referred, and m is the order of the reaction.

Substituting equation 7 into equation 4 yields

$$\delta_m \Delta G^\ddagger = -RT \ln \frac{k(r)_2}{k(r)_1} \quad 8$$

Where $k(r)_1$ is the rate constant for the reaction in the reference solvent, and $k(r)_2$ is the rate constant for the reaction in the new solvent.

Consider two saturated solutions of a compound, both solutions are at equilibrium, then

$$\mu(\text{pure solid}) = \mu(\text{solute, solution 1}) \quad 9$$

$$\mu(\text{pure solid}) = \mu(\text{solute, solution 2}) \quad 10$$

Since the activity of the solid is the same in each case, then

$$\mu(\text{solute, solution 1}) = \mu(\text{solute, solution 2}) \quad 11$$

The chemical potentials of the solutes are given by

$$\mu_2(\text{I}) = \mu_2^\ominus(\text{I}) + RT \ln S(\text{I}) f_2(\text{I}) \quad 12$$

$$\mu_2(\text{II}) = \mu_2^\ominus(\text{II}) + RT \ln S(\text{II}) f_2(\text{II}) \quad 13$$

Then

$$\mu_2^\ominus(\text{II}) - \mu_2^\ominus(\text{I}) = RT \ln S(\text{I}) f_2(\text{I}) / S(\text{II}) f_2(\text{II}) \quad 14$$

If $f_2(\text{I})/f_2(\text{II})$ is assumed to be unity

$$\delta_m \mu^\ominus = RT \ln \frac{S(\text{I})}{S(\text{II})} \quad 15$$

Where S(I) is the solubility (in mol dm⁻³) of the compound in the reference solvent, and S(II) the solubility in the new solvent.

For an electrolyte S(I) and S(II) must be replaced by the respective solubility products, again with the assumption that the ratio of the appropriate activity coefficients is unity.

For a range of solvent mixtures a plot can be constructed of $\delta_m \Delta G^\ddagger$, $\delta_m \mu^\ominus$, and $\delta_m \mu^\ddagger$. Then

$$\delta_m \mu(\text{transition state}) = \delta_m \mu^\ddagger \quad 16$$

$$\delta_m \mu(\text{initial state}) = \sum \delta_m \mu^\ominus(\text{reactants}) \quad 17$$

Consider the same reaction referred to previously. If the reaction has an activation enthalpy ΔH_1^\ddagger in the reference solvent, and ΔH_2^\ddagger in the new solvent, then

$$\delta_m \Delta H^\ddagger = \Delta H_2^\ddagger - \Delta H_1^\ddagger \quad 18$$

Activation enthalpies are derived from the activation energies using the following equation

$$E_{\text{act}} = \Delta H^\ddagger + RT \quad 19$$

E_{act} is the activation energy calculated from the Arrhenius equation. For a given solute

$$\delta_m \Delta H^\ominus(\text{solution}) = \Delta H_2^\ominus(\text{solution}) - \Delta H_1^\ominus(\text{solution}) \quad 20$$

Where ΔH_1^\ominus and ΔH_2^\ominus are the partial molar enthalpies of the solute in the reference solvent and the new solvent respectively. Enthalpies can be obtained directly from solution calorimetry. Then

$$\delta_m \Delta H(\text{transition state}) = \delta_m \Delta H^\ddagger \quad 21$$

$$\delta_m \Delta H(\text{initial state}) = \sum \delta_m \Delta H^\ominus(\text{reactants}) \quad 22$$

In Chapter 5 the solvatochromism of several compounds are analysed into ground state-excited state contributions:

$$\delta_m(\text{ground state}) = \delta_m \Delta H^\ominus(\text{solution}) \quad 23$$

$$\delta_m \Delta E_{ct} = \Delta E_{ct}(2) - \Delta E_{ct}(1) \quad 24$$

$$\delta_m(\text{excited state}) = \delta_m \Delta E_{ct} + \delta_m(\text{ground state}) \quad 25$$

Where $\Delta E_{ct}(1)$ and $\Delta E_{ct}(2)$ are the energies of absorption at the band maxima in the reference and new solvent respectively.

The kinetics of reactions in a range of solvent mixtures can be analysed in terms of initial state-transition state contributions. However, it must be borne in mind that the transition state may change with solvent composition.

Single Ion Thermodynamic Parameters

In the previous section the analysis of solvent effects was discussed in terms of initial state-transition state contributions. However, if the reaction under discussion involves charged species, say $\text{Fe}(\text{phen})_3^{2+}$ and OH^- , the problem arises of determining single ion quantities such as $\delta_m \Delta H^\ominus(\text{Fe}(\text{phen})_3^{2+})$, $\delta_m \Delta H^\ominus(\text{OH}^-)$, and $\delta_m \mu^\ominus(\text{Fe}(\text{phen})_3^{2+})$. Experimentally it is impossible to measure the enthalpy of solution of OH^- , or the solubility of $\text{Fe}(\text{phen})_3^{2+}$ cations.

Consider the salt A^+B^- , then

$$X^\ominus(\text{A}^+\text{B}^-) = X^\ominus(\text{A}^+) + X^\ominus(\text{B}^-) \quad 26$$

And

$$\delta_m X^\ominus(\text{A}^+\text{B}^-) = \delta_m X^\ominus(\text{A}^+) + \delta_m X^\ominus(\text{B}^-) \quad 27$$

Where X is a standard thermodynamic parameter. If the solvent effect on partial molar properties of one ion is known, then partial molar properties of other ions may be calculated. Since single ion thermodynamic parameters

cannot be determined experimentally, an estimate or assumption is required. An estimate based upon the Born equation⁵ can be used

$$\delta_m \mu^\ominus(\text{ion}) = \frac{N_a z^2 e^2}{8\pi \epsilon_0 r} \left[\frac{1}{\epsilon_s} - \frac{1}{\epsilon_r} \right] \quad 28$$

Where N_a is Avagadro's number, z is the charge on the ion, e is the unit charge, r is the crystallographic radius⁶, ϵ_0 is the permittivity of free space, ϵ_s is the relative permittivity of the solvent, and ϵ_r is the relative permittivity of the reference solvent.

Another important and usually accepted method⁷ assumes

$$\delta_m \mu^\ominus(\text{Ph}_4\text{P}^+) = \delta_m \mu^\ominus(\text{Ph}_4\text{B}^-) \quad 29$$

The anion and cation are approximately spherical, and of similar size; the peripheries of the ions are the same, and the ions are only lightly solvated. Solubilities of the appropriate salts yield the required single ion value

$$\begin{aligned} \delta_m \mu^\ominus(\text{cation}) = & 2.303RT \{ \log_{10}[\text{S(II)XBPh}_4] \\ & + 0.5 \log_{10}[\text{S(I)PPh}_4\text{BPh}_4] - 0.5 \log_{10}[\text{S(II)PPh}_4\text{BPh}_4] \\ & - \log_{10}[\text{S(I)XBPh}_4] \} \quad 30 \end{aligned}$$

Where S(I) is the solubility product of the salt in the reference solvent, S(II) is the solubility^{product} of the salt in the solvent, and X is the cation under discussion.

Similarly

$$\begin{aligned} \delta_m \mu^\ominus(\text{anion}) = & 2.303RT \{ \log_{10}[\text{S(II)XPPH}_4] \\ & + 0.5 \log_{10}[\text{S(I)PPh}_4\text{BPh}_4] - 0.5 \log_{10}[\text{S(II)PPh}_4\text{BPh}_4] \\ & - \log_{10}[\text{S(I)XPh}_4] \} \quad 31 \end{aligned}$$

Where S(I) and S(II) are the solubilities of the salt (mol dm⁻³)

in the reference solvent and new solvent respectively, and X is the anion under discussion.

Less work has been reported for evaluating single ion enthalpies of transfer. Using the same arguments for estimating Gibb's free energy of transfer, one method⁷ assumes

$$\delta_m \Delta H^\ominus(\text{Ph}_4\text{P}^+) = \delta_m \Delta H^\ominus(\text{BPh}_4^-) \quad 32$$

Thus, the enthalpies of solution of appropriate salts will yield the required single ion parameter

$$\delta_m \Delta H^\ominus(\text{anion}) = \delta_m \Delta H^\ominus(\text{XPPh}_4) - \frac{1}{2} \delta_m \Delta H^\ominus(\text{PPh}_4\text{BPh}_4) \quad 33$$

$$\delta_m \Delta H^\ominus(\text{cation}) = \delta_m \Delta H^\ominus(\text{XBPh}_4) - \frac{1}{2} \delta_m \Delta H^\ominus(\text{PPh}_4\text{BPh}_4) \quad 34$$

The choice of single ion values employed to perform initial state-transition state analysis is often limited by the availability of published data. Each assumption has its own limitations. Thus calculations involving the Born equation are complicated by the nature of solvation of the ion under discussion on going from water rich media to organic (solvent) rich media. One problem with PPh_4^+ , BPh_4^- assumption is the poor solubility of BPh_4PPh_4 in water rich media.

The choice of single ion thermodynamic parameters obviously affects conclusions drawn from initial state-transition state analysis, although overall patterns remain unaltered. Despite this, initial state-transition state dissections remain a very powerful tool for the analysis of solvent effects upon reactions.

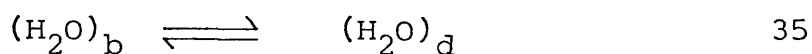
The Structure of Water

Water is the most extensively studied solvent⁸. Recently a short review has been published⁹.

Radial distribution functions for water derived from X-Ray scattering experiments show two peaks: one at 0.28 nm and the other at 0.348 nm. These experiments also indicate that the co-ordination number of water is approximately 4.4, and at its boiling point the co-ordination number increases to five.

This and other evidence suggests a structure of water consisting of a hydrogen bonded clathrate like cluster in equilibrium with non hydrogen bonded water molecules. The co-ordination numbers favour a tetrahedral arrangement around each water molecule (cf. Ice I_h); this arrangement is not closest packing, so the structure has a large amount of empty space. Upon increasing the temperature, the structure collapses, so increasing the co-ordination number. The lifetime of the clusters is estimated to be 10^{-11} s, and the non bonded water molecules would reside in the voids mentioned above.

The structure of water can be represented by the equilibrium



Where $(\text{H}_2\text{O})_b$ is the hydrogen bonded, bulky, low density form of water.

Solutes which enhance water-water interactions shift the equilibrium to favour the formation of $(\text{H}_2\text{O})_b$;

conversely, solutes which break the water structure shift the equilibrium to favour the $(\text{H}_2\text{O})_d$.

Binary Aqueous Mixtures

The reactions described in Chapters 2 and 3 were performed in binary aqueous mixtures, therefore it is of interest to consider the classification of binary aqueous mixtures.

On the basis of their molar excess thermodynamic functions binary aqueous mixtures can be divided into three classes

(1) Typically Aqueous, TA: $G^E > 0$, $|TS^E| > |H^E|$

In these cases mixing is dominated by entropy changes.

(2) Typically Non Aqueous, TNA: $|H^E| > |TS^E|$

In these cases mixing is enthalpy dominated. This class may be further divided

(a) $G^E > 0$:TNAP mixtures

(b) $G^E < 0$:TNAN mixtures

Typically Aqueous Mixtures

Examples of this class include acetone + water, alcohols + water. Fig 1 shows plots of molar excess functions against mole fraction for ethanol-water and t-butanol-water mixtures. Such mixtures may have a tendency to form lower critical solution temperatures(LCST). Some TA mixtures may undergo phase separation at increased pressures.

Fig 2 shows the variation of partial molar volumes for

some TA systems. Generally V^E is negative and this implies a net volume shrinkage when the solute is added to water: the solute does not occupy as much volume as it does in the pure liquid state. At low mole fractions water-water interactions are enhanced, providing a clathrate type structure around the solute. An exothermic H^E is associated with this behaviour. At a certain mole fraction, x_2^* , the slope of $V_2^E-x_2$ plot is zero. At this point there is insufficient water to maintain the clathrate structure. With further increase in mole fraction x_2 , the slope of $V_2^E-x_2$ plot is positive, and this is associated with "structure breaking"; at a certain mole fraction, x_2^{**} , the extended water structure is broken down. Interestingly, x_2^{**} corresponds closely to H^E minima. Some values of x_2^* and x_2^{**} are shown in Table 1.

Typically Non Aqueous Positive Mixtures

These systems are rare. Examples of this class are acetonitrile + water, ethylene carbonate + water, propylene carbonate + water, sulpholane + water. These systems may undergo phase separation at an upper critical solution temperature(UCST). The cosolvent has a depolymerizing effect on water ie. water structure breakers; there is also evidence for intercomponent hydrogen bonds¹⁰.

Typically Non Aqueous Negative Mixtures

Examples of this class include hydrogen peroxide + water¹¹ and dimethylsulphoxide + water¹² (Fig.3 and Fig.4). These mixtures have negative values of G^E and small, negative S^E values. This corresponds to increase order of the system. Evidence indicates strong intercomponent interactions occur in these systems. There is intercomponent association: in DMSO-water mixtures there is strong evidence for the formation of 2:1 DMSO/H₂O species¹³.

Solvent Polarity

In Chapters 5 and 6 the majority of the reactions discussed were performed in non aqueous solvents. As with binary aqueous mixtures, it would be useful to classify pure solvents. One physical property often used to describe solvents is their relative permittivity. Another frequently used classification is that of solvent polarity. The polarity of a solvent is commonly used to relate its ability to solvate dissolved charged or dipolar species. Although this concept is easy to grasp qualitatively, attempts to quantify this term have proved difficult. According to Reichardt¹⁴ the polarity of a solvent is determined by its solvation capability for reactants and activated complexes as well as for molecules in the ground and excited states. This in turn depends on the action of all possible specific and non specific intermolecular forces between solvent and solute molecules. These

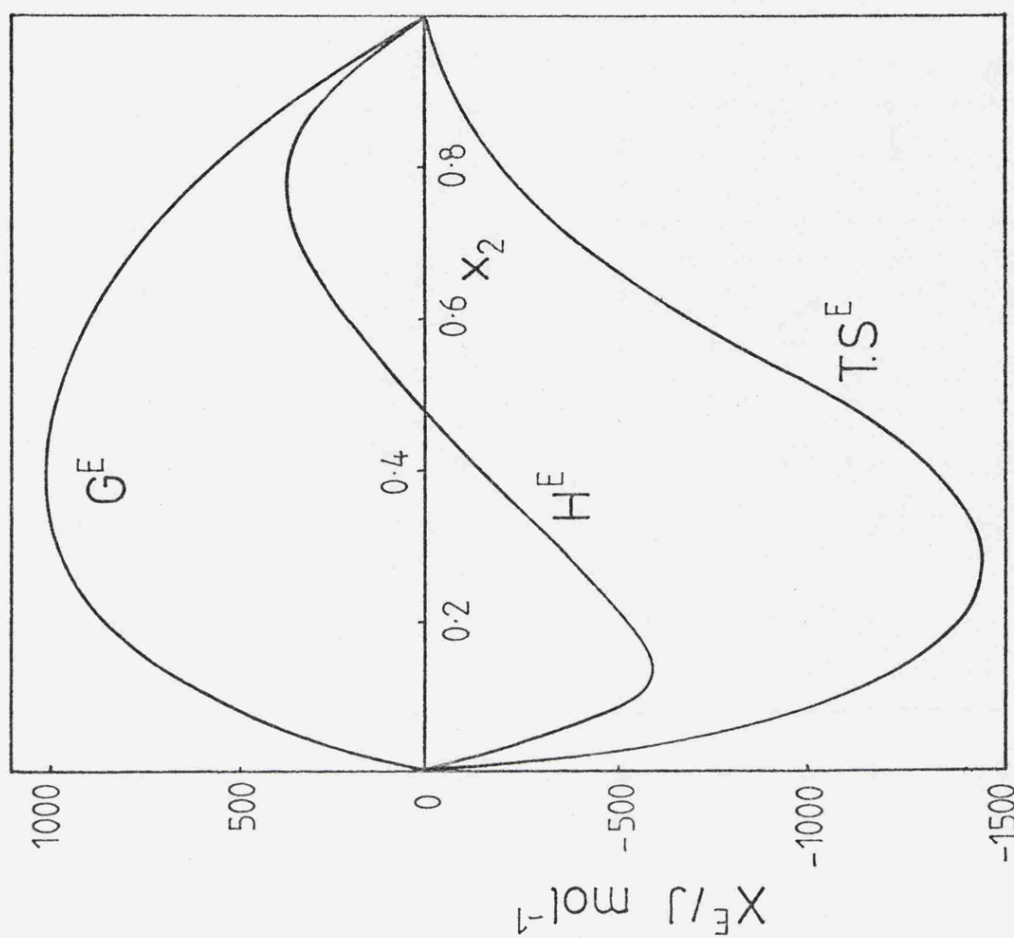
intermolecular forces include Coulomb interactions between ions, directional interactions between dipoles, inductive, dispersive, hydrogen bonding, charge transfer forces, and hydrophobic interactions. To determine solvent polarity quantitatively a process is selected which depends upon the above interactions, and where these interactions are solvent sensitive. Such processes include equilibria, rates of reaction and spectral properties. Several solvent polarity scales have been reported, and Reichardt has discussed them in detail¹⁴. For the work described in this thesis only Dimroth's $E_T(30)$ scale is used. This scale¹⁵ is based upon the transition energy of the charge transfer band of a pyridinium-N-phenoxide betaine dye (Fig.5):

$$E_T(30) = h.c.\bar{\nu}.N_a \quad 36$$

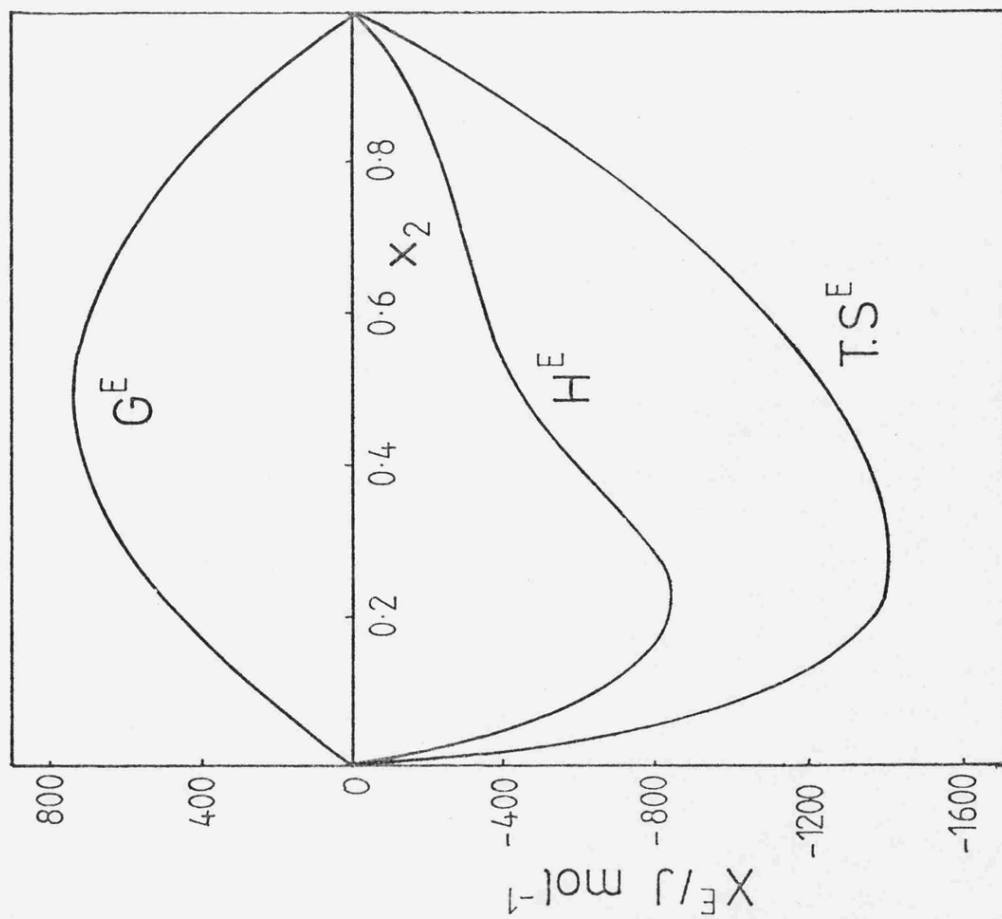
Where h is Plank's constant, c is the velocity of light, $\bar{\nu}$ is the wavenumber (cm^{-1}) of the photon producing the electronic excitation, and N_a is Avagadro's number.

$E_T(30)$ values are known for more than a hundred pure solvents and for a variety of binary mixtures¹⁶. Of all the solvent polarity scales, $E_T(30)$ is the most comprehensive. This is partly due to the solubility of the dye in such a wide range of solvents/solvent mixtures and that the dye is the most solvatochromic compound reported to date. This scale was particularly used in Chapter 5 where the effects of solvents upon Charge Transfer bands were studied.

Figure 1 Molar excess thermodynamic functions for typically aqueous mixtures.



298.2K
t-butanol/water



298.2K
Ethanol/water

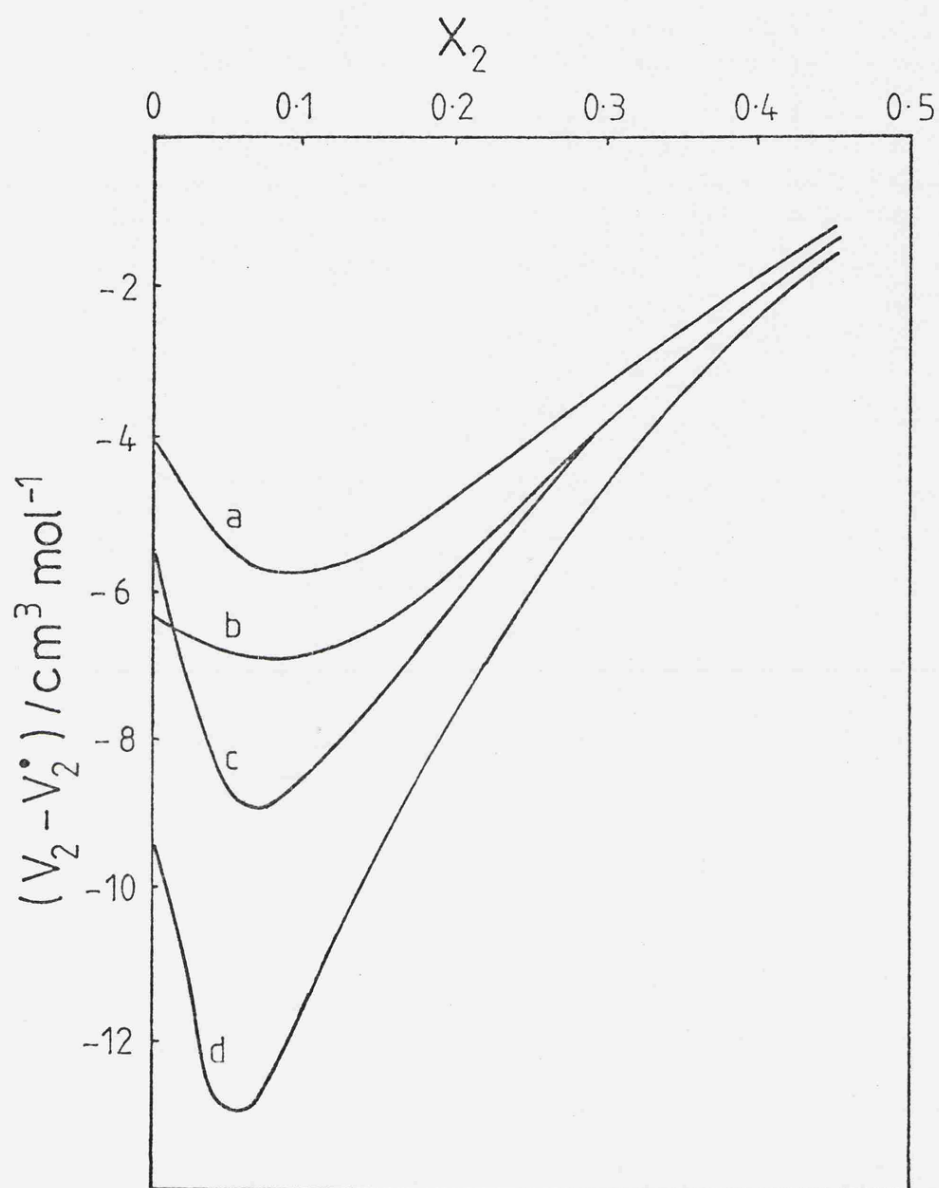


Figure 2 Dependence of relative partial molar volume, $(V_2 - V_2^*)$ for cosolvents in some typically aqueous mixtures as a function of cosolvent mole fraction at 298.2 K.

a) ethanol, b) acetone, c) n-propanol, d) t-butanol.

Figure 3 Molar excess thermodynamic functions of mixing for hydrogen peroxide/water mixtures at 298.2 K.

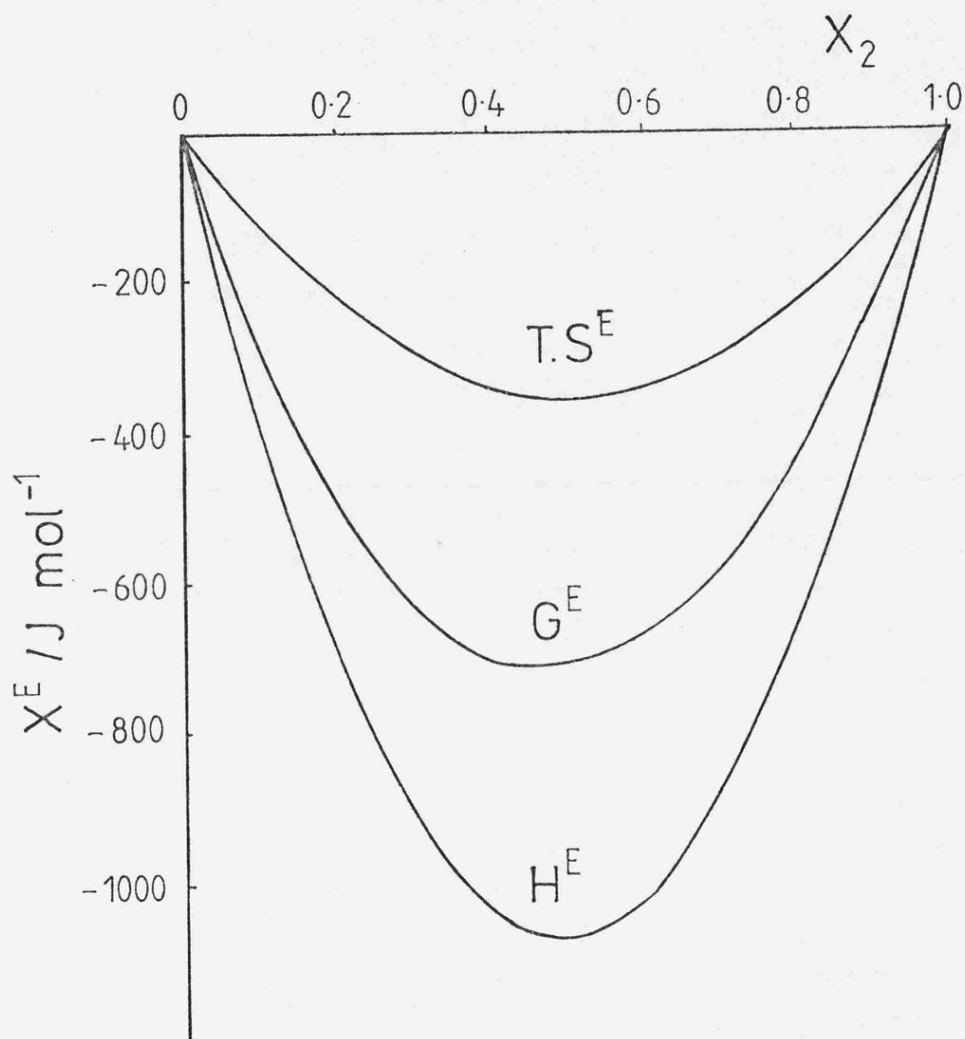


Figure 4 Molar excess thermodynamic functions of mixing for dimethylsulphoxide/water mixtures at 298.2 K.

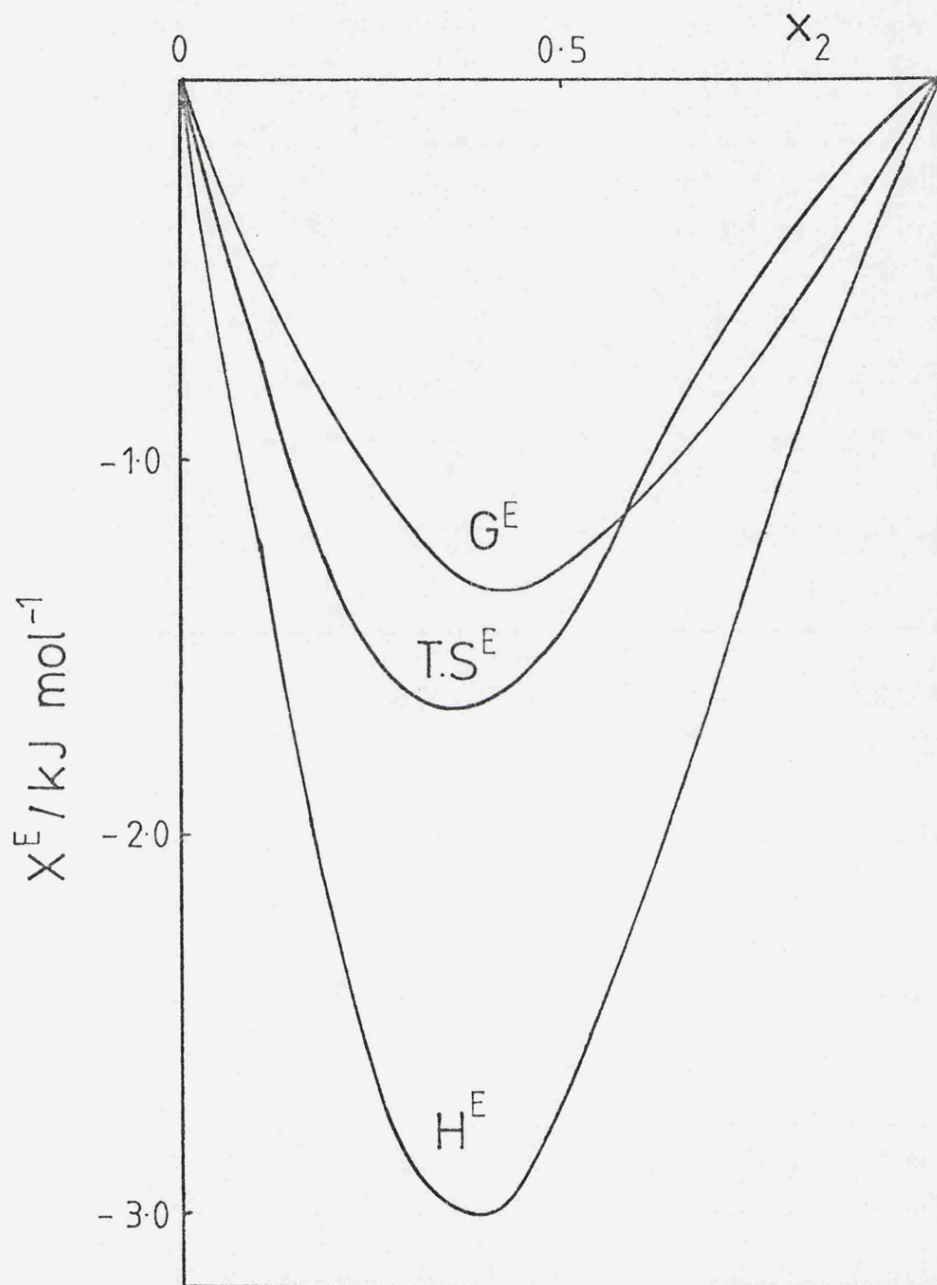


Figure 5 The betaine dye E^T(30).

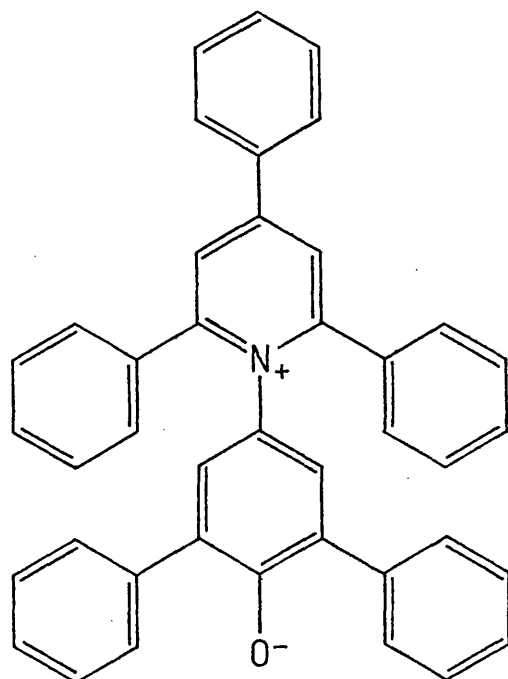


Table 1

x_2^* , x_2^{**} values for alcohols

Solute	x_2^*	x_2^{**}
Ethanol	0.09	0.20
Isopropanol	0.06	0.18
t-Butanol	0.04	0.10
[Acetone	0.06	0.35]

References Chapter 1

1. "Chemical Kinetics and Reaction Mechanisms",
J.H.Espenson, McGraw Hill, 1981
2. P.P.Duce, Ph.D Thesis, Leicester University, 1982
3. P.Moore, J.Chem.Soc.Faraday 1, 68, 1890 (1972)
4. P.J.Robinson, J.Chem.Ed., 55, 509 (1978)
5. M.Born, Z.Phys., 1, 45 (1920)
6. Latimer improved Born's equation by using an effective
radius of the ion: W.M.Latimer, K.S.Pitzer and C.M.
Slansky, J.Chem.Phys., 7, 108 (1939)
7. A.J.Parker, Chem.Rev., 69, 984 (1973)
8. "Water-A Comprehensive Treatise", ed. F.Franks, Plenum
Press, 1973
9. "Water", F.Franks, Royal Society Chemistry , London, 1983
10. D.A.Armitage, M.J.Blandamer, M.J.Foster, N.J.Hidden,
K.W.Morcom, M.C.R.Symons and M.J.Wooten, Trans.Faraday
Soc., 64, 1193 (1968)

11. G.Sachard, G.M.Kavanagh and L.B.Ticknor, J.Am.Chem. Soc., 74 3715 (1952);
A.G.Mitchell and W.F.K.Wynne-Jones, Discuss.Faraday Soc., 15, 161 (1953);
P.A.Gigùre, O.Knop and M.Falk, Canad.J.Chem., 36, 883 (1958)
12. H.L.Clever and S.P.Pigott, J.Chem.Thermodynamics, 3, 221 (1971)
13. T.Tokuhiro, L.Menafra and H.H.Szmani, J.Chem.Phys., 61, 2275 (1974)
14. "Solvent Effects in Organic Chemistry", C.Reichardt, Verlag Chemie, Weinheim, New York, 1979, Chapter 7
15. K.Dimroth, C.Reichardt, T.Siepmann and F.Bohlmann, Liebigs Ann.Chem., 661, 1 (1963); C.Reichardt, Liebigs Ann.Chem., 752, 64 (1971)
16. H.Langhals, Angew.Chem.Int.Ed.Engl., 21, 724 (1982)

CHAPTER TWO:

Initial state-transition state analysis for
the reactions $\text{Fe}(\text{phen})_3^{2+} + \text{Nu}$ ($\text{Nu} = \text{OH}^-, \text{CN}^-$)
in aqueous methanol mixtures.

Introduction

There is an extensive chemistry of complexes of the type $\text{Fe}(\text{LL})_3^{2+}$, where LL represents a diimine ligand. The choice of ligand dictates the electronic configuration, and for many diimines iron is low spin, t_{2g}^6 , eg. LL= 2,2'-bipyridine (bipy) or 1,10-phenanthroline (phen). These iron diimine systems have been used as models to study various kinetic systems such as nucleophilic attack, hydrolysis and so on. The low spin iron(II) makes them particularly attractive from the kinetic point of view.

Our interest in these systems is to study the effects of solvents, especially on nucleophilic attack, and hydrolysis. Studies¹ have been done for a variety of nucleophiles including hydroxide, cyanide, methoxide and azide, and a general expression for the rate law has been determined², and is of the form:

$$k_{\text{obs}} = k_1 + k_2[\text{nuc.}] + k_3[\text{nuc.}]^2 + k_4[\text{nuc.}]^3 \dots$$

The relative importance of each term in the rate law depends very much upon the conditions employed for each experiment. For nucleophilic attack, where the concentration of nucleophile is relatively small the rate law reduces to:

$$k_{\text{obs}} = k_1 + k_2[\text{nuc.}]$$

At high concentrations of nucleophile the $k_3[\text{nuc.}]^2$ term becomes important.

Concurrent with the kinetic discussion is the question of mechanism. The kinetics indicate a bimolecular mechanism. Because of the conceptual difficulties of nucleophilic

attack at the metal centre Gillard has proposed an alternative mechanism whereby the nucleophile attacks at the co-ordinating ligand.³

We are interested in using nucleophilic attack on $\text{Fe}(\text{phen})_3^{2+}$ as a probe for solvent effects. The mechanism of the attack is assumed to be bimolecular. It is hoped to discuss solvent effects in terms of an initial state-transition state analysis.

Experimental

$\text{Fe}(\text{phen})_3\text{Cl}_2 \cdot 6\text{H}_2\text{O}$ was prepared according to the method of Walden⁴. Thus, three equivalents of 1,10-phenanthroline and one equivalent of iron(II) chloride were dissolved in a little methanol. A red colouration formed immediately. The methanol was removed to produce a semisolid. The solid was filtered off, and washed with a little cold methanol. The solid was dried under vacuum, over P_2O_5 .

Water of crystallisation was determined by thermogravimetric analysis on a Stanton Redcroft TG 750/770 thermogravimetric balance.

Sodium chloride solution was made by direct weighing from Analar material. Sodium hydroxide solution was made by suitable dilution of standard solutions. Methanol was dried using Mg/I_2 . For kinetic runs a concentrated solution of tris(1,10-phenanthroline) iron(II) sulphate was suitably diluted.

Kinetic runs were carried out in 1cm cells in the thermostated cell compartment of either a Pye-Unicam SP

8-100 or Pye-Unicam SP 1800 fitted with a Hewlett Packard HP 9285 computer.

Optical densities were measured at 510nm for a period of 2.5 half lives. Observed first-order rate constants, k_{obs} , were either computed from recorded optical densities, or directly by the mini-computer.

Enthalpies of solution* were measured using a LKB 8700 calorimeter assembly with ancillary recording and detecting apparatus as described elsewhere⁵; the machine was calibrated using the enthalpy of solution of KCl in water.

Results

First-order rate constants for the acid aquation of $\text{Fe}(\text{phen})_3^{2+}$, in various solvent mixtures are shown in table 1. Enthalpies of activation were determined in the usual manner.

First-order rate constants, k_{obs} , for the reaction between $\text{Fe}(\text{phen})_3^{2+}$ and hydroxide, in various solvent compositions are shown in table 2. First-order rate constants were shown to be linear in hydroxide concentration.

Values for k_2 were calculated from:

$$k_2 = (k_{\text{obs}} - k_1)/[\text{nuc.}]$$

using values for k_1 from table 1. (either directly or by interpolation).

Activation enthalpies were calculated in the normal manner, using a standard unweighted least mean squares program.

First-order rate constants for cyanide attack are shown

* UNCERTAINTY ON THE ENTHALPIES OF SOLUTION IN TABLE 4 ARE \pm

in table 3 (work done by J.McCann and R.H.Reynolds as part of an undergraduate project).

Variation of enthalpies of activation with solvent composition are shown in Fig.1.

Enthalpies of solution of $\text{Fe}(\text{phen})_3\text{Cl}_2 \cdot 6\text{H}_2\text{O}$ in various solvent mixtures are incorporated in table 4 and Fig.3.

Table 4 shows the analysis of solvent effects on initial states and transition states. This table is summarised in graphical form in Fig.2. All single ion transfer enthalpies are derived from Krestov and Klopov's⁶ set of single ion enthalpies of solvation of alkali metal cations and halide ions. Estimates of $\delta_m \Delta H^\ominus(\text{OH}^-)$ were obtained from enthalpies of solution of sodium hydroxide⁷ and Krestov and Klopov's $\delta_m \Delta H^\ominus(\text{Na}^+)$ values. Similarly, $\delta_m \Delta H^\ominus(\text{CN}^-)$ were estimated using Krestov and Klopov's $\delta_m \Delta H^\ominus(\text{K}^+)$ values. From published⁸ enthalpies of mixing of methanol-water mixtures, $\delta_m \Delta H^\ominus(6\text{H}_2\text{O})$ could be calculated.

Discussion

In our analysis of the solvent effects the detailed mechanism is not important; we will assume that nucleophilic attack is a simple one step bimolecular process: this is born out by the kinetic observations; the mechanism of aquation is assumed to be unimolecular, as suggested from the volume of activation⁹.

If we concentrate at the water rich end ($\leq 40\%$ MeOH) we see that the initial state and transition state parallel each other.

The $\text{Fe}(\text{phen})_3^{2+}$ contributes significantly to the initial state. There is considerable enthalpy expenditure in getting the substrate into solution. This can be seen as a reflection of the solvent structure. If you consider water as a hydrogen bonded cage, with methanol occupying the spaces, this represents a highly co-ordinated situation, requiring expenditure of enthalpy to break up the structure sufficiently to get the large substrate into solution.

By way of contrast the effect of solvent composition upon hydroxide anion is small, reflecting the preferential solvation of the ion by water.

That the transition state parallels the initial state closely indicates that it is being formed early, its structure approximating to that of the initial reactants.

At the methanol rich end the transition state crosses over the initial state. This would seem to indicate preferential solvation of the transition state. There is no simple explanation for this. An analysis of this type requires at least one extrathermodynamic assumption, thus there may be considerable error for single ion values in 80% methanol. No other set of single ion values has yet been published for water-methanol mixtures. A set of values based upon the assumption:

$$\delta_m \Delta H^\ominus(\text{Ph}_4\text{As}^+) = \delta_m \Delta H^\ominus(\text{Ph}_4\text{B}^-)$$

is expected¹⁰. Although these values may differ significantly from Krestov and Klopov's values, the qualitative aspects of the initial state-transition state analysis will remain unchanged.

There is also the problem of obtaining accurate activation enthalpies. In 80% methanol the k_1 term becomes important and of similar magnitude for k_{obs} , thus introducing error in the calculation of k_2 . One way round this problem is to use higher concentrations of hydroxide. However this would necessitate the use of stopped flow techniques, which is unsatisfactory when using concentrated solutions.

For the aquation reaction similar trends are observed. Again the transition state is dominated by the $Fe(phen)_3^{2+}$ cation, and at high methanol concentration the transition state crosses the initial state.

With cyanide as the nucleophile similar results are observed (Fig.2). The effect of the solvent composition upon the nucleophile is small. The transition state parallels the initial state, and the $Fe(phen)_3^{2+}$ cation contributes significantly to both the initial and the transition states.

With both hydroxide and cyanide nucleophiles, and for aquation, 'enthalpic maxima' occur around 20% MeOH. This is a reflection of the solvent structure, 20% MeOH being close to x_2^{**} . It is interesting to examine the enthalpies of solution for a range of metal halides in aqueous methanol (Fig.3). Again there is an enthalpic maxima for each compound, and these occur at very similar solvent compositions. There is also a change going from trivalent to bivalent, and from bivalent to monovalent halides. In each case the enthalpies of solution become more positive. For $Fe(phen)_3Cl_2 \cdot 6H_2O$ the effect of the organic ligand can

clearly be seen.

In summary, for nucleophilic attack by hydroxide or cyanide on $\text{Fe}(\text{phen})_3^{2+}$ cation in aqueous methanol, the initial state and transition state is dominated by the $\text{Fe}(\text{phen})_3^{2+}$ cation.

Table 1

First-order rate constants, $10^4 k_{\text{obs}}$, for aquation of $\text{Fe}(\text{phen})_3^{2+}$ in hydrochloric acid ($0.133 \text{ mol dm}^{-3}$); initial $[\text{complex}] = 5 \times 10^{-5} \text{ mol dm}^{-3}$.

T/K	% methanol		T/K	% methanol	
	0	80		20	40
298.2	0.77		303.9	2.7	3.6
	0.77		308.1	5.2	6.8
	0.78		313.0	10.8	13.6
301.8	1.49	8.9	318.3	24.4	32.4
	1.49	8.9	323.5	40.8	60.7
	1.48	8.8			
304.7	2.42	13.2			
	2.39	13.2			
306.6	3.09	16.6			
308.2	4.24	22.7			
	4.13	22.6			
	4.21	23.3			

% methanol	$\Delta H^\ddagger / \text{kJ mol}^{-1}$
0	126.6 ± 2.2
20	131.0 ± 2.6
40	129.0 ± 2.6
80	115.2 ± 2.1

Table 2

First-order rate constants, $10^3 k_{\text{obs}}$, for the reaction of $\text{Fe}(\text{phen})_3^{2+}$ with hydroxide ($\underline{I} = 0.133 \text{ mol dm}^{-3}(\text{NaCl})$); initial $[\text{complex}] = 5 \times 10^{-5} \text{ mol dm}^{-3}$.

water		20% methanol		
T/K	$[\text{OH}^-] = 0.133\text{M}$	T/K	$[\text{OH}^-] = 0.107\text{M}$	0.133M
298.2	2.14	292.6	0.96	1.27
	2.11	295.9	1.72	2.32
	2.09	297.9	2.92	3.67
	2.11	298.7	3.19	4.02
301.8	3.24	299.5	3.38	4.95
	3.39	300.4	4.39	4.55
	3.23	303.2	5.01	6.62
	3.38	303.5	5.56	7.96
304.7	4.44	304.5	5.55	9.11
	4.40	306.3	7.7	10.6
306.6	5.07	307.3	9.8	12.8
308.2	6.67	308.5	10.3	14.6
	6.63	311.3	15.4	17.8
	6.69	312.9	15.7	20.1
		314.3	21.2	27.5

Table 2 continued

40% methanol			80% methanol	
T/K	[OH ⁻] = 0.107M	0.133M	T/K	[OH ⁻] = 0.0033M
298.0	0.60	0.83	300.0	1.63
300.7	0.94	1.19		1.67
302.3	1.14	1.65	301.8	1.99
309.4	3.37	4.51		1.98
311.2	3.74	5.21	304.7	2.68
312.8	5.19	6.94		2.72
313.8	6.9	7.8		2.58
316.7	7.1	8.8		2.88
318.0	7.9	12.5		2.68
321.6	11.6	15.3	306.6	3.39
				3.36
				3.36
			308.2	3.76
				4.00
				3.91
				3.83

% methanol	$\Delta H^\ddagger / \text{kJ mol}^{-1}$
0	81.1 \pm 1.8
20	89.8 \pm 2.1
40	92.9 \pm 3.1
80	46.6 \pm 5.4

Table 3

First-order rate constants, $10^4 k_{\text{obs}}$, for the reaction of $\text{Fe}(\text{phen})_3^{2+}$ with cyanide ($0.063 \text{ mol dm}^{-3}$); initial $[\text{complex}] = 5 \times 10^{-5} \text{ mol dm}^{-3}$.

T/K	% methanol				
	0	10	20	30	40
287.7	4.8	5.4	8.7	17.8	30.9
305.2	49.4	67.3	87.6	180	253
310.3	81.4	103	170	284	467
314.8	132	209	338	415	792

% methanol	$\Delta H^\ddagger / \text{kJ mol}^{-1}$
0	88.8 ± 2.9
10	97.2 ± 5.0
20	97.3 ± 3.3
30	86.2 ± 4.6
40	88.8 ± 0.9

Table 4

Initial state and transition state contributions to solvent effects on activation enthalpies (kJ mol^{-1}) for substitution reactions of the $\text{Fe}(\text{phen})_3^{2+}$ cation, at 298.2 K.

overleaf:

Table 4

	% methanol			
	0	20	40	80
$\Delta H_{\text{soln}}^{\ominus}(\text{Fe}(\text{phen})_3\text{Cl}_2 \cdot 6\text{H}_2\text{O})^{\text{a}}$	+7.3	+38.4	+31.2	+11.0
$\delta_m \Delta H^{\ominus}(\text{Fe}(\text{phen})_3\text{Cl}_2 \cdot 6\text{H}_2\text{O})$		+31.1	+23.9	+3.7
$\delta_m \Delta H^{\ominus}(6\text{H}_2\text{O})$		-1.1	-3.7	-8.3
$\delta_m \Delta H^{\ominus}(\text{Fe}(\text{phen})_3\text{Cl}_2)$		+32.1	+27.6	+12.0
$\delta_m \Delta H^{\ominus}(2\text{Cl}^-)$		+2.8	+5.6	+4.3
$\delta_m \Delta H^{\ominus}(\text{Fe}(\text{phen})_3^{2+})$		+29.4	+22.0	+7.7
<u>Aquation</u>				
ΔH^{\ddagger}	126.6	131.0	129.0	115.2
$\delta_m \Delta H^{\ddagger}$		+4.4	+2.4	-11.4
$\delta_m \Delta H(\text{ts})$		+34	+24	-4
<u>Hydroxide attack</u>				
$\delta_m \Delta H^{\ominus}(\text{OH}^-)$		+1	0	-3
$\delta_m \Delta H(\text{is})$		+30	+22	+5
ΔH^{\ddagger}	81.1	89.8	92.9	46.6
$\delta_m \Delta H^{\ddagger}$		+8.7	+11.8	-34.5
$\delta_m \Delta H(\text{ts})$		+39	+34	-30
<u>Cyanide attack</u>				
$\Delta H_{\text{soln}}^{\ominus}(\text{KCN})$	+11.5	+14.7	+12.6	
$\delta_m \Delta H^{\ominus}(\text{KCN})$		+3.2	+1.1	
$\delta_m \Delta H^{\ominus}(\text{K}^+)$		-1.2	-2.8	
$\delta_m \Delta H^{\ominus}(\text{CN}^-)$		+4.4	+3.9	
$\delta_m \Delta H(\text{is})$		+34	+26	
ΔH^{\ddagger}	88.8	97.3	88.8	
$\delta_m \Delta H^{\ddagger}$		+8.5	0	
$\delta_m \Delta H(\text{ts})$		+43	+26	

a This result compares satisfactorily with the enthalpy of solution of +4.87 kcal mol⁻¹ reported for the heptahydrate (Y.Yamamoto and T.Tarumoto, *Analyt.Lett.*, 3,537 (1970)).

Figure 1 Comparison of activation enthalpy trends with solvent composition.

Fe(phen)_3^{2+} SUBSTITUTION: ΔH^\ddagger TRENDS

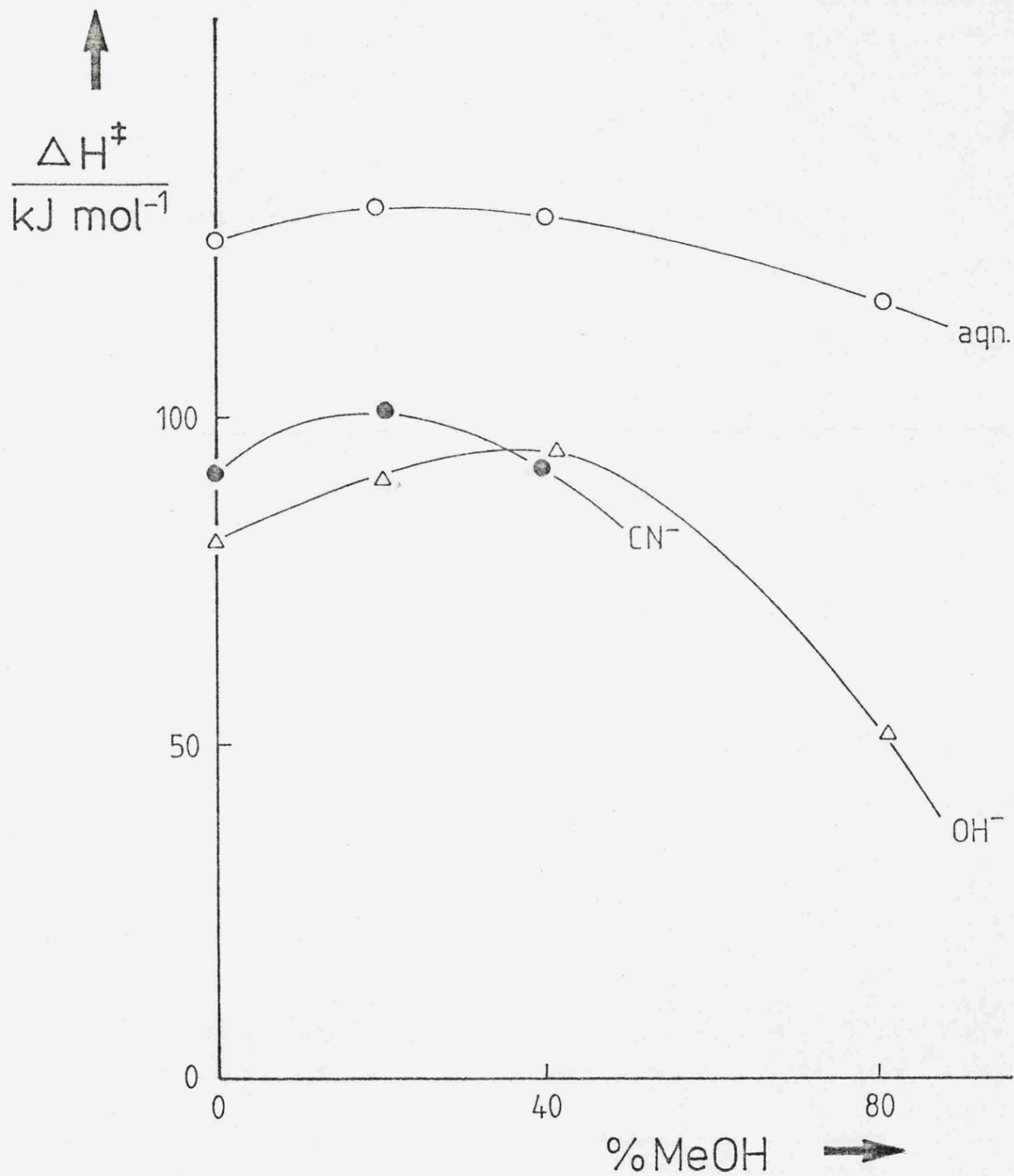


Figure 2(1) Initial state-transition state analysis for the hydroxide attack at the $\text{Fe}(\text{phen})_3^{2+}$ cation.

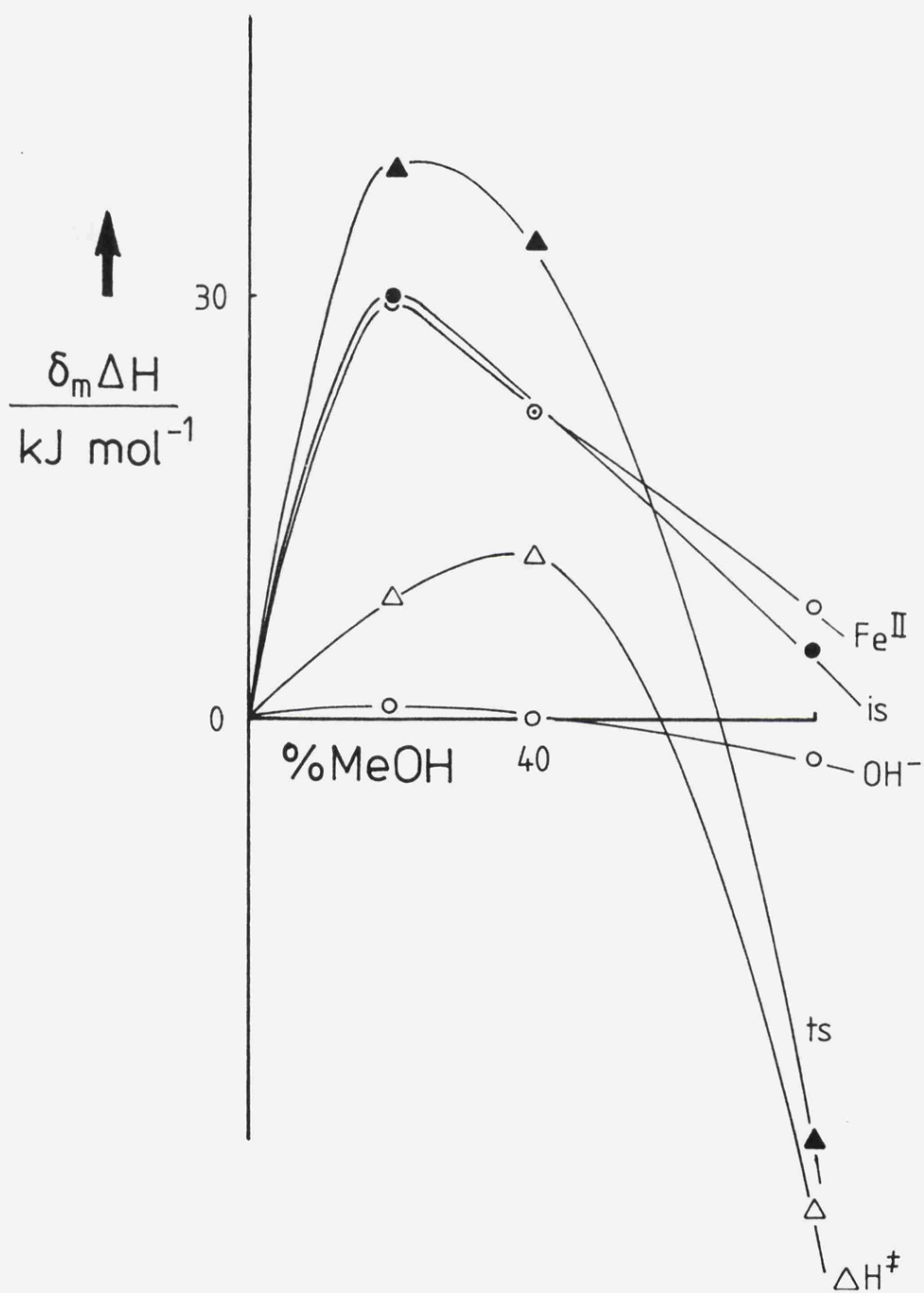


Figure 2(2) Initial state-transition state analysis for the cyanide attack at the $\text{Fe}(\text{phen})_3^{2+}$ cation.

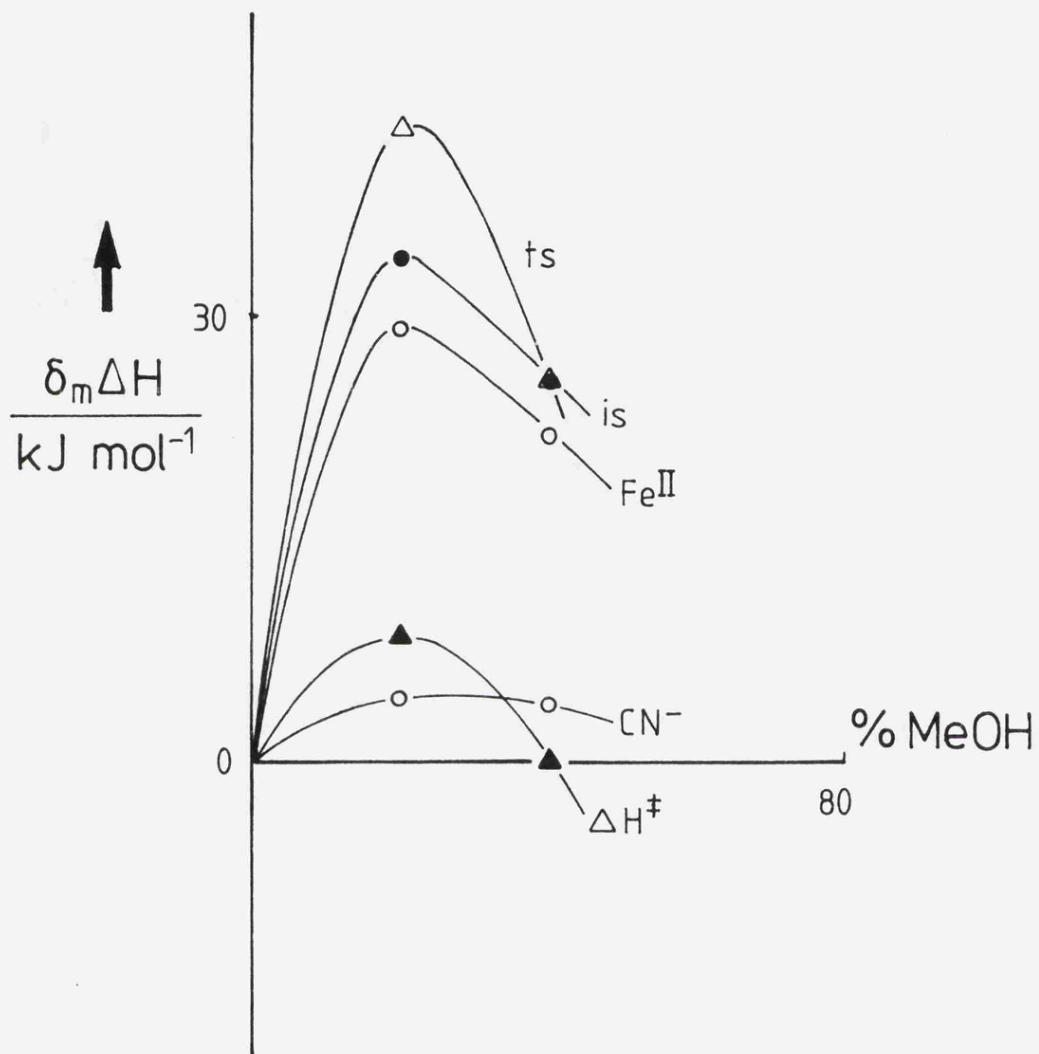


Figure 2(3) Initial state-transition state analysis for the aquation of the $\text{Fe}(\text{phen})_3^{2+}$ cation.

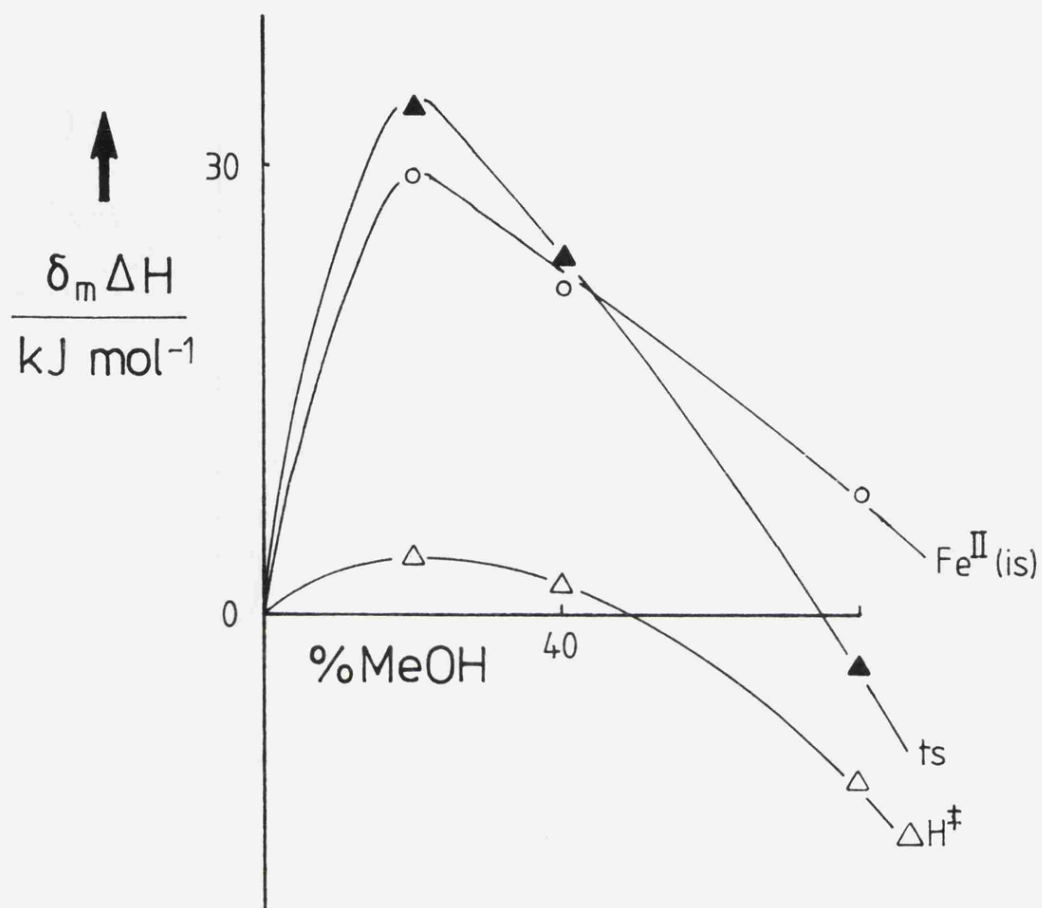
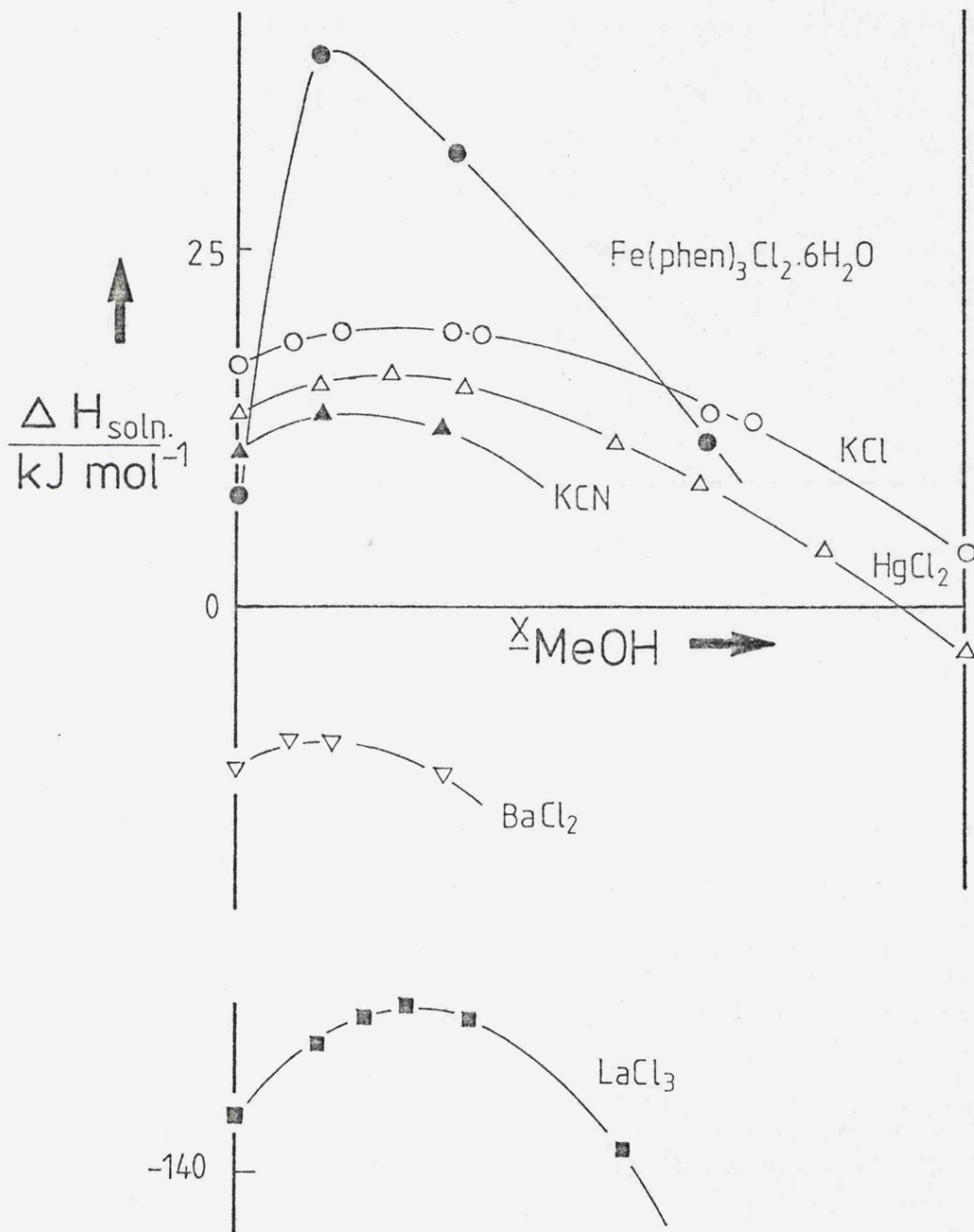


Figure 3 Comparison of enthalpy of solution trends for $\text{Fe}(\text{phen})_3\text{Cl}_2 \cdot 6\text{H}_2\text{O}$ and for KCN with those for a selection of inorganic halides, for dissolution in aqueous methanol at 298.2 K.



References Chapter 2

1. M.J.Blandamer, J.Burgess, J.G.Chambers, R.I.Haines, and H.E.Marshall, J.C.S.Dalton, 1977, 165
2. D.W.Margerum and L.P.Morgenthaler, J.Am.Chem.Soc., 84, 706 (1962)
3. R.D.Gillard, Inorg.Chim.Acta, 11, L21 (1974); Co-ord. Chem.Rev., 16, 67 (1975)
4. G.H.Walden, L.P.Hammett, and R.P.Chapman, J.Am.Chem.Soc., 55, 2649 (1933)
5. J.Burgess, I.Haigh, and R.D.Peacock, J.C.S.Dalton, 1974 1062
6. G.A.Krestov and V.I.Klopov, Zh.Strukt.Khim., 5, 829 (1964)
7. M.Bobtelsky and R.D.Larisch, J.Chem.Soc., 1950, 3612
8. F.Franks and K.J.G.Ives, Q.Rev.Chem.Soc., 20, 1, (1966) and refs. therein.
9. J.-M.Lucie, D.R.Stranks, and J.Burgess, J.C.S.Dalton, 1975, 245
10. M.H.Abraham, T.Hill, H.C.Ling, R.A.Schulz, and R.A.C.Watt, submitted to J.C.S.Far.Trans 1.

CHAPTER THREE:

Initial state-transition state analysis for the racemisation of $(-)\text{Fe}(\text{phen})_3^{2+}$ in aqueous methanol mixtures. Initial state-transition state analysis for the racemisation of $(-)\text{Fe}(\text{phen})_3^{2+}$ in aqueous DMSO mixtures. Initial state-transition state analysis for the dissociation of $\text{Fe}(\text{phen})_3^{2+}$ in aqueous methanol and aqueous DMSO mixtures. The resolution of $\text{Fe}(\text{mppm})_3^{2+}$. The kinetics of racemisation of $(-)\text{Fe}(\text{mppm})_3^{2+}$. The resolution of $\text{Fe}(\text{5NO}_2\text{phen})_3^{2+}$ and $\text{Ru}(\text{5NO}_2\text{phen})_3^{2+}$. The attempted resolution of $\text{Fe}(\text{btz})_3^{2+}$ and $\text{Ru}(\text{btz})_3^{2+}$. The preparation of d-2'-methoxy-2-nitro-6-carboxydiphenyl.

Introduction

In the previous chapter some of the problems associated with analysing solvent effects were encountered. One of the difficulties was estimating single ion values; another problem concerned the detailed mechanism for the reactions.

The effects of solvent composition upon racemisation were investigated in an attempt to overcome these problems. Initial interests were with the racemisation of metal β -diketonate complexes. However, because they were uncharged, hence removing the need for single ion values, they proved difficult to resolve. Some experiments were done to try and resolve chromium(III) tris(acetylacetonate) by the method of Moeller and Gulyas¹, but these were unsuccessful. Other techniques for resolving neutral metal β -diketonate complexes have been published², but these were not investigated.

In this chapter the racemisation of $\text{Fe}(\text{phen})_3^{2+}$ is studied. As these complexes are charged they are technically easier to resolve. However, to analyse solvent effects into initial state and transition state contributions single ion values are required.

$\text{Fe}(\text{phen})_3^{2+}$ racemises by an intramolecular pathway and a solvolytic pathway, the intramolecular pathway predominating. To minimise racemisation by the solvolytic pathway, the racemisation of iron Schiff base complexes were studied, because these complexes generally solvolise more slowly than $\text{Fe}(\text{phen})_3^{2+}$.

To overcome the problems of charged complexes the

racemisation of some hindered biphenyls was investigated; these biphenyls were uncharged and racemisation occurs by simple rotation of a carbon-carbon single bond.

Experimental

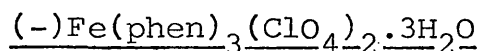
Kinetics

Rates of racemisation were determined by following the change of optical rotation for 10cm³ of sample solution contained in a 10cm³, 10cm path length polarimeter cell. The polarimeter cell was thermostated at 25°C. All rotations were measured at the sodium-D line on a Perkin-Elmer 140 polarimeter. The general procedure was to make up cold solutions from optically active substrates, filter the solutions, and rapidly transfer the filtrate to the polarimeter cell, allowing a short period of time for the solution to equilibriate at 25°C. Runs were followed for at least 2.5 half lives, the rate of racemisation being defined as:

$$k_{\text{rac}} = -1/t \ln \alpha_o / \alpha_t$$

Rates of acid aquation for the Fe(phen)₃²⁺ were determined as described in Chapter 2. For the iron Schiff base complex aqueous solutions of Na₂EDTA were employed instead of acid, because aquation is acid dependant.

Laevo tris phenanthroline iron(II) perchlorate trihydrate:



(-)Fe(phen)3(ClO4)2.3H2O was prepared according to the method of Dwyer and Gyarfás³. Thus, to a solution of

iron(II) tris phenanthroline sulphate was added an excess of concentrated potassium antimonyl tartate solution. A precipitate appeared almost immediately. This precipitate was dissolved in a 10% acetone solution and to it was added a strong aqueous solution of sodium perchlorate; the final solution was cooled in iced water, where upon fine needles of $(-)\text{Fe}(\text{phen})_3(\text{ClO}_4)_2 \cdot 3\text{H}_2\text{O}$ were obtained. The crystals were filtered off and washed with a little cold water, and finally dried over P_2O_5 . The solid was kept cold prior to use.

tris(4-methyl-N-[phenyl(2 pyridyl)methylene])iron(II) perchlorate trihydrate: $\text{Fe}(\text{mppm})_3(\text{ClO}_4)_2 \cdot 3\text{H}_2\text{O}$

1:1 stoichiometric amounts of 2-benzoyl pyridine and p-toluidine were dissolved in a small quantity of methanol. To this solution was added a one third molar equivalent of iron(II) chloride tetrahydrate dissolved in a small amount of methanol containing 1cm^3 of glacial acetic acid and a few mg of hydroxylamine hydrochloride. A deep blue colouration resulted. The solution was left for a short period of time (approx. $\frac{1}{2}$ hr.), and then filtered through celite. The filtrate was left to allow the solvent to evaporate off. An oily residue remained, and this was dried in vacuo, over P_2O_5 . The final residue was taken up into water, and filtered through celite again. To the filtrate was added a strong aqueous solution of sodium perchlorate. The solution was cooled. The blue precipitate was filtered off, and washed several times with ice cold water until the filtrate became tinted slightly blue. The product was left

to dry by evaporation.

Laevo tris(4-methyl-N-[phenyl(2-pyridyl)methylene])iron(II) antimonyl tartate dodecahydrate: $(-)\text{Fe}(\text{mppm})_3\text{SbT}\cdot 12\text{H}_2\text{O}$

This was prepared in a similar manner to $(-)\text{Fe}(\text{mppm})_3(\text{ClO}_4)_2\cdot 3\text{H}_2\text{O}$ except that a strong aqueous solution of potassium antimonyl tartate was used instead of sodium perchlorate.

Laevo tris(5NO₂phenanthroline)ruthenium(II) iodide hydrate: $(-)\text{Ru}(\text{II})(5\text{NO}_2\text{phen})_3\text{I}_2\cdot n\text{H}_2\text{O}$

The complex was prepared from $\text{K}_2[\text{RuCl}_5(\text{OH}_2)]$ and 5-nitro phenanthroline according to the method of Liu and Bailar⁴. The $\text{K}_2[\text{RuCl}_5(\text{OH}_2)]$ was prepared using Isied's method⁵.

Attempted preparation of optically active tris(bithiazine) iron(II) antimonyl tartate hydrate: $\text{Fe}(\text{btz})_3\text{SbT}\cdot n\text{H}_2\text{O}$

Btz and the racemic iron complex $\text{Fe}(\text{btz})_3^{2+}$ were prepared as described in Chapter 4. Resolution of this complex was attempted using the method described for $\text{Fe}(\text{phen})_3^{2+}$ cation, but was unsuccessful.

Laevo tris(5NO₂phenanthroline)iron(II)antimonyl tartate decahydrate:

$(-)\text{Fe}(5\text{NO}_2\text{phen})_3\text{SbT}\cdot 10\text{H}_2\text{O}$

$(-)\text{Fe}(5\text{NO}_2\text{phen})_3\text{SbT}\cdot 10\text{H}_2\text{O}$ could be prepared in a similar manner to $\text{Fe}(\text{phen})_3\text{SbT}$. An antimonyl tartate salt could be isolated, which though optically active, racemised very quickly, such that no optically active perchlorate salt could be isolated.

Attempted preparation of optically active tris(bithiazine)
ruthenium(II)iodide hydrate: $\text{Ru(II)(btz)}_3\text{I}_2 \cdot n\text{H}_2\text{O}$

This was attempted using the method of Liu and Bailar.
It did not appear to be successful.

d-2-nitro-6-carboxy-2'-methoxydiphenyl

This was prepared according to the method of Adams⁶
(scheme 1).

In each case the compounds were characterised by
microanalysis and/or uv/vis spectroscopy.

Results

For transition metal complexes the rate of racemisation
(occurring by an intramolecular pathway) is defined as:

$$k_{\text{rac}} = k_{\text{obs.rac}} - k_{\text{dissoc}}$$

where k_{rac} is the true rate of racemisation

$k_{\text{obs.rac}}$ is the observed rate of racemisation

k_{dissoc} is the rate of dissociation

All kinetics gave good first-order plots which were
reproducible to within a few percent.

The rates of racemisation of the Fe(phen)_3^{2+} cation in
aqueous methanol are taken from Van Meter and Neumann⁷, as
are the rates of dissociation and solubilities of
perchlorate salts. These results are summarised in tables
1 and 2.

The rates of racemisation of the Fe(phen)_3^{2+} cation in
aqueous DMSO, along with rates of dissociation, and
solubilities of picrate salts are summarised in tables 3
and 4. These results include work done by S. Cope as part
of an undergraduate project.

The rates of racemisation of $\text{Fe}(\text{mppm})_3^{2+}$ cation in aqueous methanol, and the rates of dissociation are shown in table 5.

$\text{Fe}(\text{5NO}_2\text{phen})_3^{2+}$ cation racemised very quickly and it was not possible to measure any rate constants.

$\text{Ru}(\text{5NO}_2\text{phen})_3^{2+}$ cation showed no tendency to racemise at 25°C.

For $\text{Ru}(\text{btz})_3^{2+}$ cation no positive result was obtained. Because the complex was highly coloured, very dilute solutions had to be used in the polarimeter. However, if there was only a small enantiomeric excess, the corresponding optical activity would be very small.

Repeated work indicated that there was only a slight enantiomeric excess, but this was "lost" due to the high dilution necessary for the polarimeter.

No optically active $\text{Fe}(\text{btz})_3^{2+}$ complex could be isolated.

Insufficient quantities of optically active biphenyl were prepared to perform kinetic experiments.

Discussion

The racemisation of tris chelate metal complexes can proceed by various mechanisms. Broadly speaking there are two sets of mechanisms: those involving bond breaking, and those which do not involve bond breaking. Principle interests are in those which do not involve bond breaking. In bond breaking one end of a ligand may be free to move around, and may also be charged; the interaction with the solvent becomes a complex pattern of free and bound ligand interaction. For octahedral complexes there are three

principle mechanisms for racemisation not involving ring opening: the Bailar twist (Fig.1), the Ray-Dutt twist (Fig.2), and the Springer-Siever twist (Fig.3). The Bailar and Ray-Dutt twists both produce a trigonal prismatic transition state, which approximates to D_{3h} and C_{2v} symmetry respectively; the Springer-Sievers twist also has a trigonal prismatic transition state which has an approximate D_{3h} symmetry. For any particular system deciding which of these mechanisms is operating, is very difficult. $Fe(phen)_3^{2+}$ is believed to be intramolecular⁸ since steric considerations rule out mechanisms involving ring opening. As phenanthroline is a planar, rigid ligand the Bailar twist mechanism is not an attractive proposition. On this basis the tentative conclusion is that either a Ray-Dutt or a Springer-Sievers twist is in operation.

The results of Van Meter and Neumann can be analysed in terms of initial state and transition state contributions. These results are summarised in table 1 and Fig.4. Van Meter and Neumann used the Born equation to calculate their single ion values for $Fe(phen)_3^{2+}$ and ClO_4^- . Other workers using the TPTB assumption have obtained very similar values⁹.

The initial state and transition state parallel each other, with the transition state dominating. Van Meter and Neumann's discussion concluded that the effect of solvent composition upon racemisation was principally due to preferential solvation of the hydrophobic ligands. The

effect of preferential solvation can be seen from the variation of $\delta_m \Delta G^\ddagger$. That the transition state dominates indicates that the transition state is more open, allowing greater access for solvent molecules. A consideration of molecular models indicates that the Ray-Dutt transition state is the more open structure leading to greater solvation.

It is interesting to contrast these results with those for aquation (Fig.5), since this is also a unimolecular process. Similar trends are found, again with the transition state dominating. Most noticeable is the relative difference in energies between the initial state and transition state: for racemisation this difference is greater than for dissociation. The mechanism for dissociation can be visualised as a gradual weakening of two iron-nitrogen bonds¹⁰ (Fig.6); for racemisation there is weakening of six iron-nitrogen bonds, followed by twisting (Fig.7). Thus, the transition state for racemisation would be expected to have a higher energy than that for dissociation. The volume of activation for racemisation is large and positive¹¹, which is compatible with the proposed mechanism.

Laevo tris(phen)iron(II) cation in aqueous DMSO

The behaviour is similar to that of aqueous methanol. With increasing percentage co-solvent the rate of racemisation increases, but then decreases. This can be seen in Fig.8. This may be due to an increase in viscosity of the solvent: thus solvent in interligand

pockets becomes more difficult to reorganise during intramolecular rearrangement. In very viscous solvents like glycerol racemisation of $(-)\text{Fe}(\text{phen})_3^{2+}$ is very slow⁷, however correlations between viscosity and the rates of racemisation are not very good (Fig.9).

Initial state-transition state analysis for racemisation and dissociation are shown in Figs.10 and 11. Single ion values were determined from the solubility of the picrate salts, and reported values for $\delta_m \mu^\ominus(\text{picrate}^-)$ ¹². Again trends are very similar to those of aqueous methanol, with the initial state closely following the behaviour of the transition state; again the transition state dominates. One interesting feature is that at low DMSO concentrations chemical potentials are positive.

This result appears anomalous since 5% DMSO ($x_2 = 0.01$) does not correspond to any thermodynamic property of aqueous DMSO mixtures eg. enthalpic minima. Solubilities of other inorganic complexes in binary aqueous organic mixtures sometimes show similar behaviour¹³.

The initial state-transition state analysis for racemisation may be compared with that for dissociation. As before, trends are similar, with energy differences for dissociation generally being smaller than for racemisation.

As well as loss of optical activity due to racemisation, by intramolecular processes, there is also loss due to dissociation of the complex. It is found that racemisation, (k_{rac}), is significantly faster than dissociation, which

is part of the evidence for the intramolecular mechanism.
Laevo tris(mppm)iron(II) cation in aqueous methanol.

The results in Fig.12 show that racemisation increases with increasing percentage of methanol in a continuous manner. In contrast with the $\text{Fe}(\text{phen})_3^{2+}$ cation there are no solvent maxima.

The rate of dissociation is of a similar order of magnitude to that of racemisation for each solvent composition. This indicates that racemisation by a dissociative pathway is now important. For this particular case it is difficult to decide which detailed mechanism is operating, and further work would be necessary to elucidate it. That there was no solvent maximum for this system has already been noted. This may be due to the preferential solvation of a ligand as it breaks away from the metal centre. At high methanol concentrations the solvation of displaced ligands probably becomes important.

Several tris oxalato complexes are believed to racemise by this dissociative mechanism¹⁴, and solvent effects on potassium tris oxalato chromate(III) have been analysed into initial state-transition state contributions¹⁵ (Fig.13). Interestingly, $\text{Ni}(\text{phen})_3^{2+}$ also racemises by an intermolecular process¹⁶.

$(-)\text{Fe}(\text{phen})_3^{2+}$ racemises in a microemulsion¹⁷ consisting of 6.89 mls of isopropanol, 0.54 mls of water and 10.46 mls of hexane with a $k_{\text{obs.rac}} = 7.0 \times 10^{-3} \text{ s}^{-1}$ ¹⁸. Unfortunately $k_{\text{dissoc.}}$ is not known for this microemulsion,

and so k_{rac} could not be calculated. Currently micro-emulsions are proving to be interesting solvent systems, and are being employed in a variety of reactions¹⁹ eg. Ni^{2+} + pada²⁰. Ni^{2+} + pada has also been investigated in ethylene carbonate solutions²¹, and this solvent is proving to be very interesting²².

Schiff base complexes have been used to probe solvent and kinetic effects²³. A few have been resolved²⁴, but no racemisation studies have been done. They may well prove to be useful models to probe detailed mechanisms for racemisation in transition metal complexes. From a practical point of view antimonyl tartates of several Schiff base complexes were crystalline solids, with low solubility in water. One problem with Schiff base complexes is the difficulty in obtaining good crystalline solids (very often oils result); antimonyl tartate could be a very useful anion in preparative chemistry and in measuring solubilities, and, hence, single ion data.

Laevo $Fe(5NO_2phen)_3^{2+}$ cation

An optically active antimonyl tartate was isolated. It was slightly soluble in water, and more so in acetone. Aqueous solutions of the complex racemised very fast such that detailed kinetics could not be undertaken. Even by cooling solutions it was not possible to follow the racemisation. Attempts to use glycerol to slow down the racemisation were also unsuccessful.

The rate of dissociation of racemic $Fe(5NO_2phen)_3^{2+}$ cation has been determined in a number of solvent mixtures.

Generally it is faster than for the corresponding phenanthroline complex²⁵. From the relationship between dissociation and racemisation for the $\text{Fe}(\text{phen})_3^{2+}$ cation, racemisation of $\text{Fe}(\text{5NO}_2\text{phen})_3^{2+}$ is expected to be very fast.

The nitro group in the five position decreases the strength of the iron-nitrogen bonds²⁶ (relative to unsubstituted phenanthroline), and this will clearly affect the rate of racemisation, where there is an initial lengthening of the iron-nitrogen bonds (ie. decrease in strength), followed by twisting.

With substitution of the phenanthroline ring there is the possibility of mer and fac isomers (Fig.14). These would be expected to have different physical properties such that resolution using antimonyl tartate would be expected to yield one isomer only.

Laevo $\text{Ru}(\text{5NO}_2\text{phen})_3^{2+}$ cation

Because the iron complex racemised so quickly the analogous ruthenium complex was prepared. This was done using the method of Liu and Bailar. The ruthenium complex was expected to be less labile than the corresponding iron complex²⁷. The laevo complex was isolated, and this showed no tendency to racemise in aqueous solution at 25°C. The corresponding phenanthroline complex is also reported to be inert²⁸.

$\text{Fe}(\text{btz})_3^{2+}$ cation

Attempts to resolve the $\text{Fe}(\text{btz})_3^{2+}$ cation were unsuccessful. The rate of dissociation of the complex in water is known

(see Chapter 3), and this suggests that racemisation would be expected to be very fast (faster than $(-)\text{Fe}(\text{5NO}_2\text{phen})_3^{2+}$), and that only a racemate would be isolated. Attempts to resolve $\text{Ru}(\text{btz})_3^{2+}$ were also unsuccessful. Possibly the method of Lui and Bailar is not suitable in this case; racemic $\text{Ru}(\text{btz})_3\text{I}_2$ was obtained.

d-2-nitro-6-carboxy-2'-methoxydiphenyl

Kinetic studies on optically active biphenyl derivatives is extensive²⁹. It was hoped to have used them to analyse solvent effects. Their main advantages are that they are uncharged, and that the mechanism for racemisation is unequivocal. Unfortunately, synthesis of d-2-nitro-6-carboxy-2'-methoxydiphenyl resulted only in a small amount of material, and as the optical rotation is small, considerable quantities would have been required for detailed studies.

One initial state-transition state analysis has been performed³⁰ (Fig.15), and recently some work has been done using charged symmetrical biphenyls³¹.

At present solubility studies are being undertaken on biphenyl analogues (Fig.16) and with published kinetic data it is hoped to perform a range of initial state-transition state analysis.

Table 1

IS/TS analysis for the racemisation of (-)Fe(phen)₃²⁺ in aqueous methanol mixtures.

x_2 (MeOH)	$10^4 \times k_{\text{rac}}$ /s ⁻¹	$\delta_m \Delta G^\ddagger$ /kJ mol ⁻¹	$\delta_m \mu^\ddagger$ (Fe(phen) ₃ ²⁺) /kJ mol ⁻¹	$\delta_m \mu^\ddagger$ (Fe(phen) ₃ ²⁺) /kJ mol ⁻¹
0	5.63	0	0	
0.1	11.5	-1.77		
0.2	20.8	-3.24	-10.29	-13.4
0.3	32.2	-4.32		
0.4	53.2	-5.57	-18.78	-24.4
0.5	71.7	-6.31		
0.6	102	-7.18	-22.3	-29.5
0.7	133	-7.84		
0.8	190	-8.72	-23.05	-31.8
0.9	212	-8.99		
1.0	187	-8.68	-22.18	-30.9

Table 2

IS/TS analysis for the dissociation of $\text{Fe}(\text{phen})_3^{2+}$ in aqueous methanol mixtures.

	x_2 (MeOH)			
	0.20	0.40	0.60	0.80
$\delta_m \Delta G^\ddagger / \text{kJ mol}^{-1}$	-0.5	-1.9	-2.8	-2.7
$\delta_m \mu^\ominus(\text{Fe}(\text{phen})_3^{2+}) / \text{kJ mol}^{-1}$	-10.3	-18.8	-22.2	-23.0
$\delta_m \mu^\ddagger(\text{Fe}(\text{phen})_3^{2+}) / \text{kJ mol}^{-1}$	-10.8	-20.7	-25.0	-25.7

This table is taken from M.J.Blandamer, J.Burgess, N.V.Reed, P.Wellings, J. Inorg. Nucl. Chem., 43, 3245 (1981)

Table 3

IS/TS analysis for racemisation of $(-)\text{Fe}(\text{phen})_3^{2+}$ in aqueous DMSO mixtures.

	% DMSO (v/v)						
	0	5	10	15	20	30	40
$10^4 \times k_{\text{rac}}^{\text{apparent}} / \text{s}^{-1}$	6.5	8.1	9.9	10.8	12.2	16.5	9.9
$10^4 \times k_{\text{dissoc}} / \text{s}^{-1}$	0.67	0.81 ^a	0.81	0.81 ^a	0.83	1.0	1.3
$10^4 \times k_{\text{rac}}^{\text{true}} / \text{s}^{-1}$	5.83	7.29	9.09	9.99	11.37	15.5	8.6
$\delta_m \Delta G^\ddagger / \text{kJ mol}^{-1}$	0	-0.55	-1.1	-1.33	-1.65	-2.42	-0.96
$\delta_m \Delta G^\ominus / \text{kJ mol}^{-1}$	0	+4.3	-5.49	-6.71	-8.2	-10.02	-12.72
$\delta_m \mu^\ominus(\text{picrate}^-) / \text{kJ mol}^{-1}$	0	-0.33 ^a	-0.49	-0.59 ^a	-0.62	-0.26	+0.36
$\delta_m \mu^\ominus(\text{Fe}(\text{phen})_3^{2+}) / \text{kJ mol}^{-1}$	0	+4.96	-4.51	-4.99	-6.96	-9.5	-13.44
$\delta_m \mu^\ddagger(\text{Fe}(\text{phen})_3^{2+}) / \text{kJ mol}^{-1}$	0	+4.41	-5.61	-6.32	-8.61	-11.92	-14.4

a) extrapolated from existing data.

Table 4

IS/TS analysis for the dissociation of $\text{Fe}(\text{phen})_3^{2+}$ in aqueous DMSO mixtures.

	% DMSO (v/v)						
	0	5	10	15	20	30	40
$10^4 \times k_{\text{dissoc}} / \text{s}^{-1}$	0.67	0.81 ^a	0.81	0.81 ^a	0.83	1.0	1.3
$\delta_m \Delta G^\ddagger / \text{kJ mol}^{-1}$	0	-0.47	-0.47	-0.47	-0.53	-0.99	-1.64
$\delta_m \Delta G^\ominus / \text{kJ mol}^{-1}$	0	+4.3	-5.49	-6.17	-8.2	-10.02	-12.72
$\delta_m \mu^\ominus(\text{picrate}^-) / \text{kJ mol}^{-1}$	0	-0.33 ^a	-0.49	-0.59 ^a	-0.62	-0.26	+0.36
$\delta_m \mu^\ominus(\text{Fe}(\text{phen})_3^{2+}) / \text{kJ mol}^{-1}$	0	+4.96	-4.51	-4.99	-6.96	-9.5	-13.44
$\delta_m \mu^\ddagger(\text{Fe}(\text{phen})_3^{2+}) / \text{kJ mol}^{-1}$	0	+4.49	-4.98	-5.46	-7.49	-10.49	-15.03

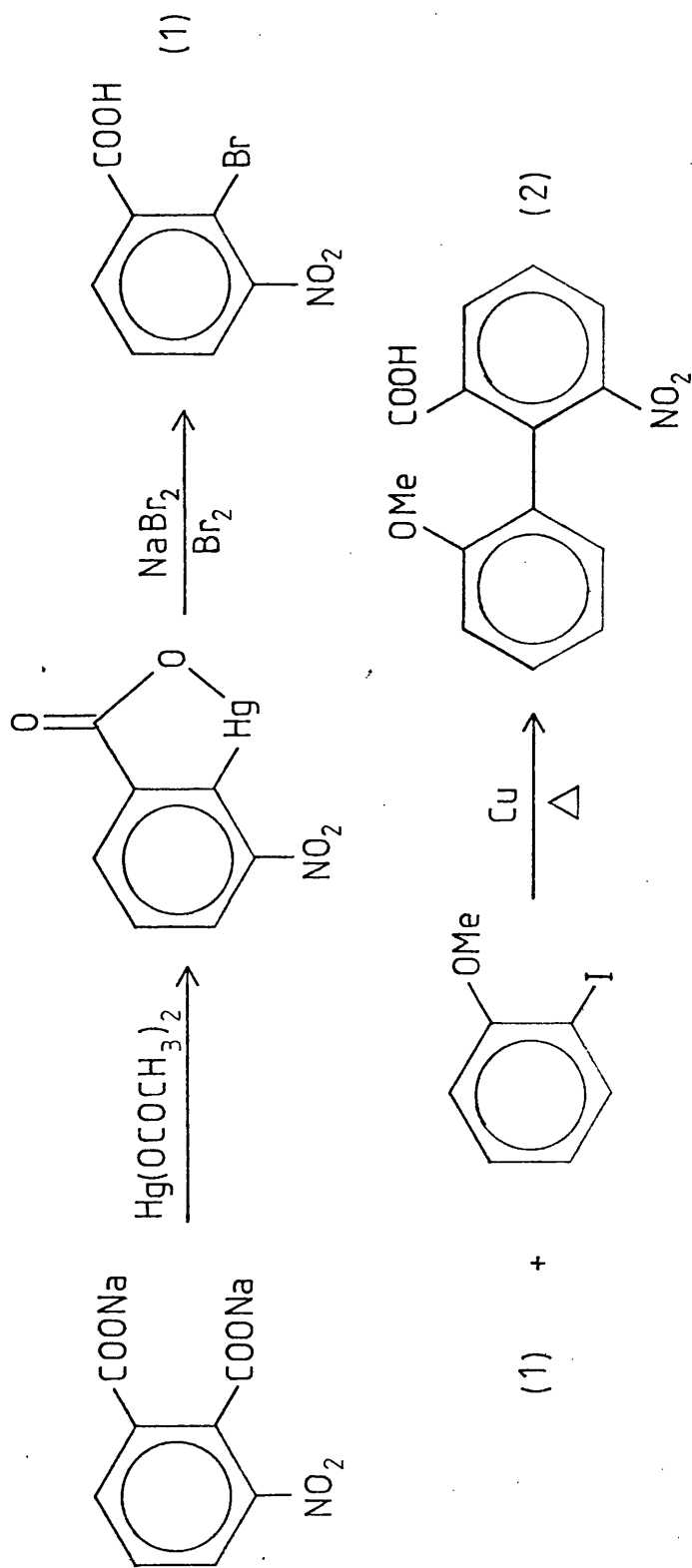
a) extrapolated from existing data

Table 5

Racemisation of $(-)\text{Fe}(\text{mppm})_3^{2+}$ at 25°C in aqueous methanol mixtures.

% MeOH (v/v)	$10^5 \times k_{\text{rac}} / \text{s}^{-1}$	$10^5 \times k_{\text{dissoc}} / \text{s}^{-1}$
0	4.14	1.774
20	3.87	2.249
40	6.81	3.400
60	11.20	8.311
80	19.59	15.197
100	46.00	26.676

Scheme 1 The preparation of d-2-Nitro-6-carboxy-2'-methoxydiphenyl.



(2) is resolved using brucine

Figure 1 Bailar Twist mechanism for racemisation.

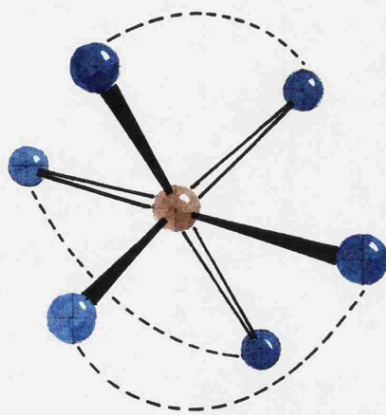
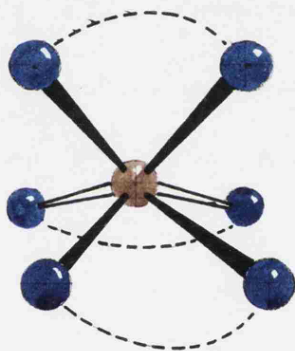
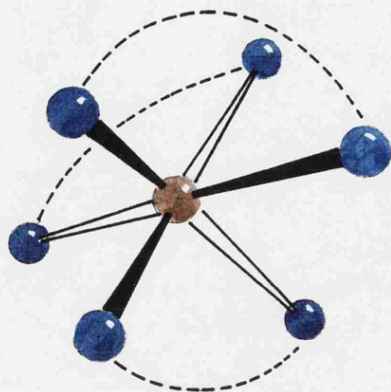


Figure 2 Ray-Dutt Twist mechanism for racemisation.

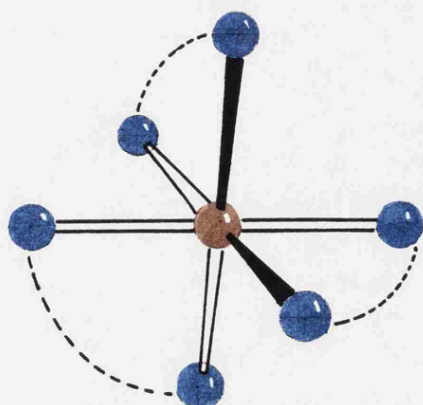
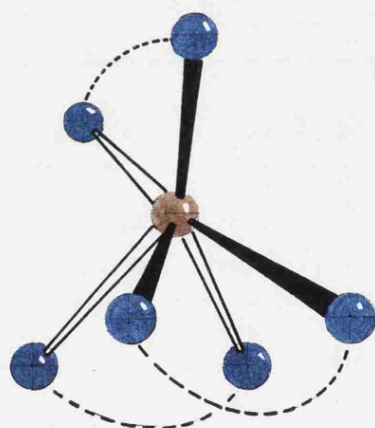
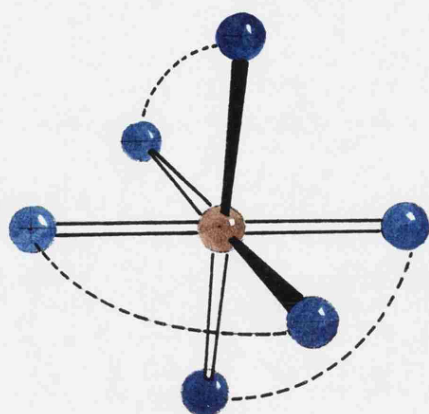


Figure 3 Springer-Sievers Twist mechanism for racemisation.

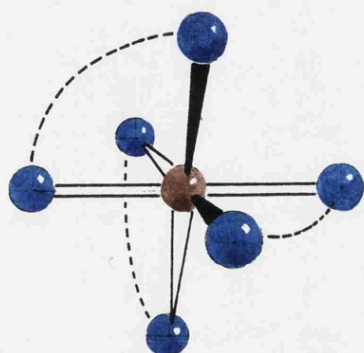
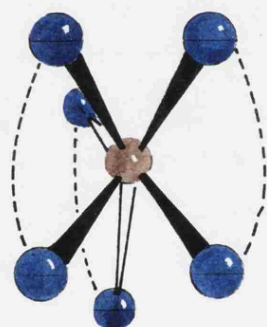
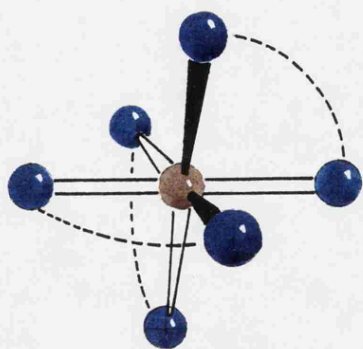


Figure 4 Initial state-transition state analysis for the racemisation of the $(-)\text{Fe}(\text{phen})_3^{2+}$ cation in aqueous methanol.

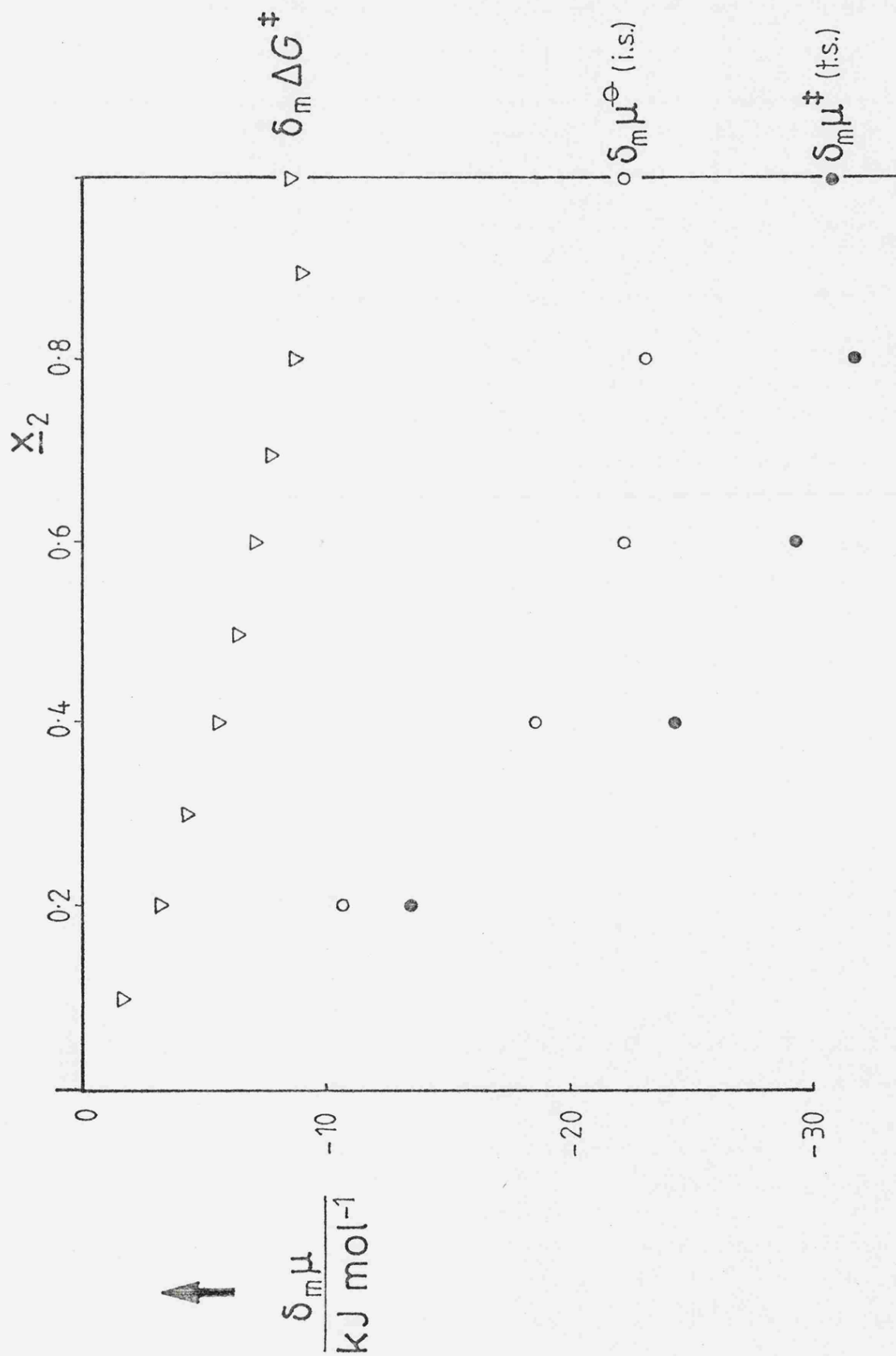


Figure 5 Initial state-transition state analysis for the dissociation of the $\text{Fe}(\text{phen})_3^{2+}$ cation in aqueous methanol.

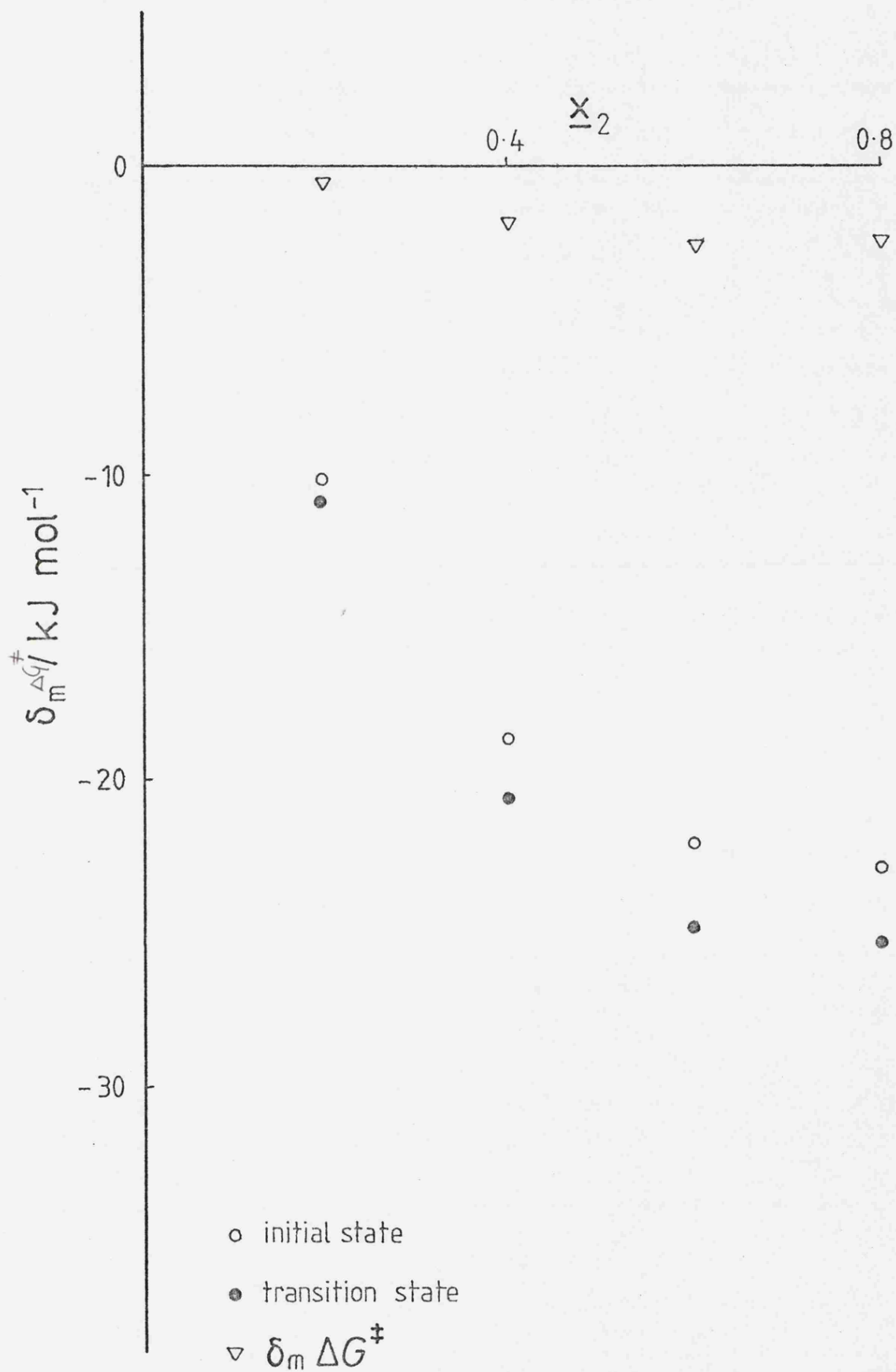


Figure 6 Schematic representation of the dissociation of the $\text{Fe}(\text{phen})_3^{2+}$ cation.

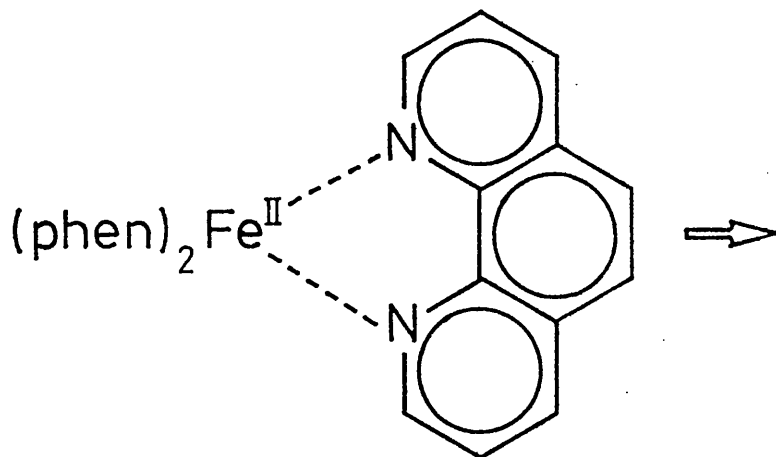


Figure 7 Schematic representation of the racemisation of the $(-)\text{Fe}(\text{phen})_3^{2+}$ cation.

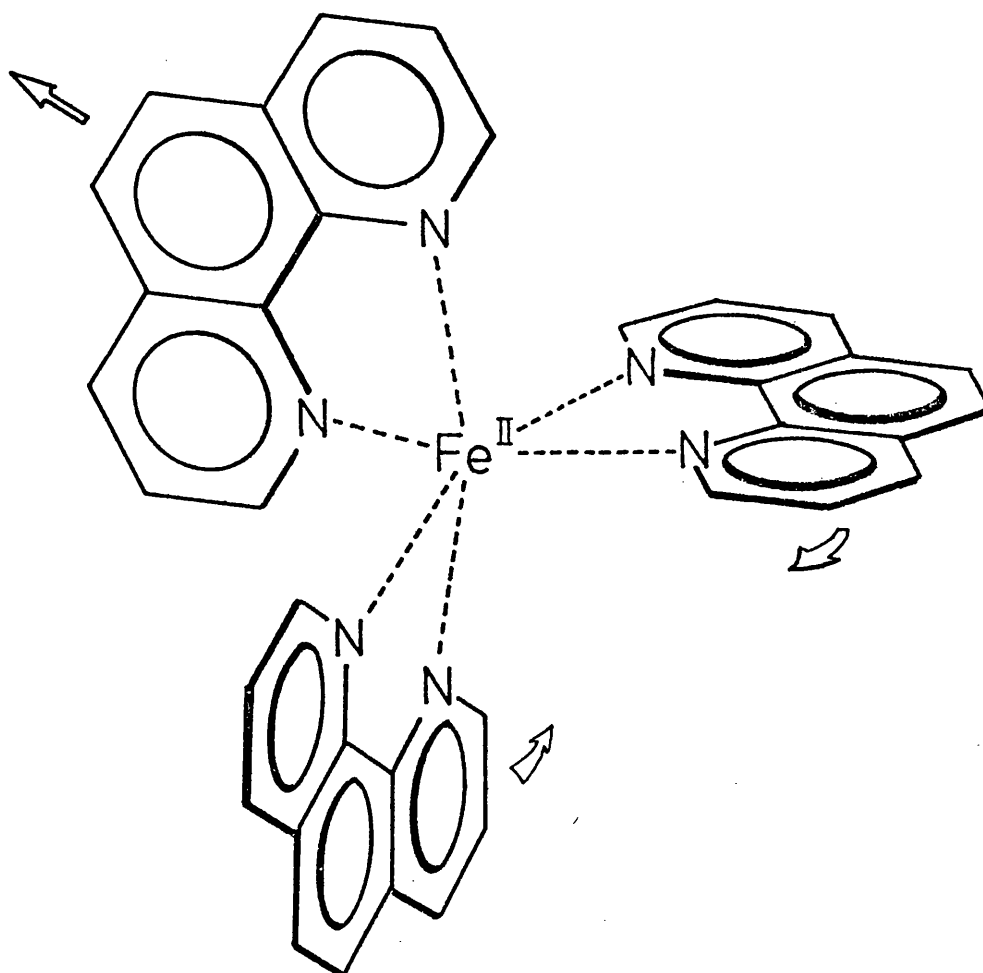


Figure 8 The rate of racemisation of the $(-)\text{Fe}(\text{phen})_3^{2+}$ cation in aqueous DMSO.

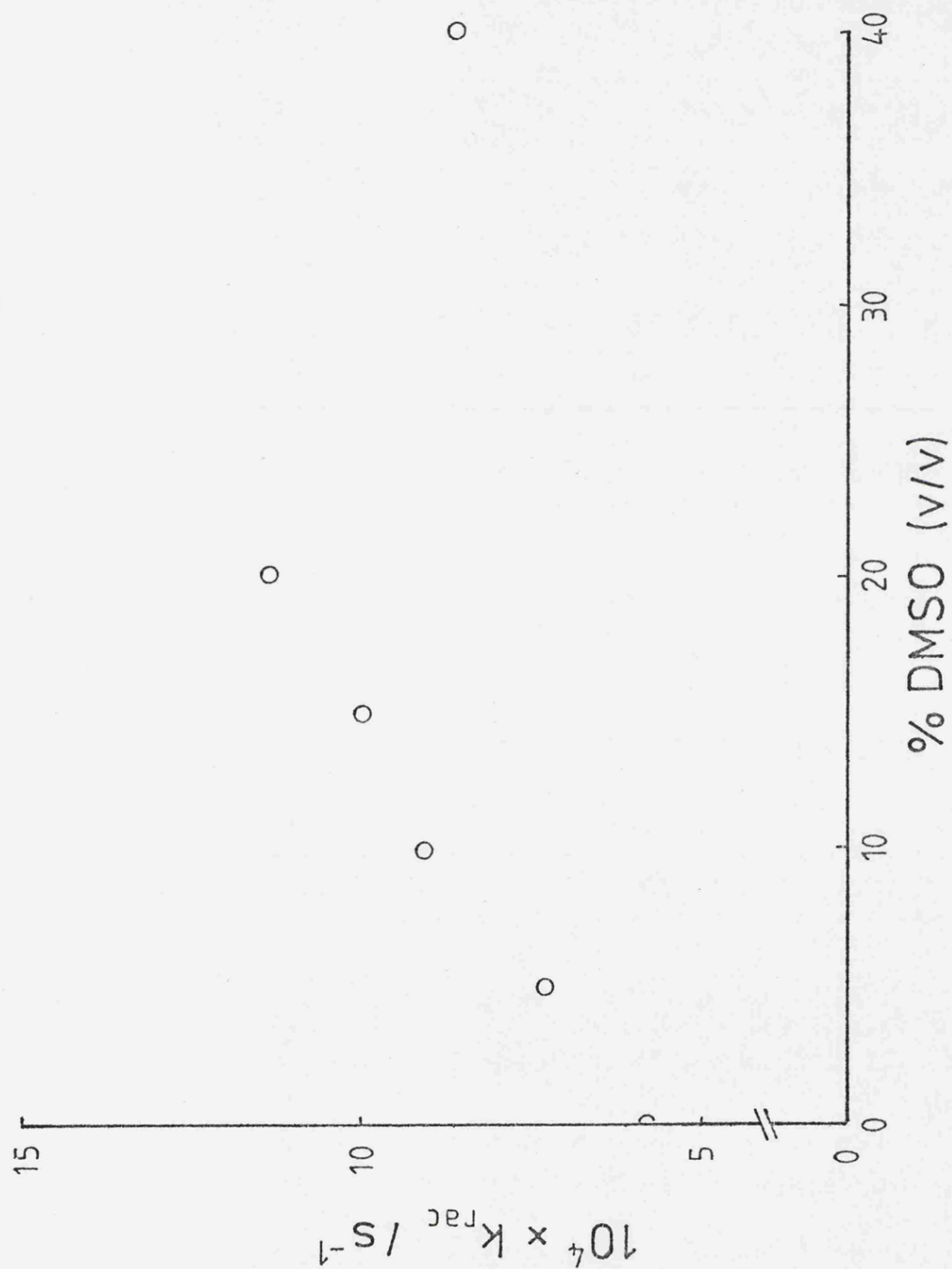


Figure 9 A plot of the rate of racemisation of $(-)\text{Fe}(\text{phen})_3^{2+}$ in aqueous DMSO mixtures (at 298.2 K) versus the viscosity of the solvent mixture.

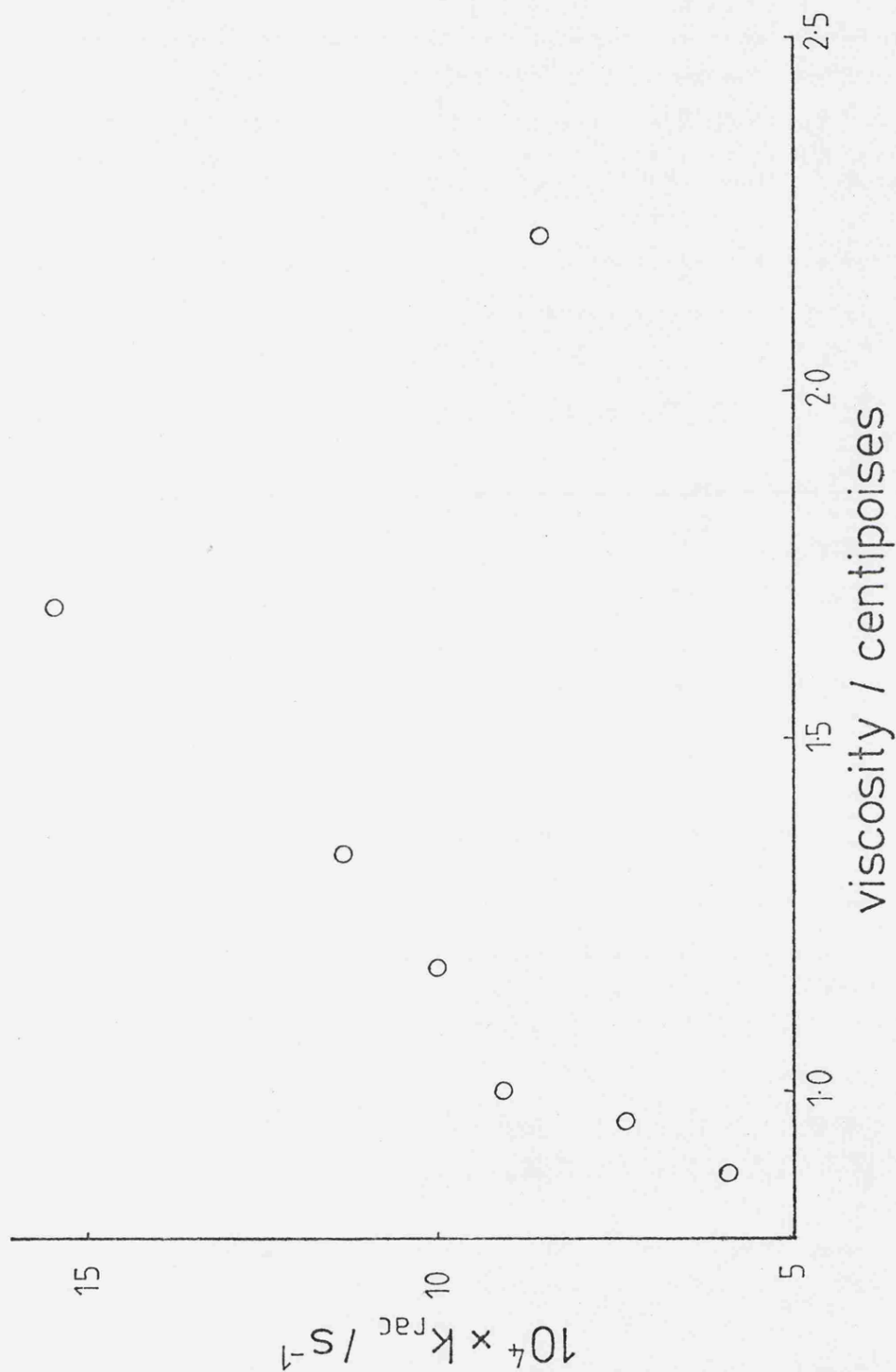


Figure 10 Initial state-transition state analysis for the racemisation of the $(-)\text{Fe}(\text{phen})_3^{2+}$ cation in aqueous DMSO mixtures.

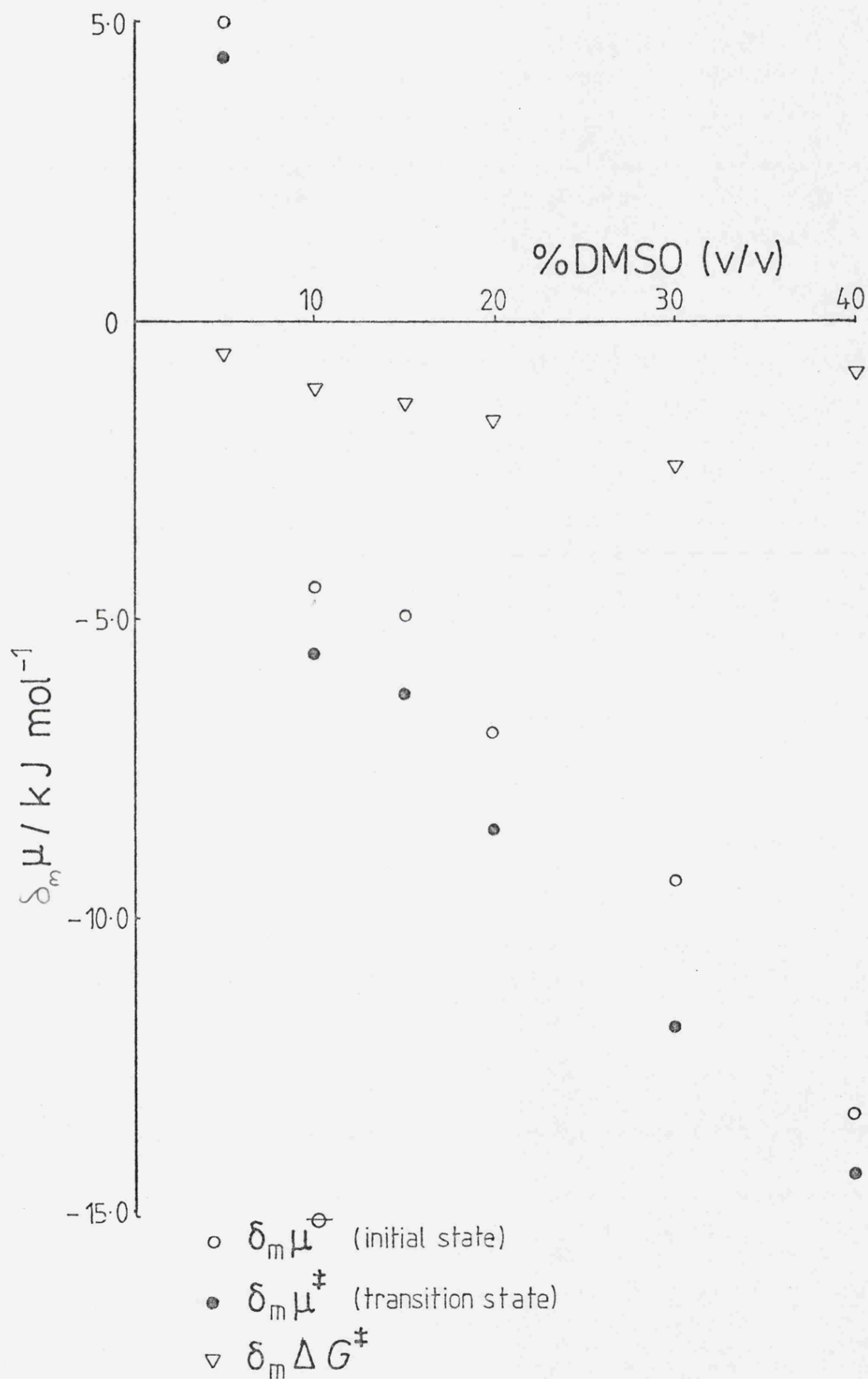


Figure 11 Initial state-transition state analysis for the dissociation of the $\text{Fe}(\text{phen})_3^{2+}$ cation in aqueous DMSO mixtures.

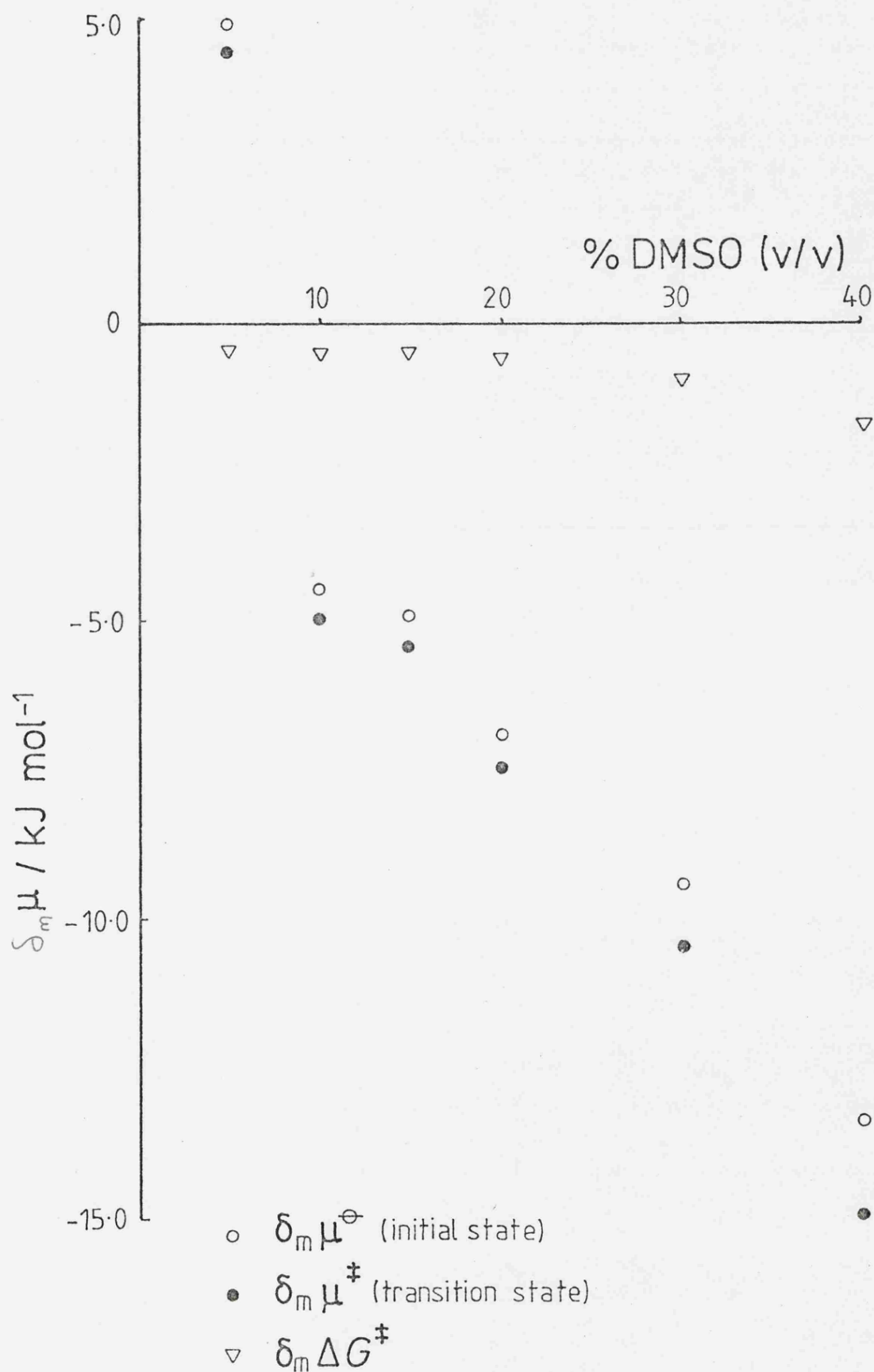


Figure 12 The rate of racemisation of the $(-)\text{Fe}(\text{mppm})_3^{2+}$ cation in aqueous methanol mixtures.

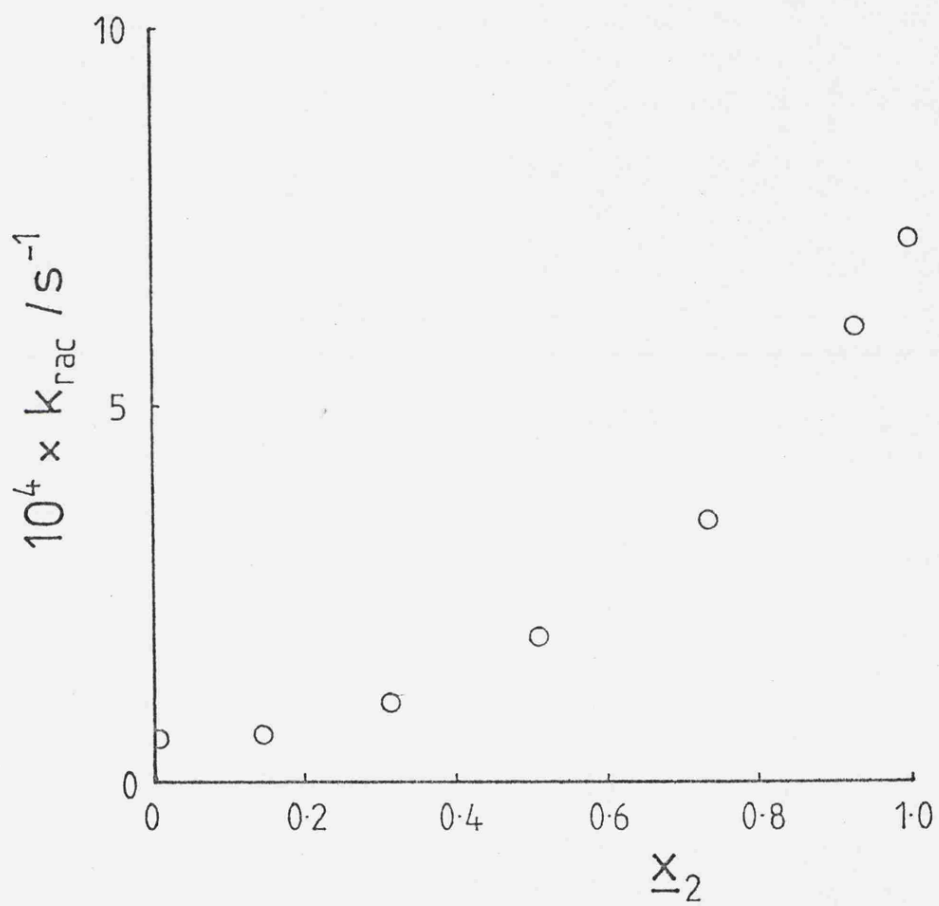


Figure 13 Initial state-transition state analysis for $\text{Cr}(\text{ox})_3^{3-}$ racemisation.

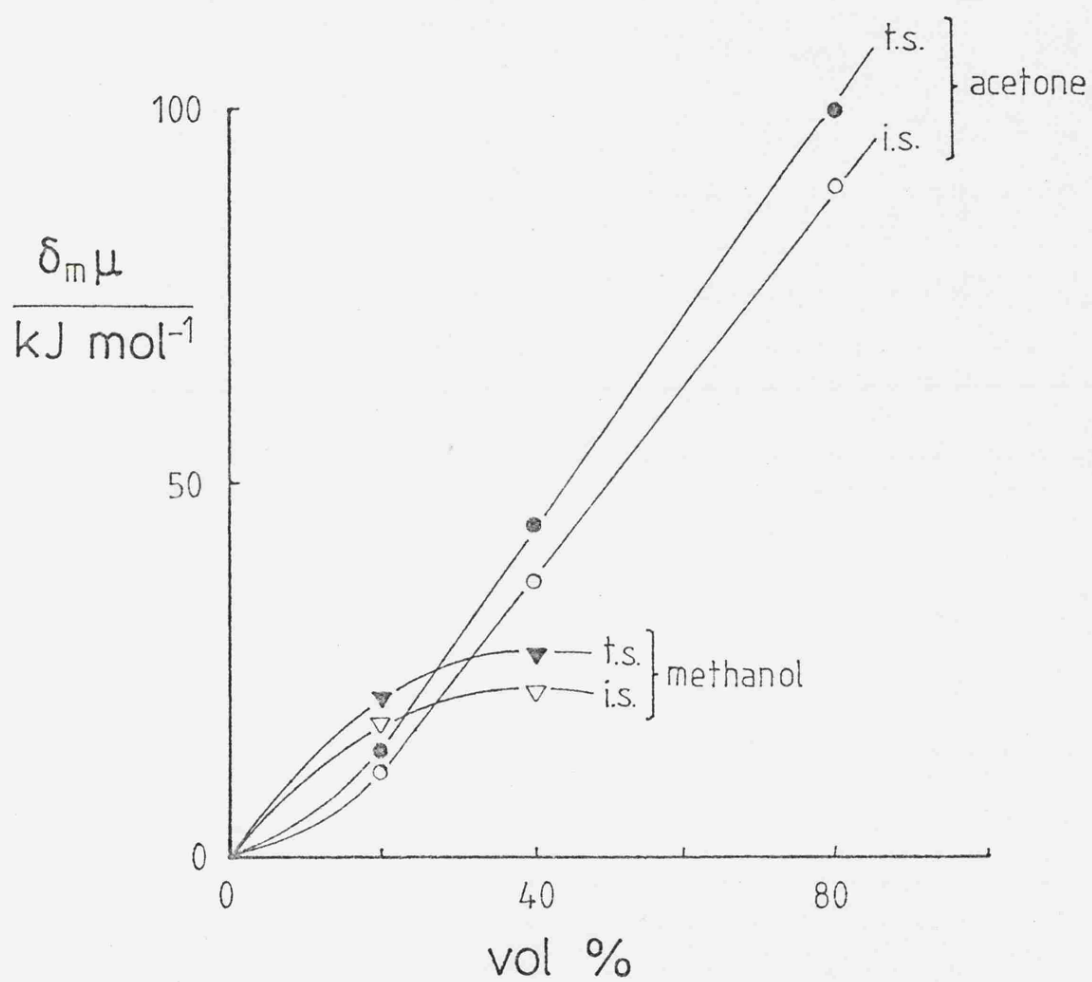


Figure 14(1) mer isomer of $\text{Fe}(\text{5NO}_2\text{phen})_3^{2+}$.

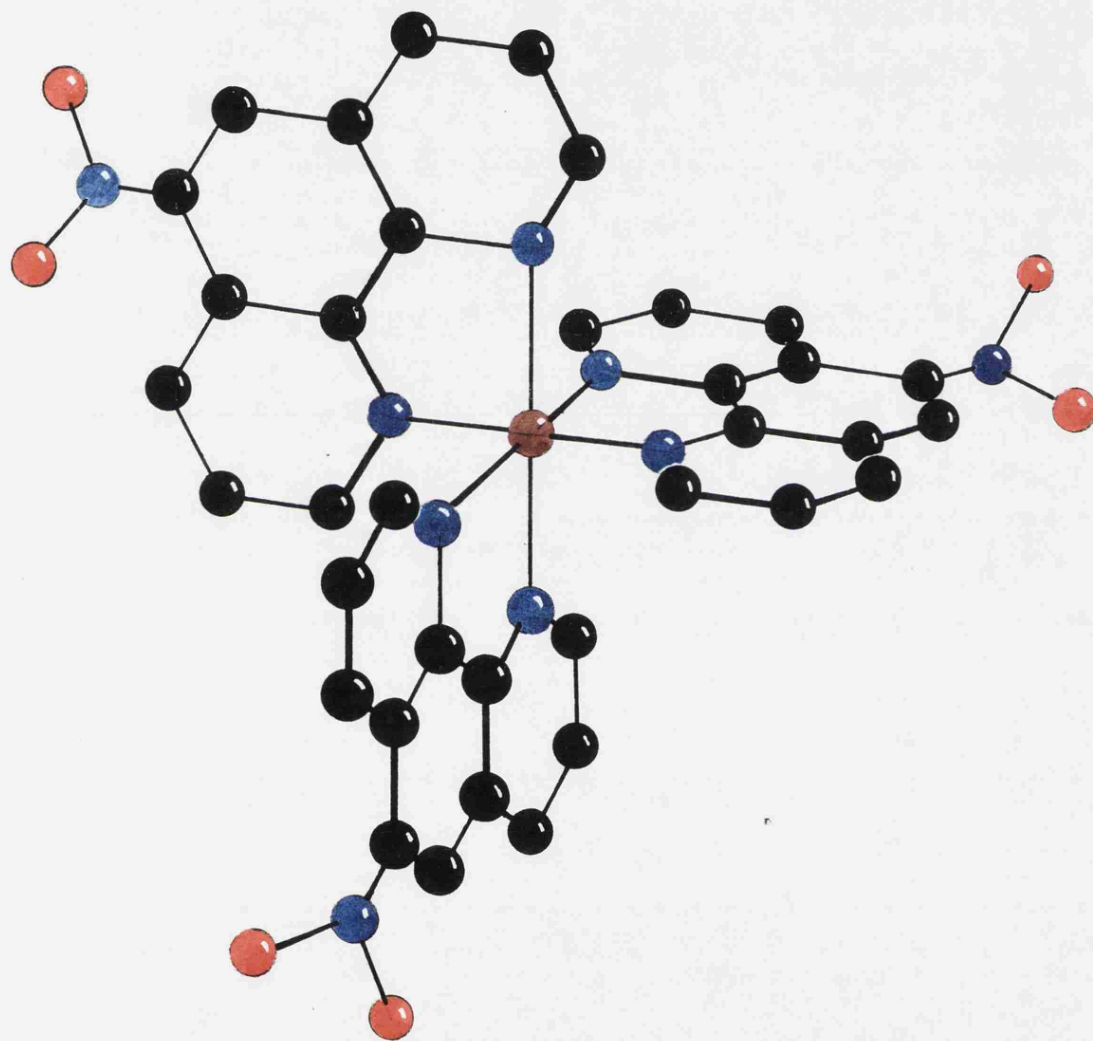


Figure 14(2) fac isomer of $\text{Fe}(\text{5NO}_2\text{phen})_3^{2+}$.

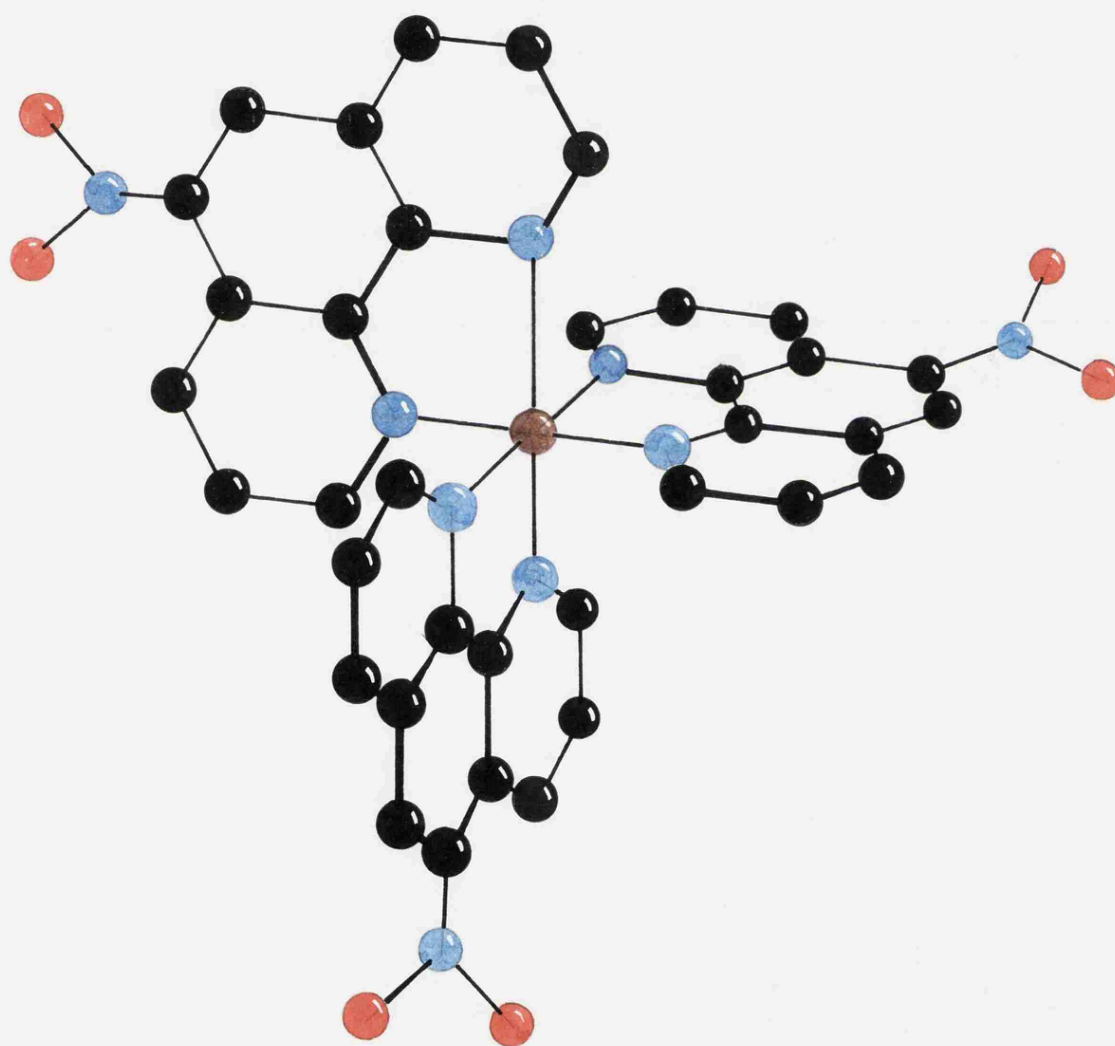


Figure 15 Initial state-transition state analysis for the hindered rotation of 2,2'-dimethoxy-6,6'-diphenamide.

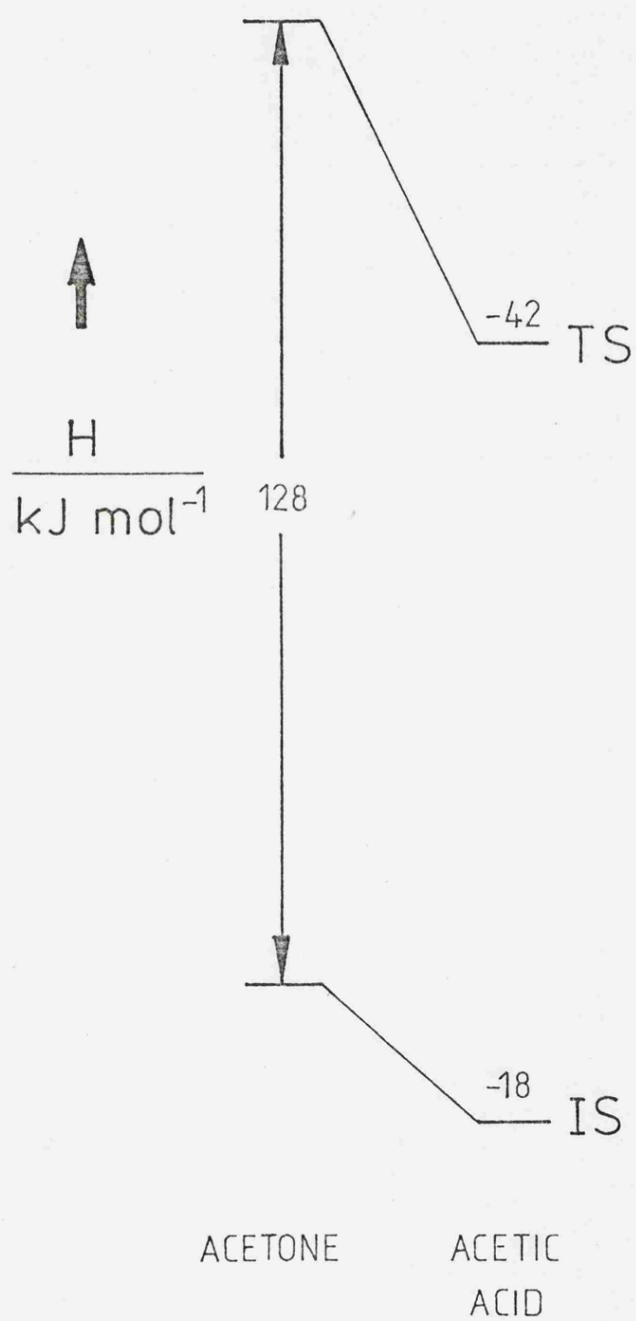
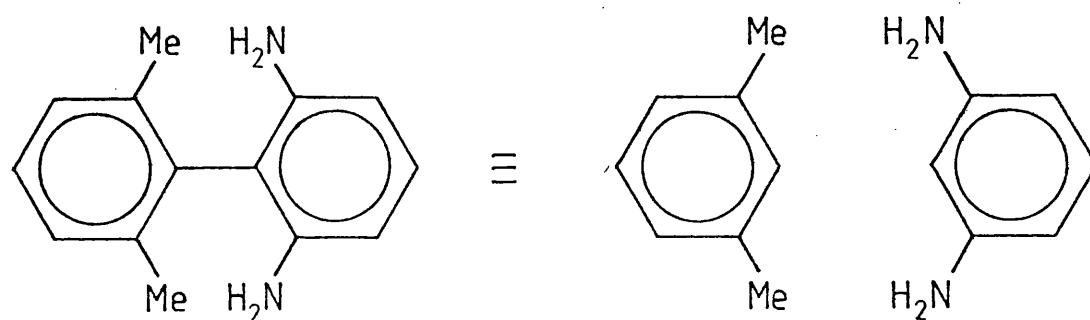
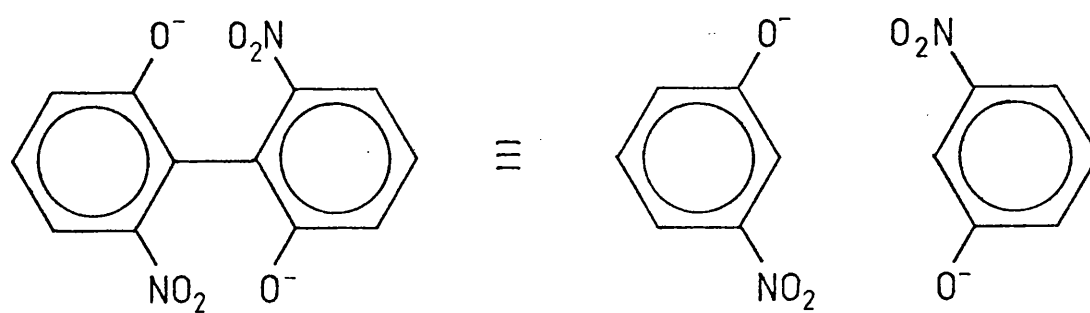
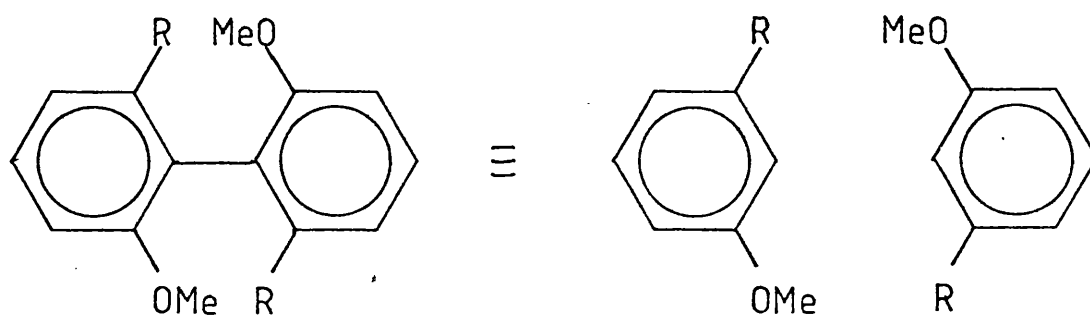
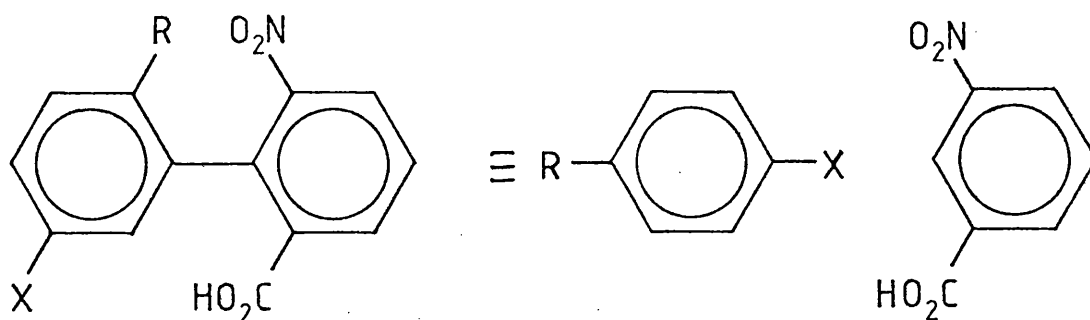


Figure 16 Hindered biphenyl analogues which could be used for initial state-transition state analyses.



References Chapter 3

1. T.Moeller and E.Gulyas, *J.Inorg.Nucl.Chem.*, 5, 245 (1958)
2. A.Yamagishi, *Inorg.Chem.*, 21, 3393 (1982)
3. F.P.Dwyer and E.C.Gyarfas, *J.Proc. N.S.W.*, 83, 263 (1949)
4. C.F.Liu, N.C.Liu and J.C.Bailar, *Inorg.Chem.*, 3, 1085 (1964)
5. S.S.Isied, *Inorg.Chem.*, 19, 911 (1980)
6. R.W.Stoughton and R.Adams, *J.Am.Chem.Soc.*, 54, 4426 (1932)
7. F.M.Van Meter and H.M.Neumann, *J.Am.Chem.Soc.*, 98, 1382 (1976); *ibid* 1388
8. F.Basolo, J.C.Hayes and H.M.Neumann, *J.Am.Chem.Soc.*, 76, 3807 (1954)
9. J.Burgess, N.Morton and J.C.McGowan, *J.C.S.Dalton*, 1977, 1775; C.Tissier, *Comptes Rendus*, 286C, 35 (1978); M.H.Abraham et al submitted to *J.C.S.Faraday 1*; C.D.Hubbard, personal communication
10. J.-M.Lucie, D.R.Stranks and J.Burgess, *J.C.S.Dalton*, 1975, 245

11. G.A.Lawrance and D.R.Stranks, *Inorg.Chem.*, 17, 1804 (1978)
12. K.K.Kundu and A.K.Das, *J.Soln.Chem.*, 8, 259 (1979)
13. N.Gosal, personal communication
14. F.A.Long, *J.Am.Chem.Soc.*, 61, 570 (1939); *ibid* 63, 1353 (1941)
15. M.J.Blandamer and J.Burgess, *Pure.Appld. Chem.*, 55, 55 (1983)
16. R.G.Wilkins and M.J.G.Williams, *J.Chem.Soc.*, 1957, 1763; see also ref. 27
17. B.A.Keiser, D.Varie, R.E.Barden and S.L.Holt, *J.Phys.Chem.*, 83, 1276 (1979)
18. J.Burgess, S.D.Cope and T.Digman, unpublished observations
19. 'Microemulsions', ed. I.D.Robb, Plenum Press, London, 1982
20. J.R.Hicks and V.C.Reinsborough, *Aus.J.Chem.*, 35, 15 (1982)

22. C.S.Hong, R.Wakslak, H.Finston and V.Fried, J.Chem.Eng.Data, 27, 146 (1982); P.T.Thompson, B.Fisher and R.H.Wood, J.Soln.Chem., 11, 1 (1982)
23. M.J.Blandamer, J.Burgess, R.I.Haines, F.M.Mekhail and P.Askalani, J.C.S.Dalton, 1978, 1001
24. F.P.Dwyer, N.S.Gill, E.C.Gyarfas and F.Lions, J.Am.Chem.Soc., 75, 3834 (1953)
25. M.J.Blandamer, J.Burgess and R.I.Haines, J.C.S.Dalton, 1976, 385
26. J.Burgess, J.Chem.Soc.A., 1967, 431
27. 'Mechanisms of Inorganic Reactions', Basolo and Pearson, 2nd ed., Wiley, New York, 1967
28. F.P.Dwyer and E.C.Gyarfas, J.Proc. N.S.W., 83, 170 (1949)
29. R.Adams and H.C.Yuan, Chem.Revs., 12, 261 (1933), J.E.Leffler and W.H.Graham, J.Phys.Chem., 63, 687 (1959); M.M.Harris and K.R.Mitchell, Proc.Chem.Soc., 367 (1959); M.M.Harris and K.R.Mitchell, J.Chem.Soc., 1960, 1905; C.C.K.Ling and M.M.Harris, Chem.Ind., 1378 (1962); A.S.Cooke and M.M.Harris, J.Chem.Soc., 1963, 2365
30. D.R.McKelvey, J.W.Frederiksen, K.R.Barrick, and G.A.Teas J.Am.Chem.Soc., 90 6568 (1968)

31. L.Balteer and N.Bergman, Acta.Chem.Scand., 36A,
31 (1982)

CHAPTER FOUR:

The reactions between $\text{Fe}(\text{btz})_3^{2+}$ and R (R = OH^- , H^+ , Hg^{2+} , Cd^{2+} , Ag^+ , $\text{S}_2\text{O}_8^{2-}$, phen, bipy). The stability constants of $\text{Fe}(\text{btz})_3^{2+}$, Agbtz^+ , Cdbtz^{2+} , Hgbtz^{2+} . The molar extinction coefficients of $\text{Fe}(\text{btz})_3^{2+}$ and $\text{Fe}(\text{btz})_2(\text{CN})_2$. Attempted preparation of $\text{Fe}(\text{bipym})_2(\text{CN})_2$. The reaction between $\text{Fe}(\text{btz})_2(\text{CN})_2$ and Hg^{2+} . The solvatochromism of $\text{Fe}(\text{btz})_2(\text{CN})_2$. The reactions between $\text{Mo}(\text{CO})_4(\text{pip})_2$ and FeL_3^{2+} (L = btz, bipym). Attempted preparation of polymerised "Fe(bipym)₂". The reactions of $\text{Fe}(\text{mba})_3^{2+}$.

Introduction

Some aspects of iron(II) tris diimine chemistry have been discussed in the previous chapter, and a continuation of this chemistry is considered here.

The ligand bithiazine (btz), (Fig.1), is known to form a variety of complexes, bonding via the nitrogens¹. Iron(II) complexes of btz and closely related ligands are known², (Fig.2). Most of the chemistry is concerned with the magnetic properties and Mössbauer spectra of these complexes.

It is of interest to extend this chemistry and in particular the chemistry of $\text{Fe}(\text{btz})_3^{2+}$, and to compare it with that of $\text{Fe}(\text{phen})_3^{2+}$.

One novel feature of btz is that it has a pair of sulphur atoms which may be used in bonding, and so it might be possible to form multinuclear species of the type shown in Fig.3. These sulphur atoms may also be used for metal catalysed aquation (Fig.4).

The ligand 2,2'-bipyrimidine (bipym) offers similar possibilities to form polynuclear complexes (Fig.5) and in metal catalysed aquation reactions.

However the principal concern is with btz complexes, although some aspects of bipym complexes are considered.

Experimental

Bipyrimidine was purchased from Lancaster Synthesis; btz was prepared according to the method of Tomalia and Paige³. The tris iron(II) complexes, were prepared by mixing stoichiometric quantities of Mohr's salt and the ligand

in water, and the mixture stirred continuously for approximately 30 minutes. The solution could then be suitably diluted for kinetic runs. Solid complexes were obtained by allowing concentrated solutions to evaporate to dryness. Perchlorates were obtained by adding a strong aqueous sodium perchlorate solution to the solutions above; the mixture was left in a refrigerator over night; the precipitate was filtered off and washed with ice cold water; finally, the precipitates were dried in vacuo over P_2O_5 .

$Fe(btz)_2(CN)_2$ and $Fe(bipym)_2(CN)_2$ were prepared by Schilt's method⁴.

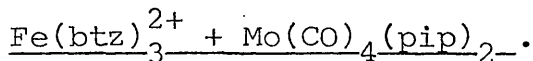
Reactions between $Fe(btz)_3^{2+}$ and R (R = OH^- , H^+ , Hg^{2+} , Cd^{2+} , $S_2O_8^{2-}$, Ag^+) were monitored at 610nm, with R in excess. All reactions were carried out in water at 25°C. Reactants and ionic strengths are shown in table 1.

Reactions between $Fe(btz)_3^{2+}$ and L (L = bipy, phen) were monitored at 610nm and 522nm (bipy) or 610nm and 510nm (phen) on a Pye-Unicam SP 8-100 spectrophotometer; reactions were carried out in aqueous methanol for solubility reasons.

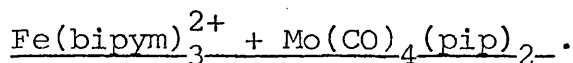
The reaction between $Fe(btz)_3^{2+}$ and Na_2EDTA was monitored at 610nm, with Na_2EDTA being in excess.

The reaction between btz and OH^- was monitored in the range 370-323nm in 50% water-acetone with sodium hydroxide in excess ($\approx 0.11M$); the reaction was repeated using 50% water-DMSO mixture. In all cases the temperature was maintained at 25°C.

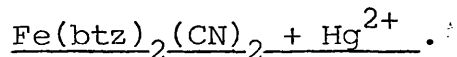
Reactions



To an aqueous solution of $\text{Fe}(\text{btz})_3^{2+}$ (prepared as described above) was added a threefold stoichiometric quantity of $\text{Mo}(\text{CO})_4(\text{pip})_2^-$ which had been dissolved in acetone. The mixture was kept in a closed vessel, shielded from light. At frequent intervals small aliquots were removed, and their uv/vis spectrum recorded.

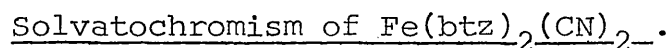


Solid $\text{Fe}(\text{bipym})_3\text{SO}_4$ was dissolved in nitromethane; to this was added a threefold stoichiometric quantity of solid $\text{Mo}(\text{CO})_4(\text{pip})_2^-$. The mixture was kept in a closed vessel, shielded from light. At frequent intervals small aliquots were removed, and their uv/vis spectrum recorded.



To an aqueous solution of $\text{Fe}(\text{btz})_2(\text{CN})_2$ was added a slight excess of mercury(II) perchlorate. A change in colour of the solution is easily detected, and a change in the uv/vis spectrum is clearly detected. This reaction may be carried out quantitatively by titrating a known solution of $\text{Fe}(\text{btz})_2(\text{CN})_2$ with a known aqueous solution of $\text{Hg}(\text{ClO}_4)_2$ (which has been stabilised by the addition of a few drops of perchloric acid).

Using concentrated solutions it is possible to obtain a red precipitate which could be isolated.



A small quantity of solid $\text{Fe}(\text{btz})_2(\text{CN})_2^-$ was dissolved in appropriate solvents, and their uv/vis spectra were recorded.

Molar Extinction Coefficient.

To an aqueous solution of a known quantity of Fe^{2+} (in the form of Mohr's salt) was added an excess of btz. The uv/vis spectrum of this solution was recorded using a Pye-Unicam SP 8-100, and hence ϵ could be calculated. For $\text{Fe}(\text{btz})_2(\text{CN})_2$, an accurately known solution was prepared by direct weighing. The uv/vis spectrum of this solution was recorded using a Pye-Unicam SP 8-100, and hence ϵ could be calculated.

Stability Constant of $\text{Fe}(\text{btz})_3^{2+}$ in water.

A stock solution of a known quantity of $\text{Fe}(\text{btz})_3(\text{ClO}_4)_2$ was made up. This stock solution was diluted by a known amount and its optical density was recorded. From theoretical and observed optical densities the stability constant, β_3 , could be calculated.

'Polymerised' $[\text{Fe}(\text{bipym})_2]_n$.

An aqueous solution of $\text{FeSO}_4 \cdot 7\text{H}_2\text{O}$ and bipym in a 1:2 stoichiometric quantity was made up, kept in a closed vessel, and shielded from light. Aliquots were taken at regular intervals and their uv/vis spectrum recorded.

Reactions of $\text{Fe}(\text{mba})_3^{2+}$.

$\text{Fe}(\text{mba})_3^{2+}$ was prepared according to the method of Krumholz⁶. To an aqueous solution was added a large excess of sodium hydroxide. To another aqueous solution was added a large excess of Na_2EDTA . The solutions were checked by eye over a period of time.

Results

All kinetics gave good first-order plots for at least 2.5 half lives. All rates are averages of two or more runs. Initial rates for the reaction with silver were determined graphically. Reaction rates are shown in table 2. Not all reactions went to completion, and those that did are indicated. For the reactions that did not go to completion, by noting initial and final optical densities it was possible to calculate stability constants for various btz complexes. The method of calculation will be discussed later.

Molar extinction coefficients in water were:

$\text{Fe}(\text{btz})_2(\text{CN})_2$: $6145 \text{ dm}^3 \text{ mol}^{-1} \text{ cm}^{-1}$ at 585nm

$\text{Fe}(\text{btz})_3(\text{ClO}_4)_2$: $10365 \text{ dm}^3 \text{ mol}^{-1} \text{ cm}^{-1}$ at 610nm

The solvatochromism of $\text{Fe}(\text{btz})_2(\text{CN})_2$ is shown in table 3. Detailed discussion of the solvatochromic behaviour will be found in chapter 5.

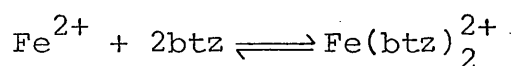
Stability constants for $\text{Fe}(\text{btz})_3^{2+}$, $\text{Cd}(\text{btz})^{2+}$, $\text{Ag}(\text{btz})^+$, $\text{Hg}(\text{btz})^{2+}$ are shown in table 4. These were calculated as follows.

$\text{Fe}(\text{btz})_3^{2+}$.

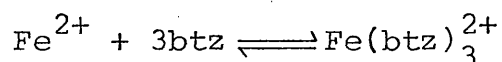
A stock solution of a known quantity of $\text{Fe}(\text{btz})_3(\text{ClO}_4)_2$ (as a solid) was prepared. Hence, from the known molarity of the stock solution, and from the extinction coefficient a theoretical optical density could be calculated. Measured optical densities were less than the theoretical values because of the equilibrium between co-ordinated and unco-ordinated iron. The equilibria involved are:



$$\beta_1 = \frac{[\text{Fe}(\text{btz})_2^{2+}]}{[\text{Fe}^{2+}][\text{btz}]}$$

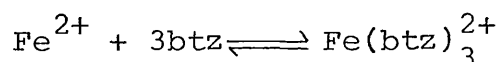


$$\beta_2 = \frac{[\text{Fe}(\text{btz})_2^{2+}]}{[\text{Fe}^{2+}][\text{btz}]^2}$$



$$\beta_3 = \frac{[\text{Fe}(\text{btz})_3^{2+}]}{[\text{Fe}^{2+}][\text{btz}]^3}$$

It is assumed that the dominant species is $\text{Fe}(\text{btz})_3^{2+}$, especially at high ligand concentration. By analogy with the phen system it is also assumed that $\beta_3 \gg \beta_2, \beta_1$ ⁷. Thus, under the experimental conditions employed the equilibrium may be considered as:

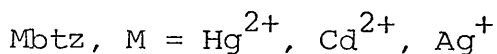


From the measured optical density, the concentration of complexed iron can be calculated. The difference between theoretical and measured concentrations of iron complex gives the concentration of free (uncomplexed) iron; three times the value of free iron concentration gives the free btz concentration. Thus, the stability constant can be calculated from:

$$\beta_3 = \frac{[\text{Fe}(\text{btz})_3^{2+}]}{[\text{Fe}^{2+}][\text{btz}]^3}$$

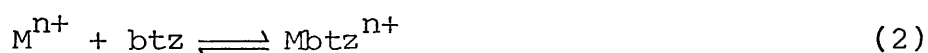
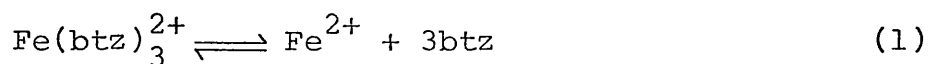
By diluting the original stock solution by a known amount, a new solution with a known concentration is created, and hence the above procedure is repeated. The average value of $\log_{10}\beta_3$ was 12.04. (β_3 must be divided

by an appropriate factor to produce a dimensionless quantity).

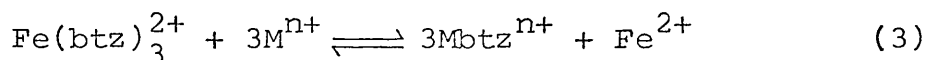


In general the reactions between Fe(btz)₃²⁺ and M (M = Hg²⁺, Cd²⁺, Ag⁺) do not go to completion. From the initial and final optical densities for these reactions it is possible to calculate stability constants for Mbtz complexes.

With M in excess with respect to free btz, it is assumed that only the mono btz complex is formed. The equilibria involved are:



(1) + 3x(2):



$$K_{\text{eq}} = \frac{[\text{Mbtz}^{n+}]^3 [\text{Fe}^{2+}]}{[\text{Fe}(\text{btz})_3^{2+}] [\text{M}^{n+}]^3}$$

From the difference in initial and final optical densities the concentration of uncomplexed iron can be calculated, and hence the concentration of free btz.

Assume all free btz is complexed with Mⁿ⁺. Thus the concentration of Mbtzⁿ⁺ can be calculated, as can the amount of free Mⁿ⁺. The equilibrium constant can then be calculated:

ΔG^\ominus for (1) is $RT \ln \beta_3$, $\beta_3 =$ stability constant

ΔG^\ominus for (2) is $-RT \ln \beta'_1$

ΔG^\ominus for (3) is $RT \ln \beta_3 - 3RT \ln \beta'_1$

now ΔG^\ominus is $-RT \ln K_{eq}$, therefore:

$$-RT \ln K_{eq} = RT \ln \beta_3 - 3RT \ln \beta'_1 \quad (4)$$

(4) \div RT:

$$-\ln K_{eq} = \ln \beta_3 - 3 \ln \beta'_1 \quad (5)$$

0.4343 x (5):

$$-\log_{10} K_{eq} = \log_{10} \beta_3 - 3 \log_{10} \beta'_1$$

$$3 \log_{10} \beta'_1 = \log_{10} \beta_3 + \log_{10} K_{eq}$$

$$\log_{10} \beta'_1 = \frac{12.04 + \log_{10} K_{eq}}{3}$$

Example calculation: $\text{Fe}(\text{btz})_3^{2+}$ reacts with Ag^+

Initial O.D. (610nm): 1.73

Final O.D. (610nm) : 0.353

Molarity of AgNO_3 in cell: 0.0099

$$\begin{aligned} \text{Initial conc. of } \text{Fe}(\text{btz})_3^{2+} &= \frac{1.73}{10365} \\ &= 1.67 \times 10^{-4} \text{ mol dm}^{-3} \end{aligned}$$

$$\begin{aligned} \text{Final conc. of } \text{Fe}(\text{btz})_3^{2+} &= \frac{0.353}{10365} \\ &= 3.4 \times 10^{-5} \text{ mol dm}^{-3} \end{aligned}$$

$$\begin{aligned} \text{therefore conc. of free iron} &= 1.67 \times 10^{-4} - 3.4 \times 10^{-5} \\ &= 1.33 \times 10^{-4} \text{ mol dm}^{-3} \end{aligned}$$

$$\begin{aligned} \text{therefore conc. of free btz} &= 3 \times 1.33 \times 10^{-4} \\ &= 3.99 \times 10^{-4} \text{ mol dm}^{-3} \end{aligned}$$

$$\text{therefore conc. of Agbtz}^+ = 3.99 \times 10^{-4} \text{ mol dm}^{-3}$$

$$\begin{aligned} \text{therefore conc. of free Ag}^+ &= 9.9 \times 10^{-3} - 3.99 \times 10^{-4} \\ &= 9.5 \times 10^{-3} \text{ mol dm}^{-3} \end{aligned}$$

therefore:

$$\begin{aligned} K_{\text{eq}} &= \frac{(3.99 \times 10^{-4})^3 (1.33 \times 10^{-4})}{(3.4 \times 10^{-5}) (9.5 \times 10^{-3})^3} \\ &= 2.89 \times 10^{-4} \end{aligned}$$

$$\log_{10} 2.89 \times 10^{-4} = -3.5378$$

therefore:

$$\begin{aligned} \log_{10} \beta'_1 &= \frac{12.04 - 3.5378}{3} \\ &= 2.86 \end{aligned}$$

$\text{Fe}(\text{btz})_3(\text{ClO}_4)_2$ and $\text{Fe}(\text{btz})_2(\text{CN})_2$ could be prepared very easily employing methods used to prepare the analogous phen complexes. Attempts to prepare $\text{Fe}(\text{bipym})_2(\text{CN})_2$ were unsuccessful. A dark red solution was obtained. It was not possible to extract any neutral complex with chloroform. By adding ZnSO_4 to the original aqueous solution a red

gelatinous precipitate was obtained.

The major product from the reaction between $\text{Mo}(\text{CO})_4(\text{pip})_2$ and $\text{Fe}(\text{btz})_3^{2+}$ was $\text{Mo}(\text{CO})_4\text{btz}$. This compound could be detected from its uv/vis spectrum. The complex could be extracted with chloroform, and the solvatochromic behaviour of the extract was identical with that of authentic $\text{Mo}(\text{CO})_4\text{btz}$ samples.

The reaction between $\text{Fe}(\text{bipym})_3^{2+}$ and $\text{Mo}(\text{CO})_4(\text{pip})_2$ gives $\text{Mo}(\text{CO})_4\text{bipym}$ as the main product, as judged from the uv/vis spectrum. The spectrum did not indicate the presence of the iron(II) tris diimine moiety; the spectrum was very similar to that of authentic $\text{Mo}(\text{CO})_4\text{bipym}$ samples.

The reaction between $\text{Fe}(\text{btz})_2(\text{CN})_2$ and Hg^{2+} results in a red coloured solution and was found to proceed in a 1:1 stoichiometric ratio. The uv/vis spectrum of the mercury adduct could be obtained, and this was different from that of $\text{Fe}(\text{btz})_2(\text{CN})_2$ (Fig.6). During large scale preparations of the adduct, precipitates could often be obtained. These could be filtered off, and dried in vacuo over P_2O_5 . However, uv/vis spectra of these precipitates were identical with that of $\text{Fe}(\text{btz})_2(\text{CN})_2$. The red solution slowly fades. Addition of sodium hydroxide or ammonia solution to this red solution returns the original blue colour of $\text{Fe}(\text{btz})_2(\text{CN})_2$, as seen by its uv/vis spectrum.

Attempts to prepare 'polymerised' $\text{Fe}(\text{bipym})_2^{2+}$ were unsuccessful. The uv/vis spectra of the original solutions indicated only $\text{Fe}(\text{bipym})_3^{2+}$ present. No precipitates were formed.

$\text{Fe}(\text{mba})_3^{2+}$ at room temperature was very resistant to hydroxide attack. Sealed tubes containing $\text{Fe}(\text{mba})_3^{2+}$ and a large excess of sodium hydroxide showed only a small deterioration of colour over several months. The same was also true for the reaction between $\text{Fe}(\text{mba})_3^{2+}$ and Na_2EDTA .

Discussion

Hydroxide reacts with $\text{Fe}(\text{btz})_3^{2+}$ to give good first-order kinetics. Fig.7 shows the dependence of observed first-order rate constants on hydroxide concentration. The points of high hydroxide concentration are at the limit of the apparatus, so confidence in these results is reduced. Ignoring these points the hydroxide dependence appears to be linear.

Acid aquation gives good first-order plots; there appears to be a slight acid dependence (Fig.8). From the acid aquation $k_{\text{dissociation}}$ can be estimated by extrapolation and is $3.00 \times 10^{-3} \text{ s}^{-1}$. $\text{Fe}(\text{bipy})_3^{2+}$ shows a curved acid dependent hydrolysis (Fig.9), and this is due to rotation and protonation of the ligand⁸. $\text{Fe}(\text{phen})_3^{2+}$ hydrolysis is acid independent, presumably because there can be no rotation of the phen ligand.

Gillard⁹ has studied hydroxide attack on the iron complex $\text{Fe}(\text{box})_3^{2+}$, where box is the oxygen analogue of btz (Fig.10). Generally reactions are two orders of magnitude faster, giving a linear dependence in hydroxide concentration (Fig.11). Gillard states the mechanism to be nucleophilic attack at the co-ordinated ligand, followed by intramolecular transfer of hydroxide to iron.

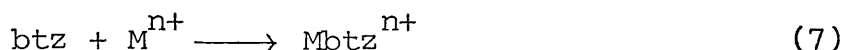
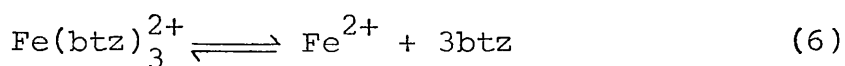
For $\text{Fe}(\text{btz})_3^{2+}$ and $\text{Fe}(\text{box})_3^{2+}$ this mechanism is difficult to visualise for two reasons: firstly, there is no possibility of charge delocalisation (with aromatic diimines like phen and bipy, charge can be delocalised, c.f. nucleophilic aromatic substitution¹⁰); secondly, it is not possible to form a Meisenheimer complex at saturated carbon. Btz is resistant to hydroxide attack: even with a very large excess of hydroxide in 50% acetone or DMSO, so as to increase the chemical potential of hydroxide, btz showed no sign of decomposition. These results strongly suggest that hydroxide is attacking directly at the metal centre, contrary to the Gillard mechanism. A recent review¹¹ has discussed the validity of the Gillard mechanism.

For $\text{Fe}(\text{mba})_3^{2+}$, the ligand is a very simple diimine, with no possibility of the Gillard mechanism operating. Consequently $\text{Fe}(\text{mba})_3^{2+}$ is very resistant to hydroxide attack, and very forceful conditions are needed to hydrolyse such complexes.

$\text{Fe}(\text{btz})_3^{2+}$ reacts with Hg^{2+} , Ag^+ and Cd^{2+} , but in general these reactions do not go to completion.

The reaction between $\text{Fe}(\text{btz})_3^{2+}$ and Ag^+ or Cd^{2+} shows an inverse dependence upon metal ion concentration (Fig. 14 and Fig. 13); the reaction between $\text{Fe}(\text{btz})_3^{2+}$ and Hg^{2+} appears to be independent of mercury ion concentration (Fig. 12).

The inverse relationships (Ag^+ , Cd^{2+}) are explained on the basis of $\text{Fe}(\text{btz})_3^{2+}$ dissociating, with the metal ion co-ordinating to the free btz:



For opposing first-order reaction (6) the overall rate is the sum of the rates for the forward and back reaction.

Thus:

$$k_{\text{obs}} = k_1 + k_{-1} \quad (8)$$

Simple dilution of $\text{Fe}(\text{btz})_3^{2+}$ solution causes the complex to dissociate a little, and it is possible to measure a rate constant for this process: this corresponds to k_1 in (6), and is approximately $2.4 \times 10^{-2} \text{ s}^{-1}$. The addition of M^{n+} alters the position of the equilibrium. When M^{n+} is in low concentration the rates observed tend towards the value of k_1 . The kinetic evidence does not support the idea of metal catalysed dissociation of $\text{Fe}(\text{btz})_3^{2+}$ (Fig.4).

For the reaction between $\text{Fe}(\text{btz})_3^{2+}$ and Hg^{2+} the situation is complicated by the fact that in neutral solutions Hg^{2+} tends to polymerize: $\text{Hg}^{2+}(\text{aq})$ has a p^*K_1 of approx. 3, where p^*K_1 is defined as:

$$p^*K_1 = -\log_{10} {}^*K_1$$

$${}^*K_1 = \frac{[\text{M}(\text{OH})^{(n-1)+}][\text{H}_3\text{O}^+]}{[\text{M}^{n+}][\text{H}_2\text{O}]}$$

Therefore in neutral solution the main species present would be HgOH^+ , which slowly polymerizes¹². Ag^+ and Cd^{2+}

both have $p^*K_1 > 7$. Unfortunately the kinetics have to be performed in neutral solution because of the acid hydrolysis of $\text{Fe}(\text{btz})_3^{2+}$. Although freshly prepared mercury(II) perchlorate solutions (unbuffered) were used, there was some delay before solutions were used.

The mechanism for the reaction is the same as before, although M^{n+} in equation (7) cannot be considered as a simple $\text{Hg}^{2+}(\text{aq})$ cation, but rather a complex polymeric species.

Because of the equilibrium involved it is possible to calculate stability constants for metal complexes using initial and final optical densities in kinetic experiments. The stabilities of the complexes are $\text{Ag}^+ \approx \text{Hg}^{2+} > \text{Cd}^{2+}$. For bipy complexes the order is $\text{Hg}^{2+}(K_1 = 9.64) > \text{Cd}^{2+}(K_1 = 3.99) > \text{Ag}^+(K_1 = 3.84)^{13}$. Generally for nitrogen complexes the stabilities of complexes are $\text{Hg}^{2+} > \text{Ag}^+ > \text{Cd}^{2+}$. Thus the general trend holds for btz complexes, although it might be expected that the mercury complex would have a larger stability constant. One reason for this might be the problems associated with neutral Hg^{2+} solutions, as indicated earlier.

$\text{Fe}(\text{btz})_3^{2+}$ reacts with phen or bipy to produce the corresponding iron complex. Again, $\text{Fe}(\text{btz})_3^{2+}$ dissociates, the free iron being complexed by the aromatic diimine ligand. Generally, all these reaction go to completion; the rate of disappearance of the btz complex,

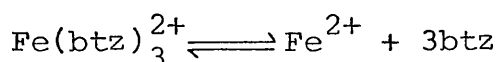
$$\frac{-d[\text{Fe}(\text{btz})_3^{2+}]}{dt},$$

gives good first-order kinetics. However, the rate of appearance of the other iron complex,

$$\frac{d \text{Fe(phen)}_3^{2+}}{dt} \quad \text{or} \quad \frac{d \text{Fe(bipy)}_3^{2+}}{dt}$$

gives first-order kinetics, although % error, and standard deviation tends to be larger. One problem is that $\text{Fe}(\text{btz})_3^{2+}$ strongly absorbs at 522 and 510nm, the λ_{max} for the bipy and phen complexes respectively.

From the mechanism:



it would be possible to calculate the stability constant for $\text{Fe}(\text{btz})_3^{2+}$. However, values obtained in this way were meaningless. The main problem was measuring very small concentrations of $\text{Fe}(\text{btz})_3^{2+}$ and $\text{Fe}(\text{phen})_3^{2+}$. With very small concentrations of phen (Fe:phen is 1:2.4), virtually all the phen is complexed. These experiments indicate that $\text{Fe}(\text{btz})_3^{2+}$ has $\log_{10} \beta_3 < \log_{10} \beta_3(\text{phen})$.

There is a slight dependence upon phen concentration (Fig.15). A more detailed analysis would require the acid dependent aquation of $\text{Fe}(\text{btz})_3^{2+}$ in 40% MeOH. The rate of dissociation of $\text{Fe}(\text{btz})_3^{2+}$ at one bipy concentration was measured. The value was very similar to those obtained for phen.

The reaction between $\text{Fe}(\text{btz})_3^{2+}$ and Na_2EDTA gave very good first-order kinetics. Here, $\text{Fe}(\text{btz})_3^{2+}$ dissociates,

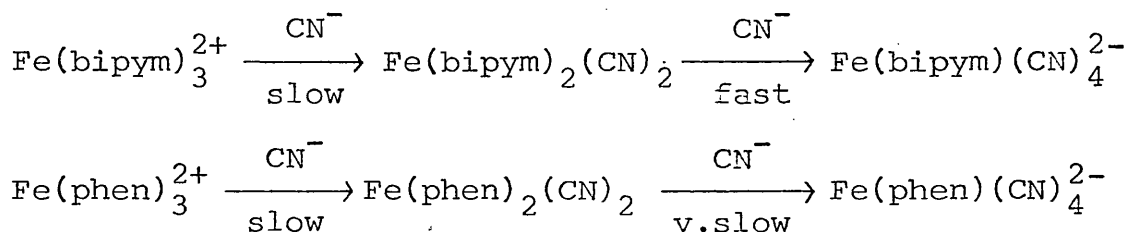
and the free iron is complexed by EDTA^{2-} . The rate of aquation at $2.4 \times 10^{-3} \text{ s}^{-1}$ agrees well with the value obtained from acid dependence.

Although it was not possible to measure the stability constant of $\text{Fe}(\text{btz})_3^{2+}$ from kinetic data, it was possible to measure it from dilution studies. An average value for β_3 was 1.1×10^{12} . Stability constants for other iron complexes are shown in table 6¹³. These values agree qualitatively with the experimental results.

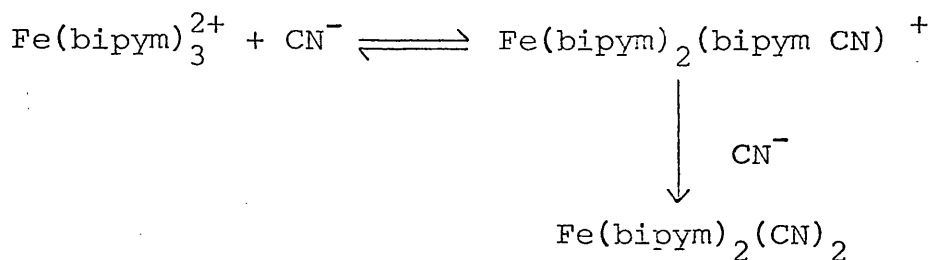
The reaction between $\text{Fe}(\text{btz})_3^{2+}$ and $\text{S}_2\text{O}_8^{2-}$ goes to completion with good first-order kinetics. The rate constants measured varied in a random fashion, and it was difficult to obtain consistent results. The values quoted in tables are averages. There is an apparent inverse dependence upon peroxodisulphate concentration (Fig.16). This is in direct contrast with peroxodisulphate oxidation of $\text{Fe}(\text{phen})_3^{2+}$ which shows a linear peroxodisulphate dependence¹⁴. Nelson has measured the redox potential for $\text{Fe}(\text{btz})_3^{3+}/\text{Fe}(\text{btz})_3^{2+}$, and this clearly indicates that peroxodisulphate can oxidise the metal centre. The aliphatic sulphur in the ligand may be oxidised¹⁵, and Levitt¹⁵ has proposed a mechanism for peroxodisulphate oxidation of thioethers to sulphoxides. The difficulty is that reactions are slower than the rate of dissociation, therefore the peroxodisulphate cannot be oxidising the metal or ligand. If the complex was dissociating first, followed by oxidation of free iron and ligand, all rate constants would approximate to the rate of dissociation. Because of the low confidence

in original experimental data, this reaction was not investigated further.

$\text{Fe}(\text{btz})_3^{2+}$, $\text{Fe}(\text{btz})_2(\text{CN})_2$, and $\text{Fe}(\text{bipym})_3^{2+}$ were very easily prepared, using methods for the analogous phen complexes. $\text{Fe}(\text{bipym})_2(\text{CN})_2$ could not be prepared. The evidence indicated that a charged complex, probably $\text{Fe}(\text{bipym})(\text{CN})_4^{2-}$ was prepared. The phen complex $\text{Fe}(\text{phen})(\text{CN})_4^{2-}$ can be prepared but usually involves refluxing $\text{Fe}(\text{phen})_3^{2+}$ with KCN^4 . $\text{Fe}(\text{bipym})(\text{CN})_4^{2-}$ was prepared under much milder conditions, thus a qualitative scheme can be stated:



The kinetics of the reaction between $\text{Fe}(\text{bipym})_3^{2+}$ and CN^- have been studied¹⁷, and the results indicate a rapid pre-equilibrium, followed by formation of the Schilt complex:



Although the complex was not isolated, it was inferred from the N.M.R. of the reaction mixture, which indicated the presence of free bipym.

The extinction coefficients of $\text{Fe}(\text{btz})_3^{2+}$ and $\text{Fe}(\text{btz})_2(\text{CN})_2$ are very typical for iron complexes, as can be seen in

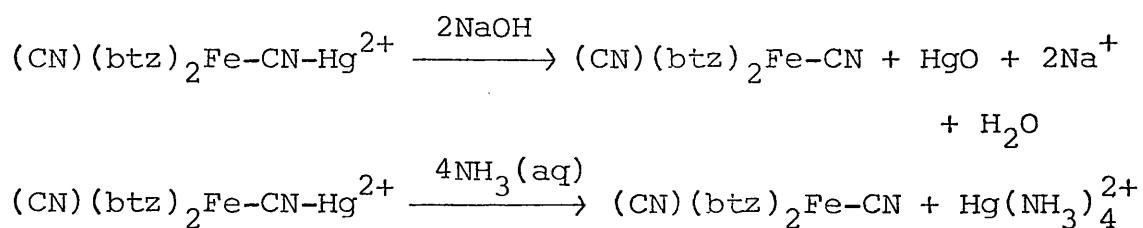
table 5.

$\text{Fe}(\text{btz})_2(\text{CN})_2$ is solvatochromic, (table 3), as is $\text{Fe}(\text{phen})_2(\text{CN})_2$ and $\text{Fe}(\text{bipy})_2(\text{CN})_2$. The solvatochromism of $\text{Fe}(\text{btz})_2(\text{CN})_2$ is discussed in a later chapter.

$\text{Fe}(\text{btz})_2(\text{CN})_2$ reacts with Hg^{2+} in aqueous solution to produce an adduct with a characteristic uv/vis spectrum. The stoichiometry of the reaction is 1:1. The adduct produces a red solution, and this colour fades over a period of time.

The structure of the adduct is unknown although i.r. spectra of the phen and bipy adducts are known which indicates structures as shown in Fig.17¹⁸. The adduct under discussion was found to deteriorate in solid form to produce $\text{Fe}(\text{btz})_2(\text{CN})_2$.

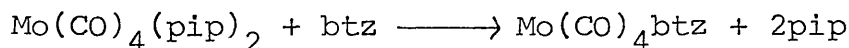
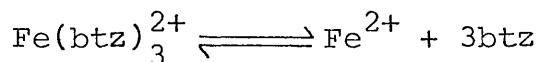
The adduct reacts with NaOH (solid or solution) and aqueous ammonia to yield $\text{Fe}(\text{btz})_2(\text{CN})_2$. These reactions may be represented by the following equations:



The driving force of the reaction is the thermodynamic stability of the reaction products. (The structure of the mercury adduct as depicted above is for convenience only.) The phen and bipy adducts react in a similar fashion.

The reaction between $\text{Fe}(\text{btz})_3^{2+}$ and $\text{Mo}(\text{CO})_4(\text{pip})_2$ was an attempt to prepare multinuclear complexes. The main

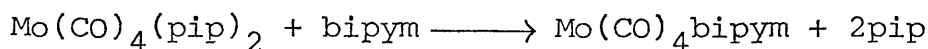
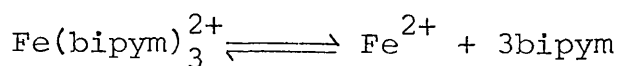
product of the reaction was $\text{Mo}(\text{CO})_4\text{btz}$. This is in line with the other reactions discussed, and the following mechanism is proposed:



The stability of $\text{Mo}(\text{CO})_4\text{btz}$ appears to be the driving force for this and other reactions to be discussed in a later chapter.

The reaction between $\text{Fe}(\text{bipym})_3^{2+}$ and $\text{Mo}(\text{CO})_4(\text{pip})_2$ was again an attempt to prepare multinuclear complexes. The product of the reaction is believed to be $\text{Mo}(\text{CO})_4\text{bipym}$, as judged from uv/vis data. The solvent for the reaction was nitromethane. It was found that $\text{Fe}(\text{bipym})_3^{2+}$ would decompose in some aqueous organic mixtures especially acetone and methanol. A variety of solvents were tried, and it was found that solid $\text{Fe}(\text{bipym})_3\text{SO}_4$ could dissolve in pure nitromethane without decomposition. Unfortunately chloroform is miscible with nitromethane, and so it was not possible to extract any neutral reaction products for detailed investigations.

The stability constant for $\text{Fe}(\text{bipym})_3^{2+}$ ($\beta_3 = 7.53$) is less than that of $\text{Fe}(\text{btz})_3^{2+}$, so a reasonable mechanism for the reaction would be:



This is very similar to the corresponding $\text{Fe}(\text{btz})_3^{2+}$ reaction; there was no evidence for $[\text{Mo}(\text{CO})_4]_2\text{bipym}$, formed by $\text{Mo}(\text{CO})_4\text{bipym}$ reacting with $\text{Mo}(\text{CO})_4(\text{pip})_2$. The complex $[\text{Mo}(\text{CO})_4]_2\text{bipym}$ is known¹⁹, but $[\text{Mo}(\text{CO})_4]_2\text{btz}$ is not.

Attempts to prepare polymerized $\text{Fe}(\text{bipym})_2$ were unsuccessful. The stability constant of $\text{Fe}(\text{bipym})_3^{2+}$ in water is 7.53×10^{13} . Presumably with other metal ions coordinated to the ligand the stability of the complex formed is less than that of the parent complex.

Table 1

Ionic strength of reactions discussed.

Reaction	Ionic strength /mol dm ⁻³	Ionic strength maintained with
$\text{Fe}(\text{btz})_3^{2+} + \text{OH}^-$	0.0667	NaCl
$\text{Fe}(\text{btz})_3^{2+} + \text{H}^+$	0.0667	NaCl
$\text{Fe}(\text{btz})_3^{2+} + \text{Ag}^+$	0.098	NaNO ₃
$\text{Fe}(\text{btz})_3^{2+} + \text{Cd}^{2+}$	0.32	K ₂ SO ₄
$\text{Fe}(\text{btz})_3^{2+} + \text{Hg}^{2+}$	0.03	Mg(ClO ₄) ₂
$\text{Fe}(\text{btz})_3^{2+} + \text{S}_2\text{O}_8^{2-}$	0.2	K ₂ SO ₄

Table 4

Stability constants of Mbtz⁺ complexes in water at 25°C.

Metal	log ₁₀ K _{eq}
Cd ²⁺	1.3
Hg ²⁺	2.6
Ag ⁺	2.7

Stability constants of metal phenanthroline complexes in water at 25°C.

Metal	log ₁₀ K ₁	log ₁₀ K ₂	log ₁₀ K ₃
Ag ⁺	5.02	7.05	
Cd ²⁺	5.93	4.59	3.78

Stability constants of metal bipyridine complexes in water at 25°C.

Metal	log ₁₀ K ₁	log ₁₀ K ₂	log ₁₀ K ₃
Ag ⁺	3.84		
Cd ²⁺	3.99		
Hg ²⁺	9.64	7.10	2.8

Table 2

$\text{Fe}(\text{btz})_3^{2+} + \text{OH}^-$ in water at 25°C *

$10^3 \times [\text{NaOH}]/\text{mol dm}^{-3}$	$10^3 \times k_{\text{obs}}/\text{s}^{-1}$
3.34	4.44
8.33	6.51
11.6	8.65
16.7	9.73
25.0	11.35
33.4	11.2
41.6	16.6
58.3	15.5
66.7	12.6

$\text{Fe}(\text{btz})_3^{2+} + \text{H}^+$ in water at 25°C *

$10^3 \times [\text{HCl}]/\text{mol dm}^{-3}$	$10^3 \times k_{\text{obs}}/\text{s}^{-1}$
3.34	2.96
10.0	3.20
16.7	3.71
33.4	4.07
50.0	3.86
66.7	4.60

$\text{Fe}(\text{btz})_3^{2+} + \text{Hg}^{2+}$ in water at 25°C

$10^3 \times [\text{Hg}(\text{ClO}_4)_2]/\text{mol dm}^{-3}$	$10^3 \times k_{\text{obs}}/\text{s}^{-1}$
10.0	2.91
8.00	3.36
6.00	3.25
4.00	3.07
2.00	2.97
1.00	2.52
0.50	3.02
0.20	2.73
0.10	2.81

Table 2 cont.

$\text{Fe}(\text{btz})_3^{2+} + \text{S}_2\text{O}_8^{2-}$ in water at 25°C *

$10^2 \times [\text{K}_2\text{S}_2\text{O}_8] / \text{mol dm}^{-3}$	$10^3 \times k_{\text{obs}} / \text{s}^{-1}$
6.67	1.44
3.34	2.03
1.67	2.60

$\text{Fe}(\text{btz})_3^{2+} + \text{Cd}^{2+}$ in water at 25°C

$10^2 \times [\text{Cd}(\text{SO}_4)_2] / \text{mol dm}^{-3}$	$10^3 \times k_{\text{obs}} / \text{s}^{-1}$
8.00	3.67
6.00	4.54
4.00	6.39
1.00	13.9

$\text{Fe}(\text{btz})_3^{2+} + \text{Ag}^+$ in water at 25°C

$[\text{AgNO}_3] / \text{mol dm}^{-3}$	$10^3 \times \text{initial rate} / \text{s}^{-1}$	$10^3 \times k_{\text{obs}} / \text{s}^{-1}$
0.098	3.96	3.27
0.0396	3.66	2.48
0.0198	3.85	3.69
0.0099	3.72	4.51
0.0035	3.29	9.32

$\text{Fe}(\text{btz})_3^{2+} + 1,10 \text{ phen}$ in 40% methanol (v/v) at 25°C

$[\text{phen}] / \text{mol dm}^{-3}$	$-\frac{d}{dt} \text{Fe}(\text{btz})_3^{2+}$ $10^3 \times k_{\text{obs}} / \text{s}^{-1}$	$+\frac{d}{dt} \text{Fe}(\text{phen})_3^{2+}$ $10^3 \times k_{\text{obs}} / \text{s}^{-1}$
0.889	2.229	2.038
0.692	2.094	1.733
0.469	1.688	1.746

Table 2 cont.

$\text{Fe}(\text{btz})_3^{2+} + \text{bipy}$ in 40% methanol (v/v) at 25°C

$[\text{bipy}] / \text{mol dm}^{-3}$	$-\frac{d}{dt} \text{Fe}(\text{btz})_3^{2+}$ $10^3 \times k_{\text{obs}} / \text{s}^{-1}$	$+\frac{d}{dt} \text{Fe}(\text{bipy})_3^{2+}$ $10^3 \times k_{\text{obs}} / \text{s}^{-1}$
0.984	1.105	1.791

$\text{Fe}(\text{btz})_3^{2+} + \text{Na}_2\text{EDTA}$ in water at 25°C, Na_2EDTA in excess

$$k = 2.474 \times 10^{-3} \text{ s}^{-1}$$

$\text{Fe}(\text{btz})_3^{2+} + \text{H}_2\text{O}$ (2cm^3 of stock solution diluted to 3cm^3 at 25°C)

$$k = 2.413 \times 10^{-2} \text{ s}^{-1}$$

Reactions marked with \star went to completion, the other reactions did not go to completion.

Table 3

Solvatochromism of $\text{Fe}(\text{btz})_2(\text{CN})_2$.

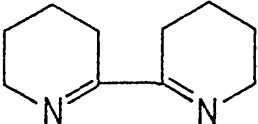
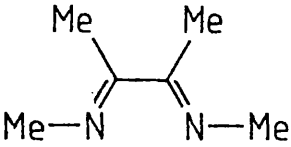
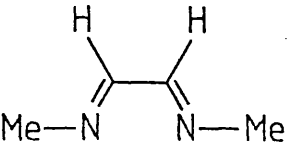
Solvent	λ_{max} /nm
Methanol	606
Ethanol	616
n-Propanol	618
n-Butanol	618
Acetone	660
Acetonitrile	648
Nitromethane	646
Trifluoroethanol	586
Water	585
Glycerol	598

Table 6

Stability constants of some iron complexes in water at 25° C.

$\text{Fe}^{2+} + \text{EDTA}$	$\log_{10} K_1 = 14.2$	
$\text{Fe}^{2+} + 3\text{phen}$	$\log_{10} \beta_3 = 21.2$	
$\text{Fe}^{2+} + 3(5\text{NO}_2\text{phen})$	$\log_{10} \beta_3 = 17.8$	
$\text{Fe}^{2+} + 3(2,9\text{Me}_2\text{phen})$	$\log_{10} \beta_3 = 10.8$	} both high spin FeL_3^{2+}
$\text{Fe}^{2+} + 3(2\text{Me-phen})$	$\log_{10} \beta_3 = 10.8$	
$\text{Fe}^{2+} + 3\text{bipy}$	$\log_{10} \beta_3 = 17.5$	
$\text{Fe}^{2+} + 3\text{en}$	$\log_{10} \beta_3 = 9.7$	

Table 5

L	Complex	$\lambda_{\text{max}} / \text{nm}^{\text{a}}$	$\epsilon^{\text{a}} / \text{dm}^3 \text{ mol}^{-1} \text{ cm}^{-1}$
bipy	FeL_3^{2+}	522	8.7×10^3
phen	FeL_3^{2+}	510	1.15×10^4
	FeL_3^{2+}	568	1×10^4
	FeL_3^{2+}	568	1.07×10^4
	FeL_3^{2+}	554	8.8×10^3
btz	FeL_3^{2+}	510	1.0365×10^4
box	FeL_3^{2+}	500	1.6×10^3
$\text{Fe}(\text{btz})_2(\text{CN})_2$		585	6.145×10^3
$\text{Fe}(\text{phen})_2(\text{CN})_2$		516	
$\text{Fe}(\text{bipy})_2(\text{CN})_2$		515	5.5×10^3

a) water as solvent

Figure 1 2,2'-bi-4,5-dihydrothiazine, bithiazine (btz).

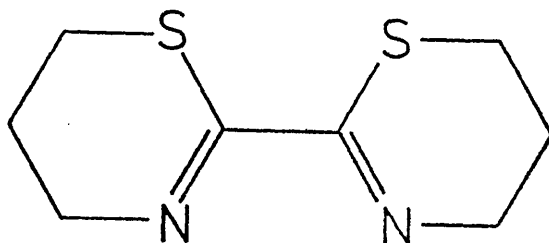


Figure 2 Ligands related to btz, for which iron(II) complexes are known.

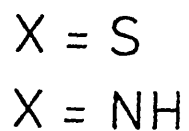
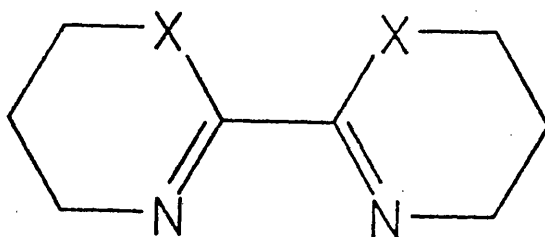
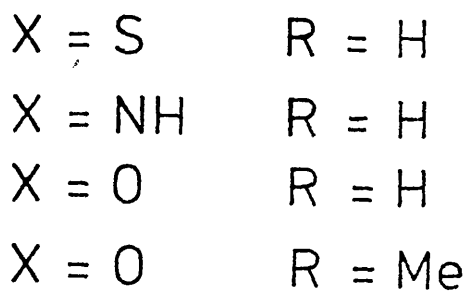
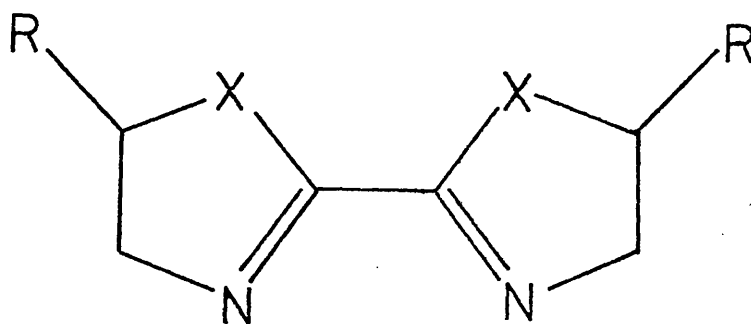


Figure 3 Schematic representation of some multinuclear complexes incorporating the ligand btz.

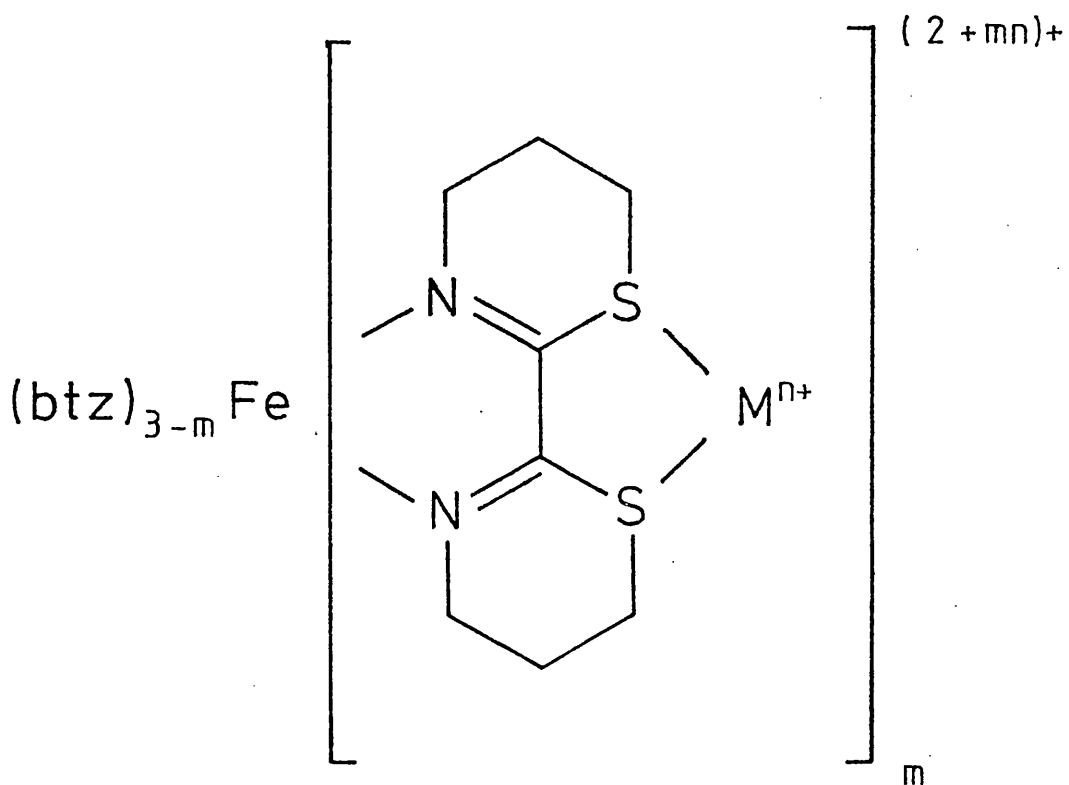


Figure 4 A mechanism for the metal catalysed dissociation of $\text{Fe}(\text{btz})_3^{2+}$.

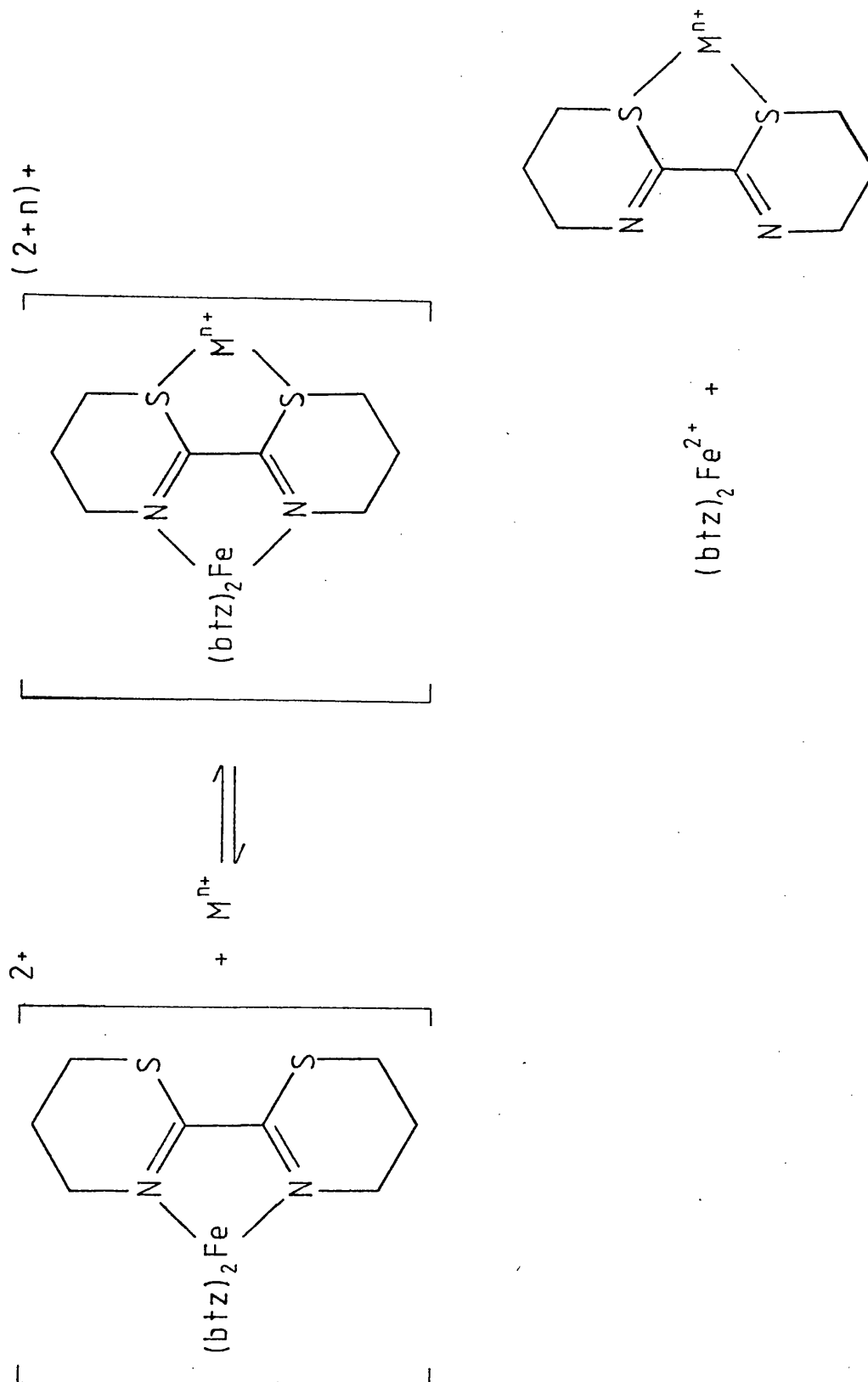


Figure 5 Schematic representation of some multinuclear complexes incorporating the ligand bipym.

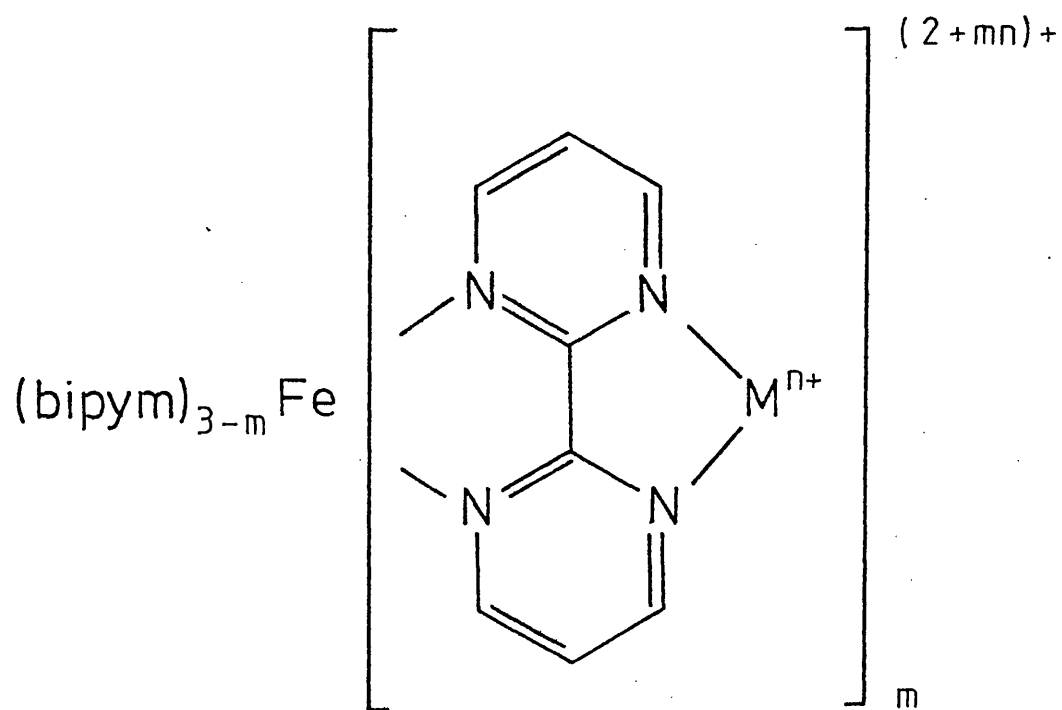


Figure 6 Uv/vis spectra of $\text{Fe}(\text{btz})_2(\text{CN})_2$ and $\text{Fe}(\text{btz})_2(\text{CN})_2\text{Hg}^{2+}$ in water at 298.2 K.

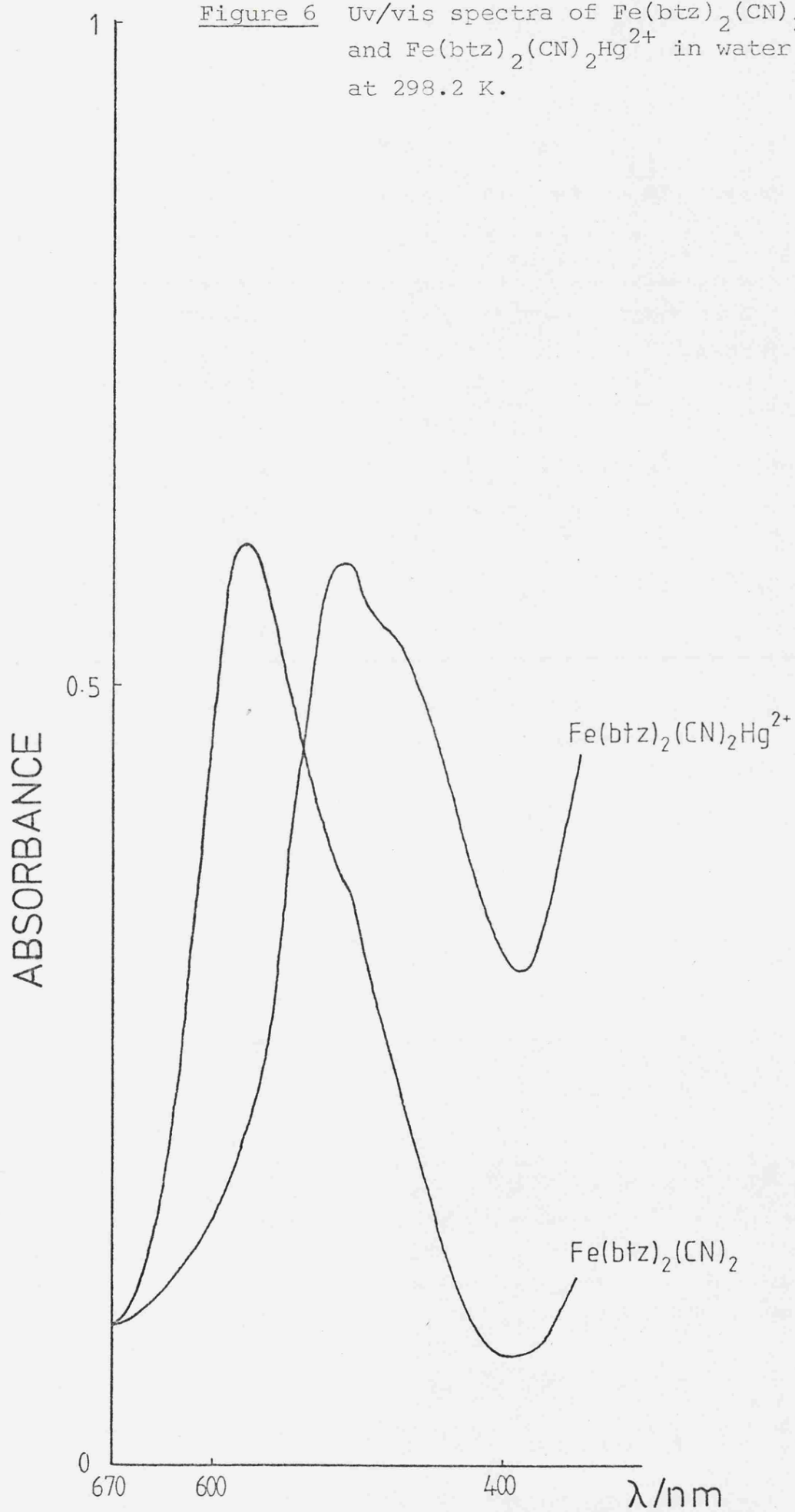


Figure 7 Dependence of the observed first order rate constant upon hydroxide concentration for the reaction between $\text{Fe}(\text{btz})_3^{2+}$ and OH^- , in water at 298.2 K.

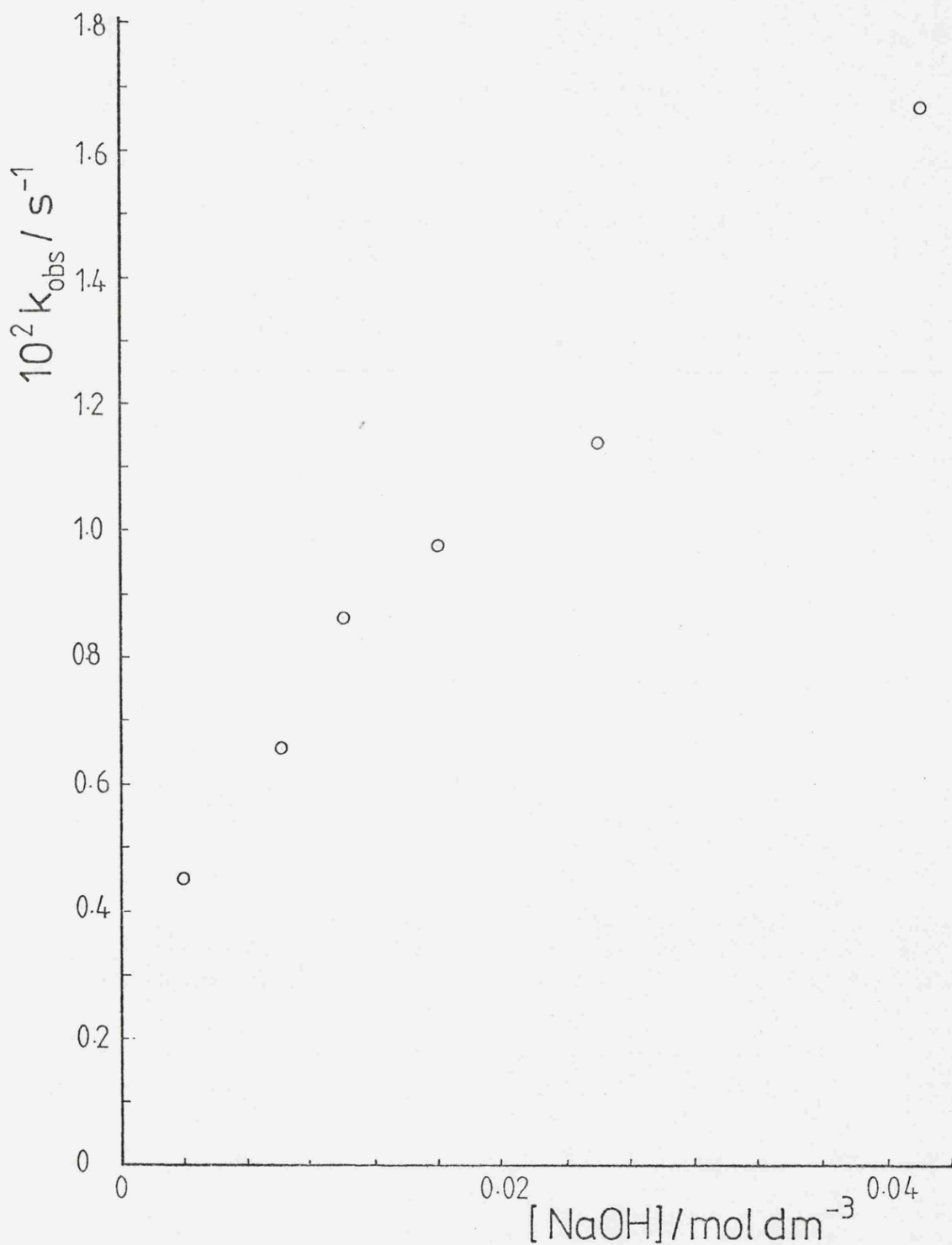


Figure 8 Dependence of the observed first order rate constant upon acid concentration for the reaction between $\text{Fe}(\text{btz})_3^{2+}$ and H^+ , in water at 298.2 K.

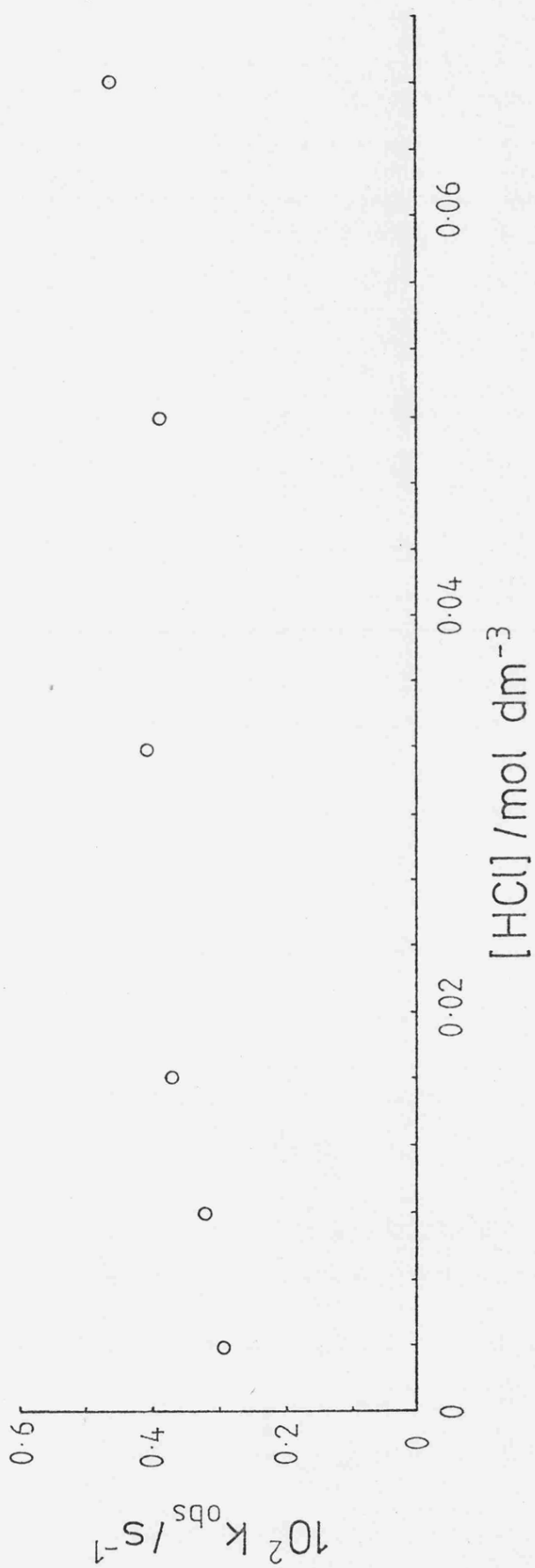


Figure 9 The effect of hydrogen-ion concentration on the first order rate constant in the hydrolysis of $\text{Fe}(\text{bipy})_3^{2+}$.

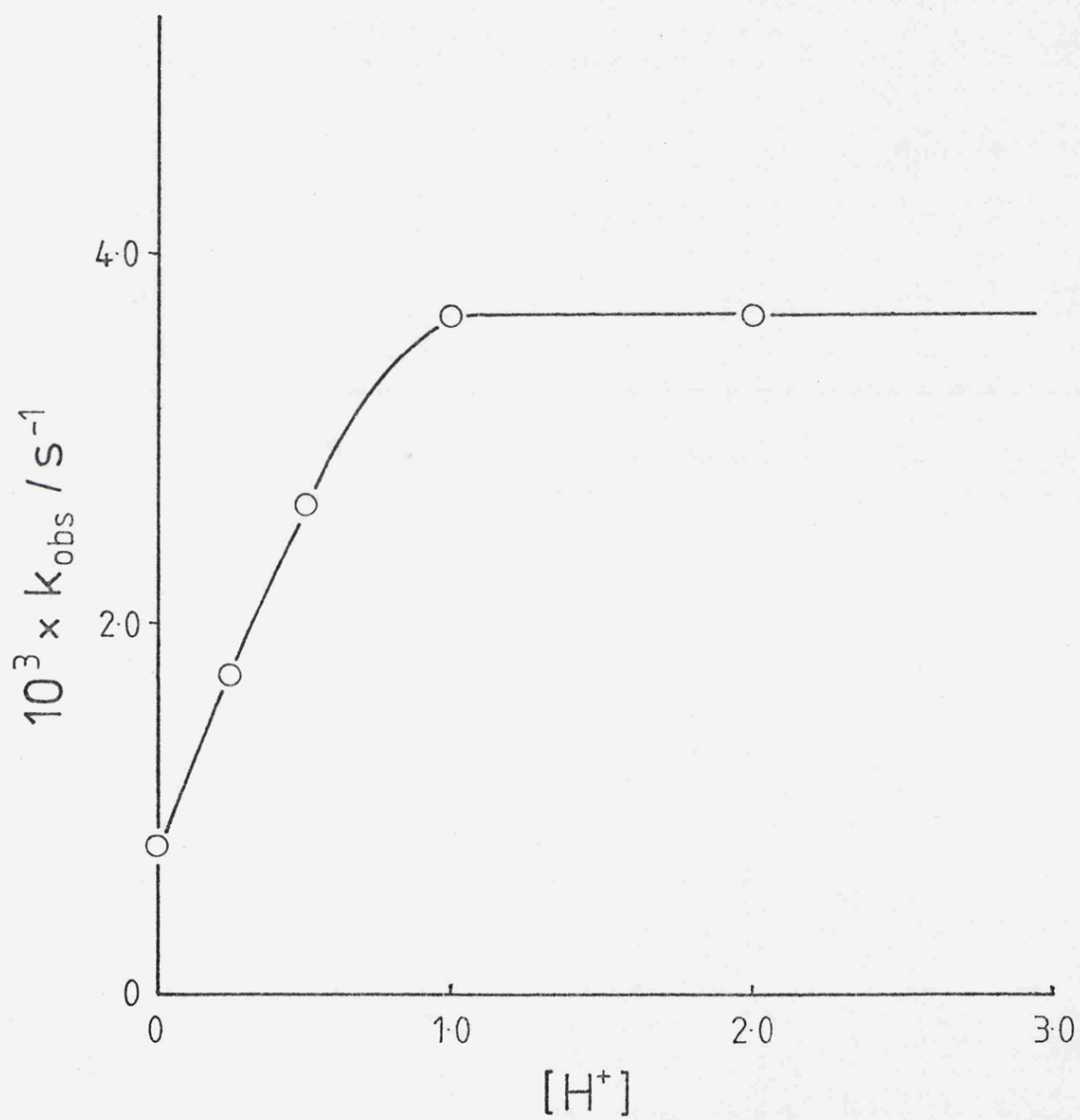


Figure 10 2,2'-bi-4,5-dehydrooxazine, box.

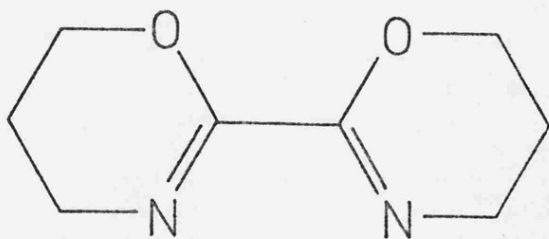


Figure 11 The effect of hydroxide concentration on the observed first order rate constant for the reaction between $\text{Fe}(\text{box})_3^{2+}$ and OH^- .

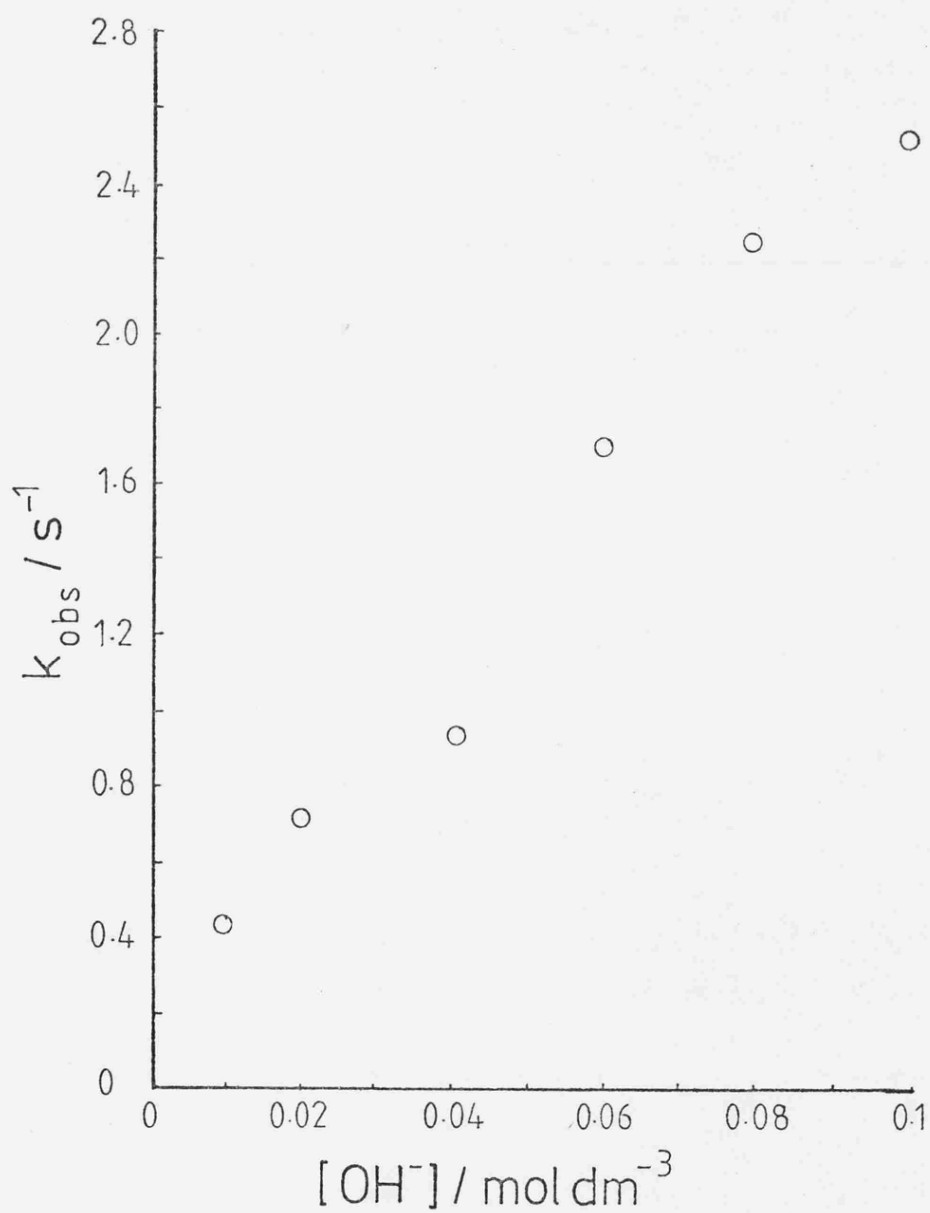


Figure 12 The effect of Hg^{2+} concentration on the observed first order rate constant for the reaction between $\text{Fe}(\text{btz})_3^{2+}$ and Hg^{2+} , in water at 298.2 K.

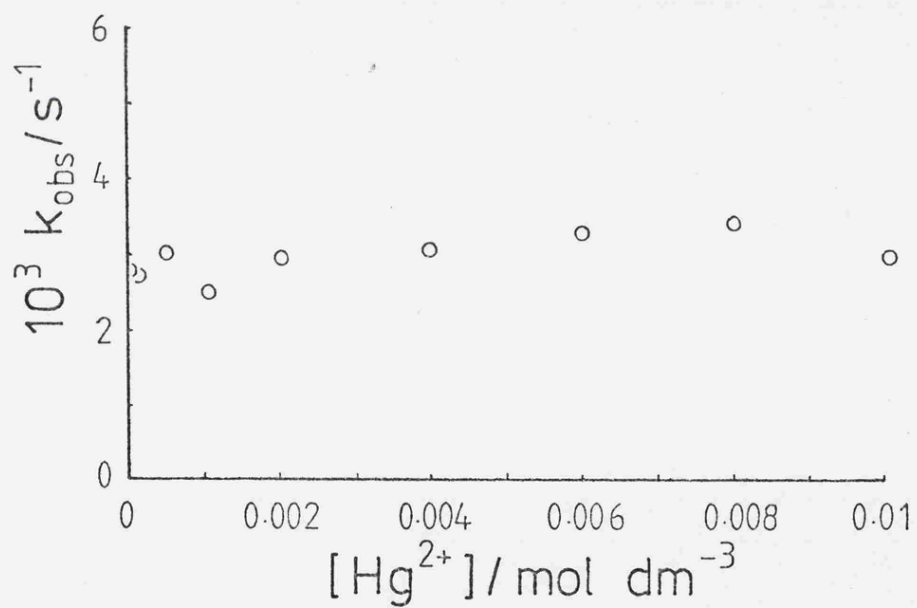


Figure 13 The effect of Cd^{2+} concentration on the observed first order rate constant for the reaction between $\text{Fe}(\text{btz})_3^{2+}$ and Cd^{2+} , in water at 298.2 K.

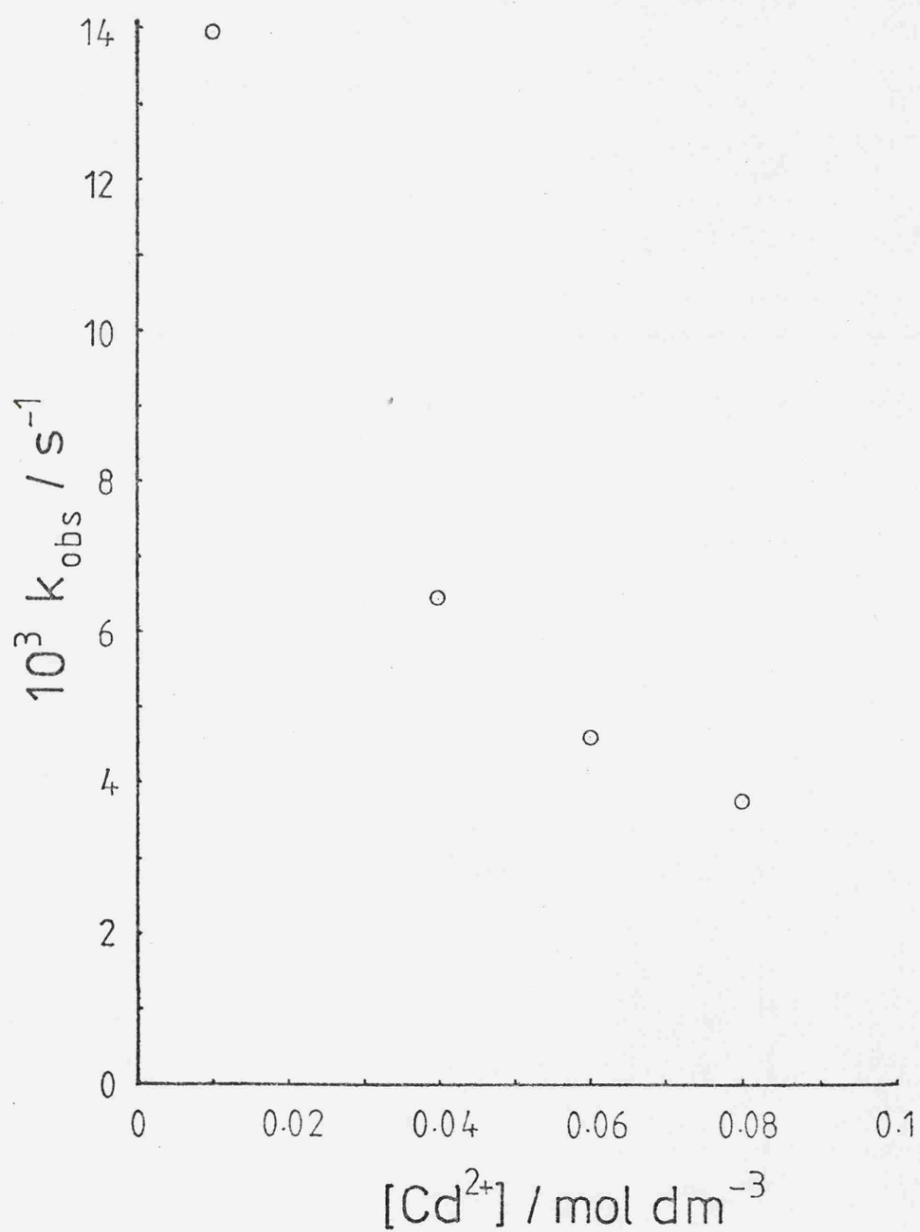


Figure 14 The effect of Ag^+ concentration on the observed first order rate constant for the reaction between $\text{Fe}(\text{btz})_3^{2+}$ and Ag^+ , in water at 298.2 K.

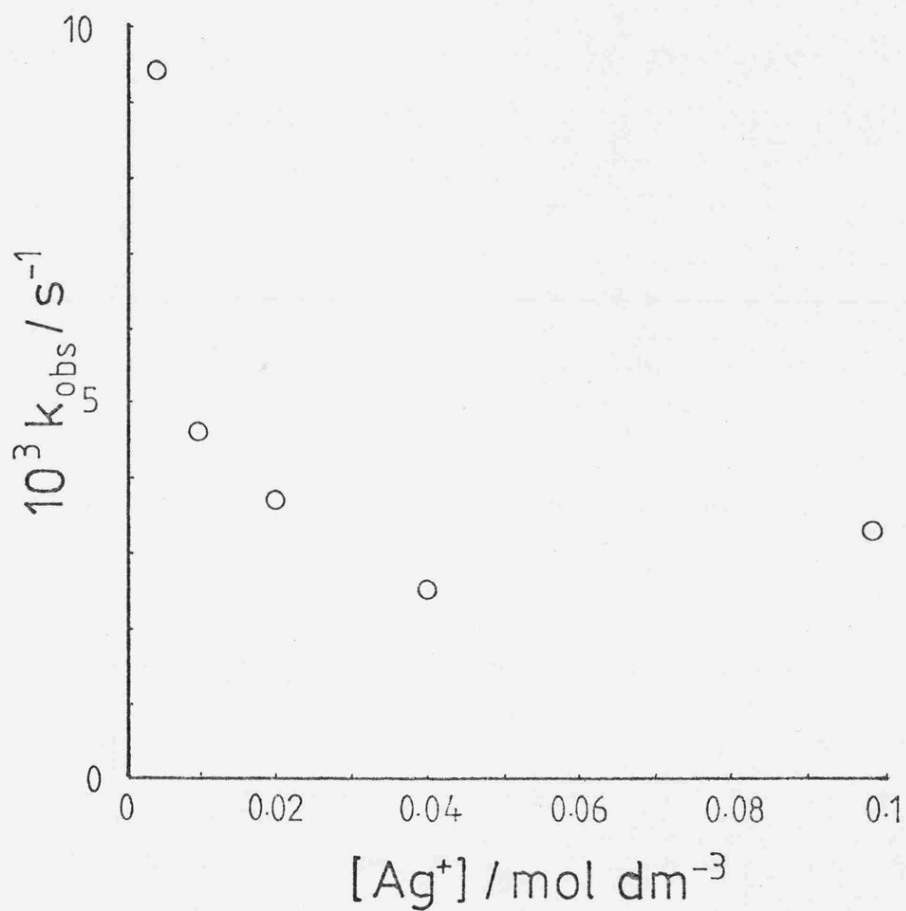
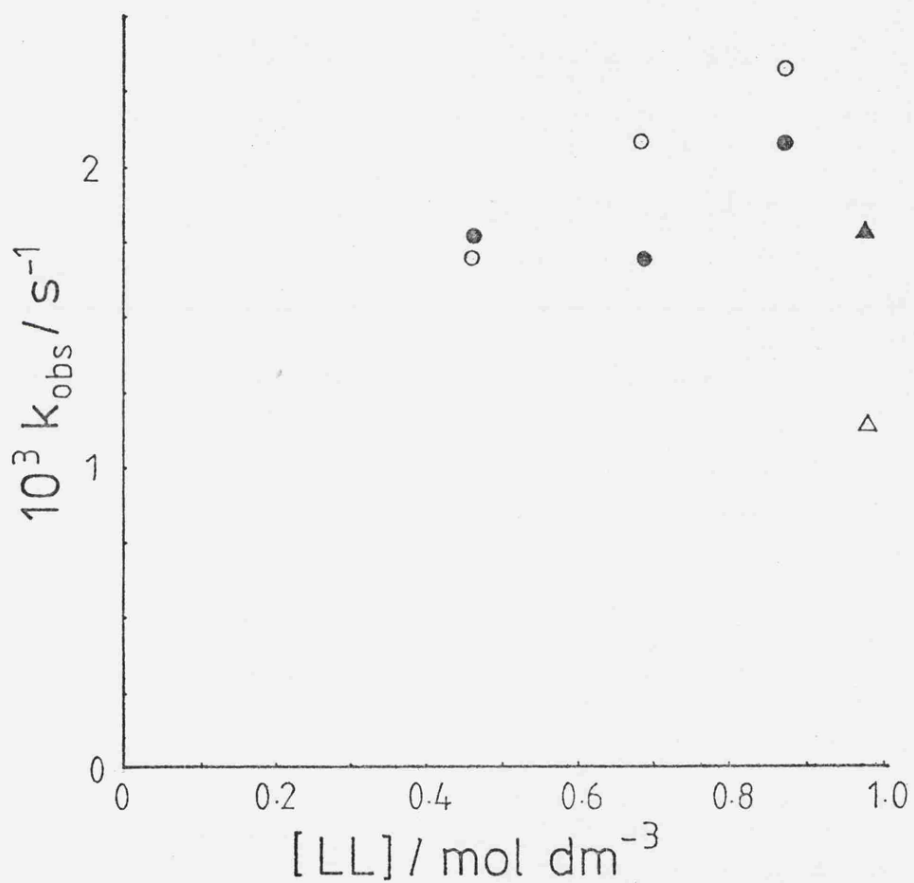


Figure 15 The effect of phen and bipy concentration on the observed first order rate constants for the reaction $\text{Fe}(\text{btz})_3^{2+} + \text{LL}$ (LL = phen, bipy), in 40% (v/v) aqueous methanol, at 298.2 K.



- phen $-\frac{d}{dt} [\text{Fe}(\text{btz})_3^{2+}]$
- △ bipy $-\frac{d}{dt} [\text{Fe}(\text{btz})_3^{2+}]$
- phen $\frac{d}{dt} [\text{Fe}(\text{LL})_3^{2+}]$
- ▲ bipy $\frac{d}{dt} [\text{Fe}(\text{LL})_3^{2+}]$

Figure 16 The effect of $S_2O_8^{2-}$ concentration on the observed first order rate constant for the reaction between $Fe(btz)_3^{2+}$ and $S_2O_8^{2-}$, in water at 298.2 K.

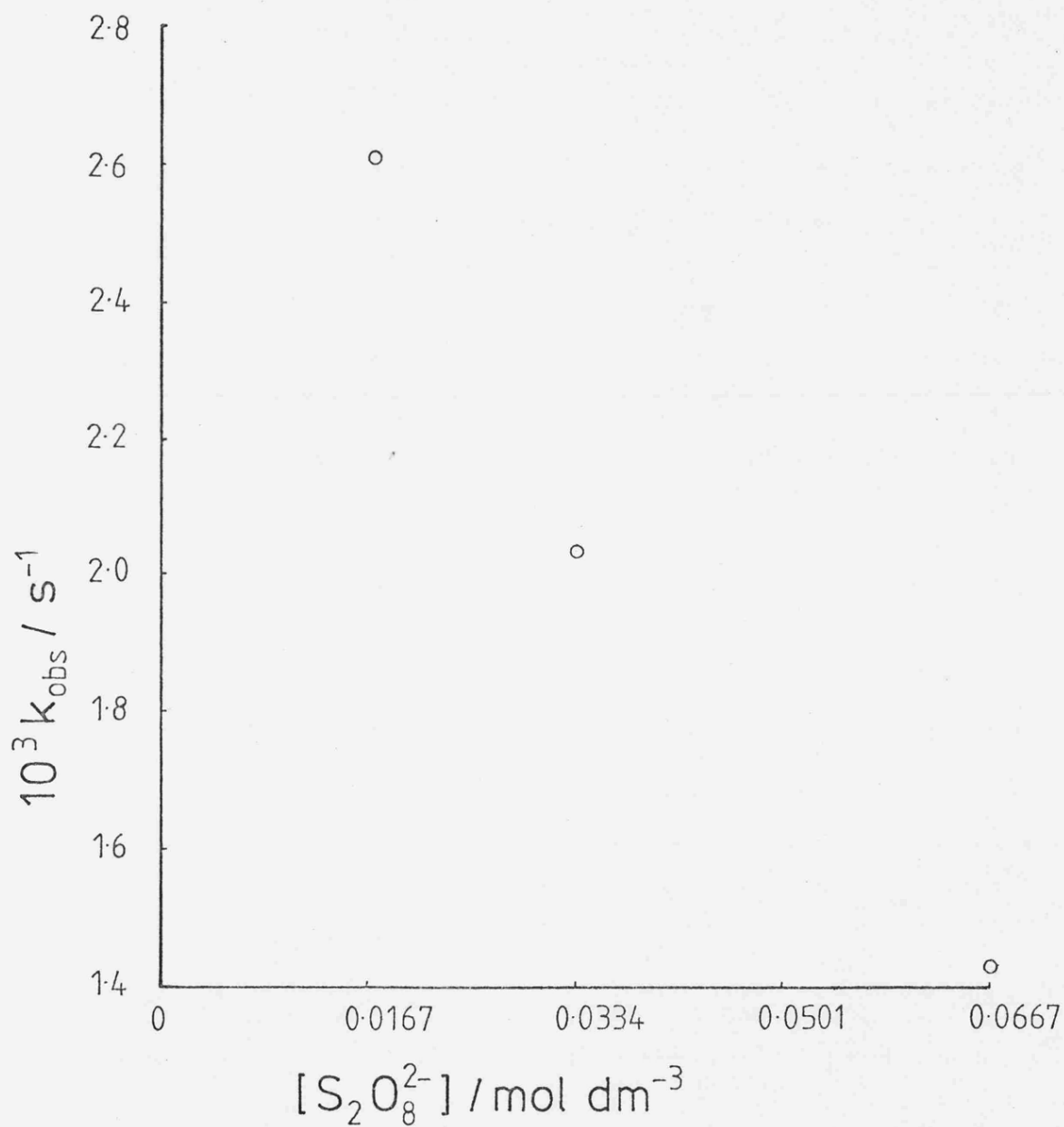
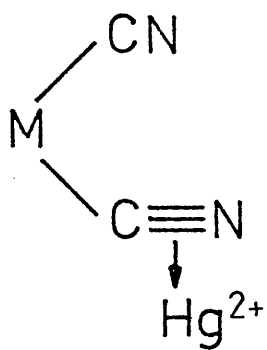
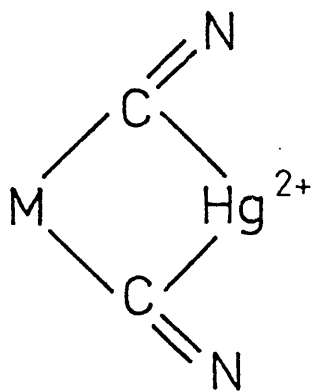
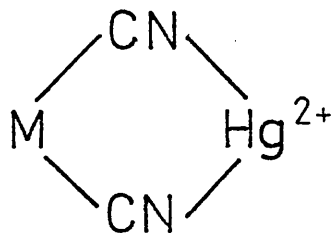


Figure 17 Schematic representation of the possible bonding involved in the $\text{Fe}(\text{btz})_2(\text{CN})_2\text{Hg}^{2+}$ adduct.



References Chapter 4

1. J.Nelson, S.M.Nelson and W.D.Perry, J.C.S.Dalton, 1976, 1282
2. M.G.Burnett, V.McKee, and S.M.Nelson, J.C.S.Dalton, 1981, 1492
3. D.A.Tomalia and J.N.Paige, J.Org.Chem., 38, 3949 (1973)
4. A.A.Schilt, J.Am.Chem.Soc., 82, 3000 (1960)
5. D.J.Darensbourg and R.L.Kump, Inorg.Chem., 17, 2680 (1978)
6. P.Krumholz, J.Am.Chem.Soc., 75, 2163 (1953)
7. L.F.Undoy and S.Livingstone, Co-ord.Chem.Rev., 3, 173 (1967)
8. 'Mechanisms of Inorganic Reactions', Basolo and Pearson, 2nd Edition, Wiley, New York, 1967
9. R.D.Gillard, D.W.Knight and P.A.Williams, Trans.Met. Chem., 4 375 (1979)
10. 'Advanced Organic Chemistry', J.March, 2nd ed.

11. N.Serpone, G.Ponterini, and M.A.Jamieson, Co-ord. Chem.Rev., 50, 209 (1983)
12. "The Hydrolysis of Cations", C.F.Bais and R.E.Mesmer, Wiley, 1976
13. Sillén,L.G. and Martell,A.E., "Stability Constants of Metal-Ion Complexes", Chemical Society Special Publications 17 and 25 (Supplement 1), The Chemical Society, London (1964, 1971)
14. J.Burgess and R.H.Prince, J.Chem.Soc.A., 1966, 1772
15. D.A.House, Chem.Rev., 62, 185 (1962)
16. L.S.Levitt, J.Org.Chem., 20, 1297 (1955)
17. R.J.Wademan and P.A.Williams, Trans.Met.Chem., 4, 333 (1979)
18. M.T.Beck and É.Cs.Porzolt, J.Co-ord.Chem., 1, 57 (1971)
19. J.A.Connor and C.Overton, Poly., 1, 53 (1982)

CHAPTER FIVE:

The preparation of $\text{Mo}(\text{CO})_4\text{bipym}$ and $\text{Mo}(\text{CO})_4\text{btz}$.
The structure of $\text{Mo}(\text{CO})_4\text{btz}$. Initial state-
transition state analysis for the solvolysis
of $\text{Mo}(\text{CO})_4\text{btz}$. Ground state-excited state
analysis for the solvatochromism of $\text{Mo}(\text{CO})_4\text{btz}$,
DMIA, PNA. The effect of temperature on the
uv/vis spectrum of $\text{Mo}(\text{CO})_4\text{btz}$. The effect of
pressure on the uv/vis spectrum of $\text{Mo}(\text{CO})_4\text{btz}$.

Introduction

There is an extensive chemistry of the group VIb metal carbonyls and their derivatives. These include spectroscopic, kinetic and structural investigations. As indicated in the previous chapter the ligand btz offers interesting comparisons with other diimine ligands such as phen and bipy. Compounds of the type $M(\text{CO})_4\text{LL}$ where $M = \text{Cr}, \text{Mo}, \text{W}$; $\text{LL} = 1, 10\text{-phenanthroline}, 2, 2'\text{-bipyridine}$ are well characterised; by contrast, there are very few btz complexes, only the molybdenum compound is well characterised.

Unlike phen or bipy, btz is an aliphatic diimine; the pair of sulphur atoms may greatly influence the solution properties of group VIb complexes. Zero valent metal complexes are useful for probing solvent effects of a range of physical properties (eg. kinetic, spectroscopic) because they are uncharged and so eliminate the need for single ion values.

One prominent feature of $\text{Mo}(\text{CO})_4\text{LL}$ complexes is their solvatochromic behaviour. Solvatochromism as defined here is the effect of solvents on charge transfer bands in the uv/visible region; there are also observed solvent effects in n.m.r., i.r. and fluorescent spectra. Although considerable work has been done to quantify solvent effects, very little has been done on ground state-excited state contributions.

One principle use of solvatochromism is in trying to quantify solvent polarity. There is considerable work

being done to try and correlate solvent polarity with spectroscopic parameters¹ though some workers feel this is misleading².

This chapter is concerned with the spectroscopic properties of $\text{Mo}(\text{CO})_4\text{btz}$, and comparing these with analogous complexes. Spectroscopic studies will include piezosolvatochromism and thermosolvatochromism. It is hoped to quantify solvent effects especially for solvatochromism.

Experimental

p-nitroanisole (PNA) and dimethylindoaniline (DMIA) were recrystallised from ethanol. Bipyrimidine (Lancaster) was used as received.

Btz was prepared by the method of Tomalia and Paige³.

$\text{Mo}(\text{CO})_4\text{btz}$ was prepared by the method of Nelson and Perry⁴. An alternative preparation was as follows: stoichiometric quantities of $\text{Mo}(\text{CO})_4(\text{piperidine})_2$ ⁵ and btz were gently refluxed in dichloromethane for ten minutes. The solution was allowed to cool, and the solvent removed. The product was allowed to dry in vacuo over P_2O_5 .

$\text{Mo}(\text{CO})_4\text{bipym}$ was prepared in the same manner as for $\text{Mo}(\text{CO})_4\text{btz}$.

$\text{Mo}(\text{CO})_4\text{btz}$ and $\text{Mo}(\text{CO})_4\text{bipym}$ were characterised by uv/vis spectroscopy, in conjunction with published spectra.

$\text{Mo}(\text{CO})_3(\text{PPh}_3)\text{btz}$ was prepared according to the method of Dobson and Houk⁶. Kinetics and calorimetry were done as described in Chapter 2.

Uv/vis spectra were run on a Pye-Unicam SP 800 or SP 8-100 using 10 mm pathlength cells.

Solubilities were determined in the usual manner⁷.

Variable temperature uv/vis spectra were performed on a specially adapted Perkin-Elmer 340 spectrophotometer as described previously⁸.

High pressure uv/vis spectra were kindly undertaken by R. van Eldik of Frankfurt University.

The structure of $\text{Mo}(\text{CO})_4\text{btz}$ was determined using X-ray methods, this work being done by Leslie Sherry and David Russell.

Results

$\text{Mo}(\text{CO})_4\text{btz}$ and $\text{Mo}(\text{CO})_4\text{bipym}$ could be obtained in nearly quantitative yields from $\text{Mo}(\text{CO})_4(\text{pip})_2$.

This method generally gave higher yields than preparations using Stiddard's method⁹.

Rates of solvolysis and corresponding enthalpies of activation are shown in table 1.

λ_{max} for $\text{Mo}(\text{CO})_4\text{btz}$, $\text{Mo}(\text{CO})_4\text{bipym}$, PNA and DMIA in various solvents are summarised in tables 2, 3, 4 and 5.

Solubility and thermochemical data are contained in tables 6, 7 and 8.

Ground state-excited state analyses were performed in terms of H. The ground state and initial state (for solvolysis) are equivalent. Enthalpies of transfer of the excited state are derived from the corresponding wavelength change using the relationship:

$$1\text{kJmol}^{-1} = 83.54\text{cm}^{-1}$$

Ground state-excited state analysis, and initial state-transition state analysis are summarised in Figs. 1, 2, 3, 4, and 5.

Changes in the uv/vis spectra of $\text{Mo}(\text{CO})_4\text{btz}$ due to temperature are shown in Fig.6. High pressure uv/vis spectra of $\text{Mo}(\text{CO})_4\text{btz}$ were unsatisfactory due to solvolysis of the compound.

Structural parameters for $\text{Mo}(\text{CO})_4\text{btz}$ are summarised in tables 9 and 10; representations of the structure are shown in Figs. 7 and 8.

Discussion

Compounds of the type $\text{Mo}(\text{CO})_4\text{LL}$, where LL is a diimine ligand, can be conveniently prepared from $\text{Mo}(\text{CO})_4(\text{piperidine})_2$ in high yield. This subject will be considered further in Chapter 6.

$\text{Mo}(\text{CO})_4\text{btz}$ as reported by Nelson and Perry was purple crystalline solid, which in acetonitrile had $\tilde{\nu}_{\text{max}}$ of 18500cm^{-1} . Our compound was a red crystalline solid which in acetonitrile gave $\tilde{\nu}_{\text{max}}$ of 20800cm^{-1} .

This large discrepancy prompted the determination of the structure of our compound which consequently was shown to be $\text{Mo}(\text{CO})_4\text{btz}$.

The structure around the molybdenum is that of a distorted octahedron with approximate C_{2v} symmetry, with btz behaving as a bidentate ligand bonding via the α -diimine group. The ligand is not planar, with C7 and C10

bent out of the plane in opposite directions (Fig.7).

Carbon-sulphur and carbon-nitrogen bond lengths are typical of those for heterocyclic systems.

Initial state-transition state analysis for solvolysis is shown in Figs.4 and 5. The analysis assumes a limiting dissociative mechanism.

For μ the effect of solvent on the initial state and transition state is small; in acetonitrile the initial state dominates; in DMSO the transition state dominates. This supports the idea of a dissociative mechanism for solvolysis.

For H the behaviour is similar. In acetonitrile the initial state dominates; in DMSO the transition state dominates.

For the corresponding bipy complex, $\text{Mo}(\text{CO})_4\text{bipy}$, the initial state-transition state analysis for solvolysis¹⁰ is shown in Fig.9. Again the transition state dominates, and the effect of the solvent is small.

One of the most notable properties of $\text{Mo}(\text{CO})_4\text{btz}$ is its solvatochromism. Table 2 gives the λ_{max} for the complex in a range of solvents, and Fig.10 gives an indication of the appearance of some solutions.

Graphs of $\lambda_{\text{max}}(\text{complex})$ vs. $E_{\text{T}}(30)$ (Figs.11 and 12) show fairly good correlations. For $\text{Mo}(\text{CO})_4\text{LL}$ complexes (LL = btz, bipym, bipy) these show very similar trends. The graphs show two distinct regions corresponding to hydroxylic and non-hydroxylic solvents¹¹.

A graph of $\lambda_{\text{max}}\text{Mo}(\text{CO})_4\text{bipy}$ vs. $\lambda_{\text{max}}\text{Mo}(\text{CO})_4\text{btz}$ (Fig.13) shows a very good correlation, with a slope close to unity.

For complexes of the type $\text{Fe}(\text{LL})_2(\text{CN})_2$ (LL = bipy, phen¹²; btz) similar trends are observed, again showing good correlations with the solvent parameter $E_T(30)$. Unfortunately, these complexes are not as soluble as the corresponding molybdenum analogues so the range of solvents is limited.

Graphs of $\lambda_{\text{max}}^{\text{Mo}(\text{CO})_4\text{bipy}}$ vs. $\lambda_{\text{max}}^{\text{Fe}(\text{btz})_2(\text{CN})_2}$ do not show a very good correlation.

Thus, analogous compounds have very similar solvatochromic behaviour. It is interesting that for a range of ligands in complexes of the type $\text{Mo}(\text{CO})_4\text{LL}$ the solvatochromism is virtually ligand independent. To understand this it is necessary to explain how solvents affect the uv/vis spectra of molecules. This has been extensively discussed and a brief description is given here.

When a molecule absorbs light an electron is transferred from one energy level to another. This electron transfer occurs over a very short period of time (approx. 10^{-15} s), such that atomic nuclei have no time to change their position (Franck-Condon principle). Thus the geometry of the excited state is the same as the ground state. This is known as the Franck-Condon excited state.

In molecules of the type $\text{M}(\text{CO})_4\text{LL}$ (M = Cr, Mo, W) there is usually a small permanent dipole¹⁴ and upon excitation there is transient change in dipole moment. Two situations can be identified: one in which the excited state dipole moment is greater than the ground state dipole moment

$(\mu_{e.s.} > \mu_{g.s.})$ and vice versa ie. $\mu_{g.s.} > \mu_{e.s.}$.

In non-polar solvents forces contributing to solvation are dipole-induced dipole and dispersion. If the solute dipole moment increases during the electronic transition, the Franck-Condon excited state becomes more solvated by dipole-solvent polarisation and a red shift is expected. Conversely if the dipole moment decreases during the transition the Franck-Condon excited state becomes less solvated and a blue shift is expected.

In polar solvents the ground state is solvated mainly by dipole-dipole interactions. If during the electronic transition the dipole moment decreases then the dipole-dipole interactions are diminished leading to less stabilisation of the Franck-Condon excited state. Thus increasing the solvent polarity will generally lead to increased stabilisation of the ground state. For the Franck-Condon excited state greater stabilisation is expected when $\mu_{e.s.} > \mu_{g.s.}$. These situations are shown diagrammatically in Fig.16.

It must be borne in mind that this is a very qualitative picture of solvent effects, and that other factors undoubtedly contribute. A more detailed description may be found in McRae¹³.

For $M(CO)_4LL$ compounds ($M = Cr, Mo, W$; $LL = diimine$) the ground state dipole moment is approx. 3.0×10^{-29} Cm. For the excited state the dipole moment is approx. 1.3×10^{-29} Cm¹⁴ (Fig.17) ie. $\mu_{g.s.} > \mu_{e.s.}$.

These dipole moments are not significantly different for

a range of diimines, thus if solvent effects are explained in terms of change in dipole moment alone, the behaviour of $\text{Mo}(\text{CO})_4\text{LL}$ complexes (LL = bipy, phen, bipym, btz) would be expected to be very similar. The solvatochromic behaviour of these complexes is indeed similar, so the qualitative description of solvent effects appears to be in good agreement.

For complexes of the type $\text{Fe}(\text{LL})_2(\text{CN})_2$ the excited state dipole would be expected to be greater than the ground state dipole ($\mu_{\text{g.s.}} < \mu_{\text{e.s.}}$), although no values have been reported.

Using enthalpy and spectral data, solvent effects can be analysed into ground state and excited state contributions (g.s.-e.s.).

These are shown for $\text{Mo}(\text{CO})_4\text{btz}$, PNA, and DMIA in Figs. 1, 2 and 3. For PNA¹⁵ and DMIA¹⁶ the Franck-Condon excited state dipole is greater than the ground state dipole.

For $\text{Mo}(\text{CO})_4\text{btz}$, increasing the solvent polarity generally destabilises the ground state. The Franck-Condon excited state is destabilised in acetonitrile, but stabilised in methanol; in methanol the Franck-Condon excited state dominates.

For PNA increasing the solvent polarity destabilises the ground state. The Franck-Condon excited state is both stabilised (MeCN) and destabilised (MeOH).

For DMIA increasing solvent polarity destabilises the ground state and stabilises the Franck-Condon excited

state.

These examples show that the trends are not as simple as expected from the earlier discussion. Other workers have observed complicated patterns of ground state-excited state effects¹⁷.

This indicates that solute-solvent interactions are more complex than originally assumed and that more quantitative work, especially in terms of H, needs to be done before any clear patterns will emerge.

The effect of temperature upon the uv/vis spectrum of $\text{Mo}(\text{CO})_4\text{btz}$ can be seen in Fig.6. The metal to ligand charge transfer band becomes broader with an increase in temperature. The band does not shift, as in the case of pyridinium-N-phenol-betain dyes¹⁸, and so this is not an example of thermosolvatochromism as defined by Staab¹⁹.

Presumably with increasing temperature ground state rotational levels become more populated, so leading to a broadening of the band shape²⁰.

The effect of pressure upon the uv/vis spectrum of $\text{Mo}(\text{CO})_4\text{btz}$ could not be measured for technical reasons. Because of the long times necessary for equilibration upon increasing pressure, the compound solvolised giving unsatisfactory spectra.

Table 1

Rates of solvolysis of $\text{Mo}(\text{CO})_4\text{btz}$.

DMSO

T/K	$10^5 \times k_1 / \text{s}^{-1}$
297.6	2.64
303	7.65
308.7	13.0
313	25.7

$$\Delta H^\ddagger = 106.8 \text{ kJ mol}^{-1}$$

MeCN

T/K	$10^5 \times k_1 / \text{s}^{-1}$
297.6	2.20
303	6.19
308.7	12.1
313	20.9

$$\Delta H^\ddagger = 108.8 \text{ kJ mol}^{-1}$$

MeOH

T/K	$10^6 \times k_1 / \text{s}^{-1}$
297.6	7.73
303	13.9
308.7	36.9
313	81.9

$$\Delta H^\ddagger = 116.7 \text{ kJ mol}^{-1}$$

Table 2

Wavelength of maximum absorption (λ) for charge-transfer band of $\text{Mo}(\text{CO})_4\text{btz}$.

Solvent	λ_{max} /nm
DMSO	477
MeCN	480
MeNO ₂	483
DMF	483
Acetone	490
Ethyl methyl ketone	497
Acetophenone	500
Methanol	500
Cyclohexanone	500
Benzyl alcohol	502
Dichloromethane	507
Ethanol	510
n-Propanol	510
Phenetole	513
Anisole	515
Ethyl bromide	515
i-Propanol	515
n-Butanol	518
t-Butanol	518
Chlorobenzene	523
Chloroform	523
Diethyl ether	526
Benzene	529
Carbon tetrachloride	555

Table 3

Wavelength of maximum absorption (λ) for charge-transfer band of $\text{Mo}(\text{CO})_4$ bipyrimidine.

Solvent	λ_{max} /nm
DMSO	460
Acetone	460
Acetophenone	470
Ethyl methyl ketone	475
Cyclohexanone	480
Ethanol	490
Methanol	490
Anisole	495
Benzyl alcohol	496
Ethyl bromide	500
Chlorobenzene	506
Phenetole	508
n-Propanol	510
i-Propanol	510
Diethyl ether	512
n-Butanol	514
Chloroform	522
Carbon tetrachloride	556

Table 4

Wavelength of maximum absorption for PNA.

Solvent	λ_{\max} /nm
Ethanol	302
Toluene	304
i-Propanol	305
t-Butanol	306
Methanol	307
Acetonitrile	309
Chloroform	309

Table 5

Wavelength of maximum absorption for DMIA.

Solvent	λ_{\max} /nm
Diethyl ether	562
Toluene	576
Acetonitrile	587
Nitroethane	591
Dichloromethane	593
Acetophenone	599
Chloroform	599
Ethanol	603
t-Butanol	603
i-Propanol	607
Methanol	612

Table 6

Ground state-excited state analysis of Mo(CO)₄btz.

	MeOH	MeCN	DMSO
$\Delta H_{sol}^e / \text{kJ mol}^{-1} \text{ }^a$	+23.3	+29.7	+23.2
$\therefore \delta_m(\text{GS}) / \text{kJ mol}^{-1}$		+6.4	-0.1
$\Delta E_{ct} / \text{kJ mol}^{-1}$	+239.2	+249.2	+250.6
$\therefore \delta_m \Delta E_{ct} / \text{kJ mol}^{-1}$		+10	+11.4
$\therefore \delta_m(\text{ES}) / \text{kJ mol}^{-1}$		+16.4	+11.3

Initial state-transition state analysis (G) for the solvolysis of Mo(CO)₄btz.

	MeOH	MeCN	DMSO
$10^6 \times k / \text{s}^{-1}$	7.73	22.0	26.4
$\therefore \delta_m \Delta G^\ddagger / \text{kJ mol}^{-1}$		-2.59	-3.04
$\delta_m \mu^*(\text{Mo(CO)}_4\text{btz}) / \text{kJ mol}^{-1} \text{ }^*$		+4.81	-0.08
$\therefore \delta_m \mu^\ddagger(\text{Mo(CO)}_4\text{btz}) / \text{kJ mol}^{-1}$		+2.22	-3.12

Initial state-transition state analysis (H) for the solvolysis of Mo(CO)₄btz.

	MeOH	MeCN	DMSO
$\Delta H_{act} / \text{kJ mol}^{-1}$	116.71	108.81	106.80
$\therefore \delta_m \Delta H^\ddagger / \text{kJ mol}^{-1}$		-7.9	-9.91
$\delta_m(\text{IS}) / \text{kJ mol}^{-1}$		+6.4	-0.1
$\therefore \delta_m(\text{TS}) / \text{kJ mol}^{-1}$		-1.5	-10.01

* Calculated from the solubilities of Mo(CO)₄btz in the solvents: DMSO, $2.41 \times 10^{-2} \text{ mol dm}^{-3}$; MeCN, $3.34 \times 10^{-3} \text{ mol dm}^{-3}$; MeOH, $2.33 \times 10^{-2} \text{ mol dm}^{-3}$.

^a: UNCERTAINTY IN ENTHALPIES OF SOLUTION ARE $\pm 5\%$

Table 7

Ground state-excited state analysis (H) for PNA.

	Toluene	MeCN	MeOH
$\Delta H_{\text{sol}} / \text{kJ mol}^{-1}$	+19.57	+21.1	+22.86
$\therefore \delta_m(\text{GS}) / \text{kJ mol}^{-1}$		+1.53	+3.29
$\Delta E_{\text{ct}} / \text{kJ mol}^{-1}$	+392.3	+386.5	+389.6
$\delta_m \Delta E_{\text{ct}} / \text{kJ mol}^{-1}$		-5.8	-2.7
$\therefore \delta_m(\text{ES}) / \text{kJ mol}^{-1}$		-4.27	+0.59

Table 8

Ground state-excited state analysis (H) DMIA.

	Toluene	MeCN	MeOH
$\Delta H_{\text{sol}} / \text{kJ mol}^{-1}$	+23.91	+25.76	+26.38
$\therefore \delta_m(\text{GS}) / \text{kJ mol}^{-1}$		+1.85	+2.47
$\Delta E_{\text{ct}} / \text{kJ mol}^{-1}$	+207.6	+203.8	+195.4
$\delta_m \Delta E_{\text{ct}} / \text{kJ mol}^{-1}$		-3.8	-12.2
$\therefore \delta_m(\text{ES}) / \text{kJ mol}^{-1}$		-1.95	-9.73

A schematic representation of $\text{Mo}(\text{CO})_4\text{btz}$ to be used in conjunction with tables 9 and 10.

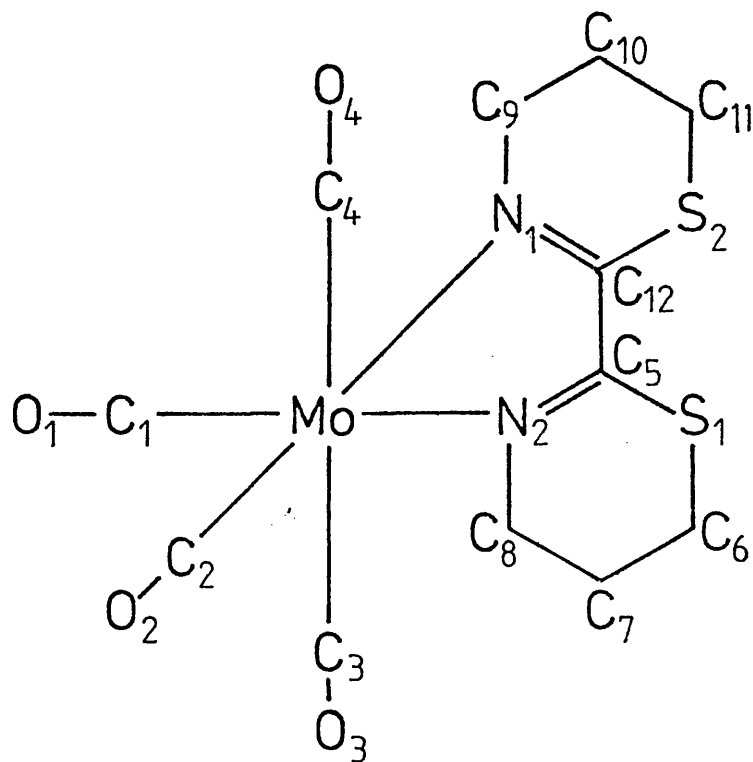


Table 9

Bond angles (°) of Mo(CO)₄btz.

N(2)-MO-N(1)	71.9(0.1)
C(1)-MO-N(1)	96.4(0.1)
C(1)-MO-N(2)	166.7(0.1)
C(2)-MO-N(1)	170.8(0.1)
C(2)-MO-N(2)	101.5(0.1)
C(2)-MO-C(1)	90.8(0.2)
C(3)-MO-N(1)	103.0(0.1)
C(3)-MO-N(2)	90.2(0.1)
C(3)-MO-C(1)	86.2(0.2)
C(3)-MO-C(2)	83.1(0.2)
C(4)-MO-N(1)	90.8(0.1)
C(4)-MO-N(2)	99.1(0.1)
C(4)-MO-C(1)	87.1(0.2)
C(4)-MO-C(2)	83.9(0.1)
C(4)-MO-C(3)	165.3(0.1)
C(6)-S(1)-C(5)	102.0(0.2)
C(12)-S(2)-C(11)	101.5(0.2)
C(9)-N(1)-MO	121.1(0.2)
C(12)-N(1)-MO	117.0(0.2)
C(12)-N(1)-C(9)	121.2(0.3)
C(5)-N(2)-MO	117.8(0.2)
C(8)-N(2)-MO	120.4(0.2)
C(8)-N(2)-C(5)	121.0(0.3)
O(1)-C(1)-MO	176.7(0.4)
O(2)-C(2)-MO	178.8(0.3)
O(3)-C(3)-MO	169.5(0.3)
O(4)-C(4)-MO	169.5(0.4)
N(2)-C(5)-S(1)	128.9(0.3)
C(12)-C(5)-S(1)	115.2(0.2)
C(12)-C(5)-N(2)	115.8(0.3)
H(61)-C(6)-S(1)	108.8(0.1)
H(62)-C(6)-S(1)	108.8(0.2)
H(62)-C(6)-H(61)	109.5
C(7)-C(6)-S(1)	112.0(0.3)
C(7)-C(6)-H(61)	108.8(0.2)
C(7)-C(6)-H(62)	108.8(0.2)
H(71)-C(7)-C(6)	108.9(0.2)
H(72)-C(7)-C(6)	108.9(0.2)
H(72)-C(7)-H(71)	109.5
C(8)-C(7)-C(6)	111.8(0.4)
C(8)-C(7)-H(71)	108.9(0.2)
C(8)-C(7)-H(72)	108.9(0.2)
C(7)-C(8)-N(2)	115.9(0.3)
H(81)-C(8)-N(2)	107.9(0.2)
H(81)-C(8)-C(7)	107.9(0.2)
H(82)-C(8)-N(2)	107.8(0.2)
H(82)-C(8)-C(7)	107.8(0.2)
H(82)-C(8)-H(81)	109.5
H(91)-C(9)-N(1)	108.0(0.2)
H(92)-C(9)-N(1)	108.0(0.2)
H(92)-C(9)-H(91)	109.5
C(10)-C(9)-N(1)	115.4(0.3)
C(10)-C(9)-H(91)	108.0(0.2)
C(10)-C(9)-H(92)	108.0(0.2)
H(101)-C(10)-C(9)	109.0(0.2)

Table 9 cont.

H(102)-C(10)-C(9)	109.0(0.2)
H(102)-C(10)-H(101)	109.5
C(11)-C(10)-C(9)	111.4(0.3)
C(11)-C(10)-H(101)	109.0(0.2)
C(11)-C(10)-H(102)	109.0(0.2)
C(10)-C(11)-S(2)	111.6(0.3)
H(111)-C(11)-S(2)	109.0(0.1)
H(111)-C(11)-C(10)	109.0(0.2)
H(112)-C(11)-S(2)	108.9(0.2)
H(112)-C(11)-C(10)	108.9(0.2)
H(112)-C(11)-H(111)	109.5
N(1)-C(12)-S(2)	129.2(0.2)
C(5)-C(12)-S(2)	114.5(0.2)
C(5)-C(12)-N(1)	116.3(0.3)

Table 10

Bond lengths (Å) of Mo(CO)₄btz.

MO-N(1)	2.252(3)
MO-N(2)	2.253(3)
MO-C(1)	1.966(4)
MO-C(2)	1.954(3)
MO-C(3)	2.028(4)
MO-C(4)	2.035(4)
S(1)-C(5)	1.751(3)
S(1)-C(6)	1.800(4)
S(2)-C(11)	1.808(4)
S(2)-C(12)	1.745(3)
N(1)-C(9)	1.476(4)
N(1)-C(12)	1.298(4)
N(2)-C(5)	1.284(4)
N(2)-C(8)	1.480(4)
O(1)-C(1)	1.170(5)
O(2)-C(2)	1.158(4)
O(3)-C(3)	1.144(5)
O(4)-C(4)	1.143(5)
C(5)-C(12)	1.498(4)
C(6)-H(61)	1.080
C(6)-H(62)	1.080
C(6)-C(7)	1.499(6)
C(7)-H(71)	1.080
C(7)-H(72)	1.080
C(7)-C(8)	1.528(5)
C(8)-H(81)	1.080
C(8)-H(82)	1.080
C(9)-H(91)	1.080
C(9)-H(92)	1.080
C(9)-C(10)	1.522(5)
C(10)-H(101)	1.080
C(10)-H(102)	1.080
C(10)-C(11)	1.521(6)
C(11)-H(111)	1.080
C(11)-H(112)	1.080

Figure 1 Ground state-excited state analysis for the solvatochromism of $\text{Mo}(\text{CO})_4\text{btz}$.

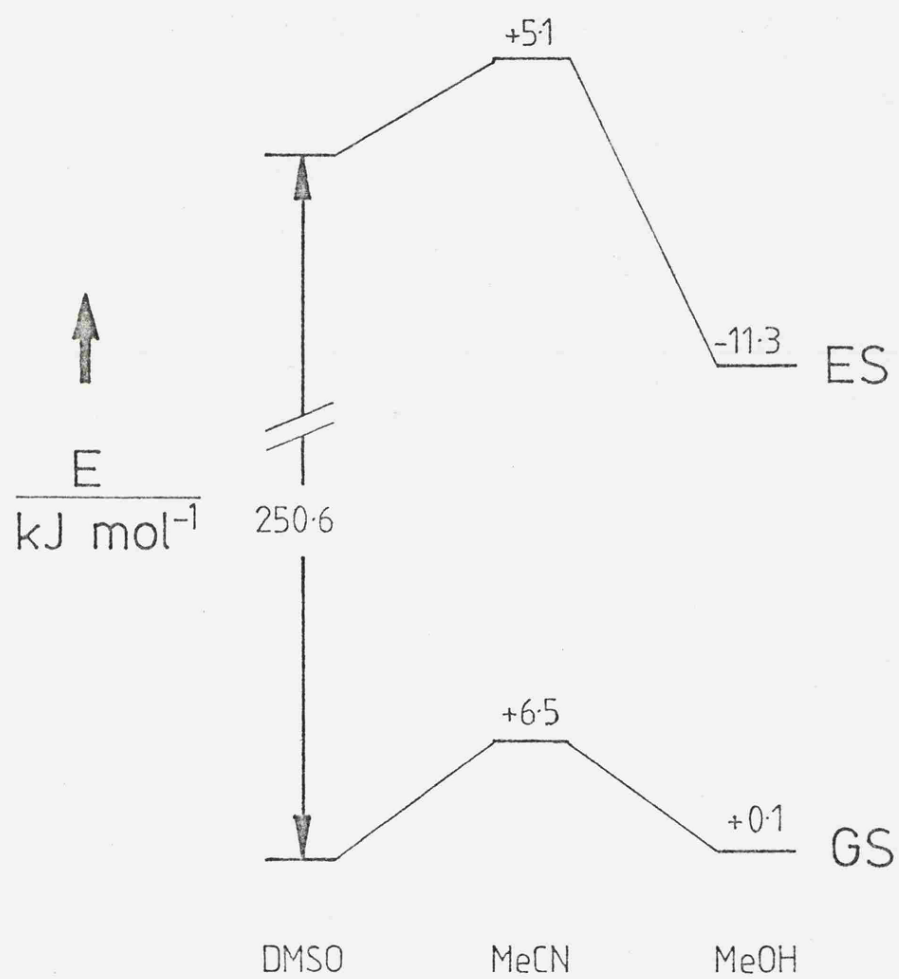


Figure 2 Ground state-excited state analysis for the solvatochromism of PNA.

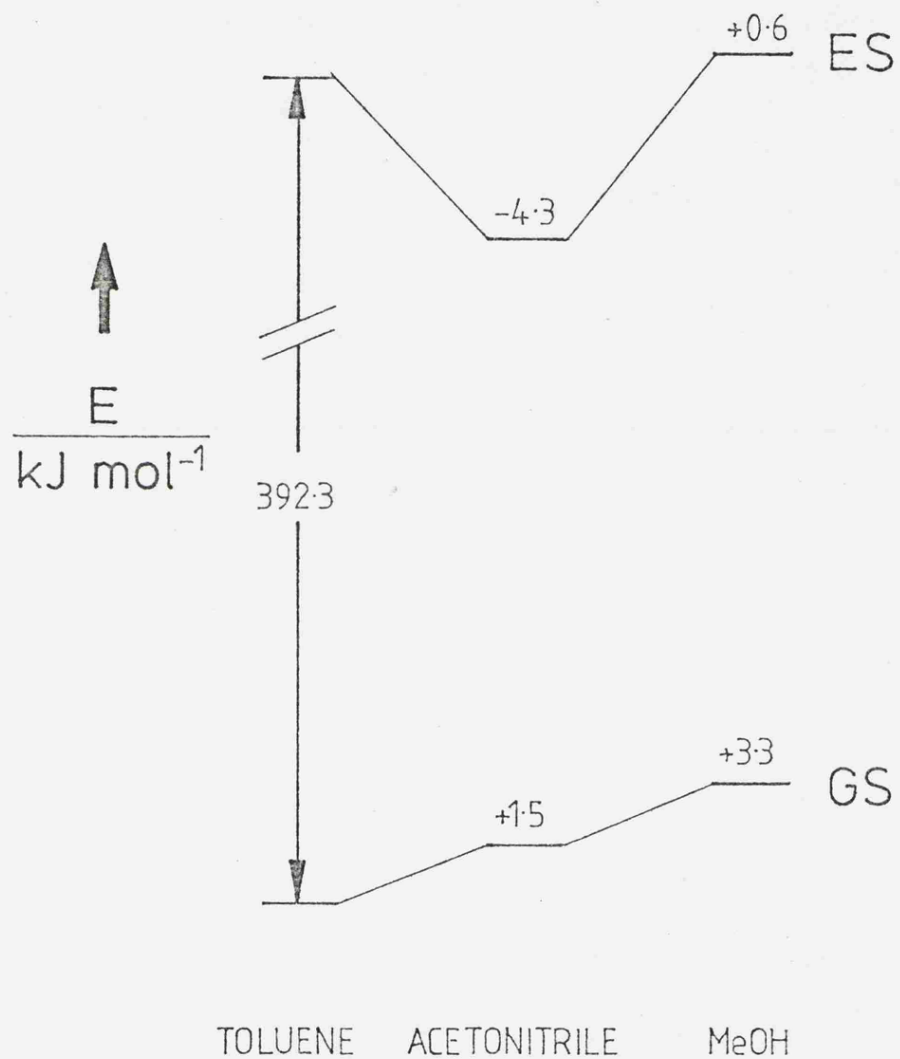


Figure 3 Ground state-excited state analysis for the solvatochromism of DMIA.

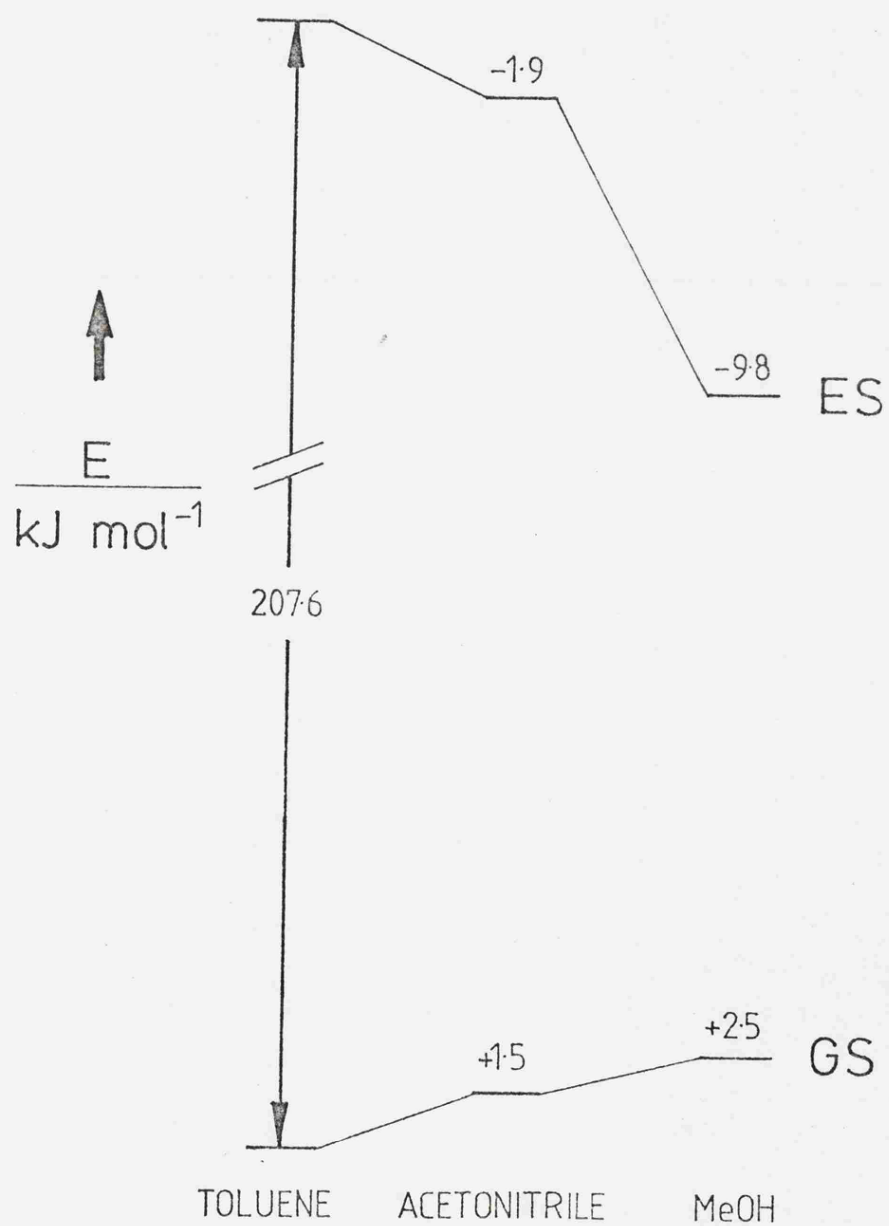


Figure 4 Initial state-transition state analysis (G) for the solvolysis of $\text{Mo}(\text{CO})_4\text{btz}$.

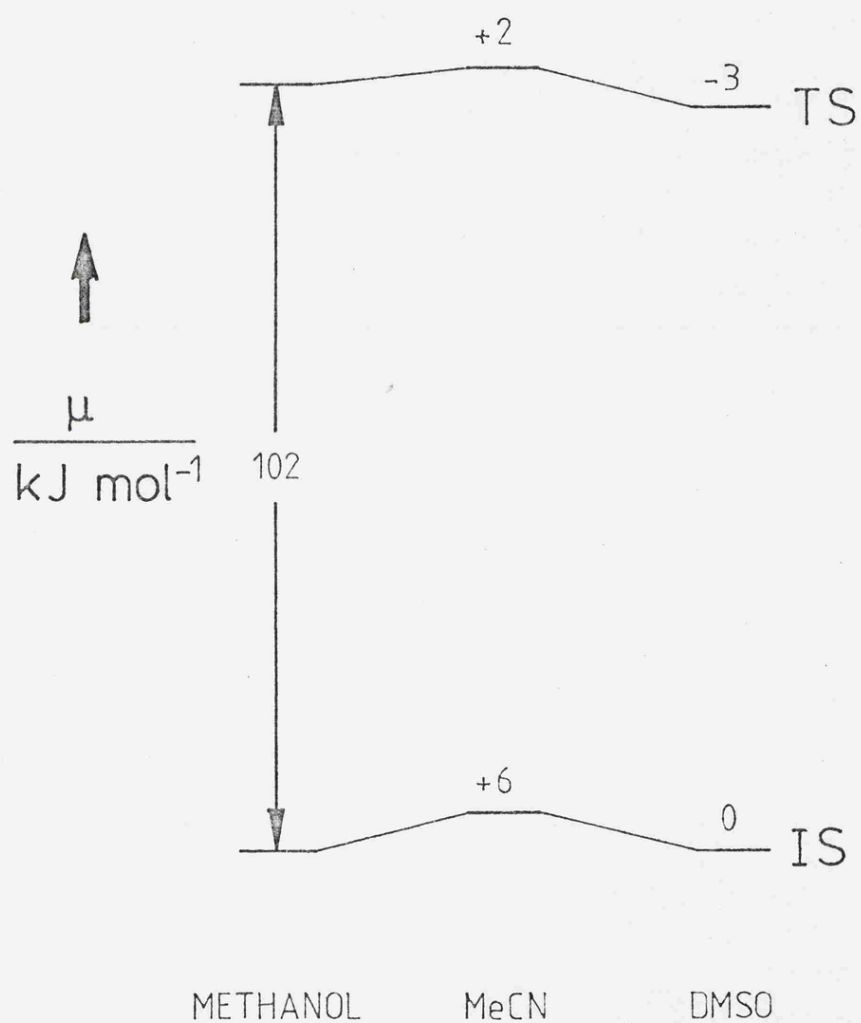


Figure 5 Initial state-transition state analysis (H) for the solvolysis of $\text{Mo}(\text{CO})_4\text{btz}$.

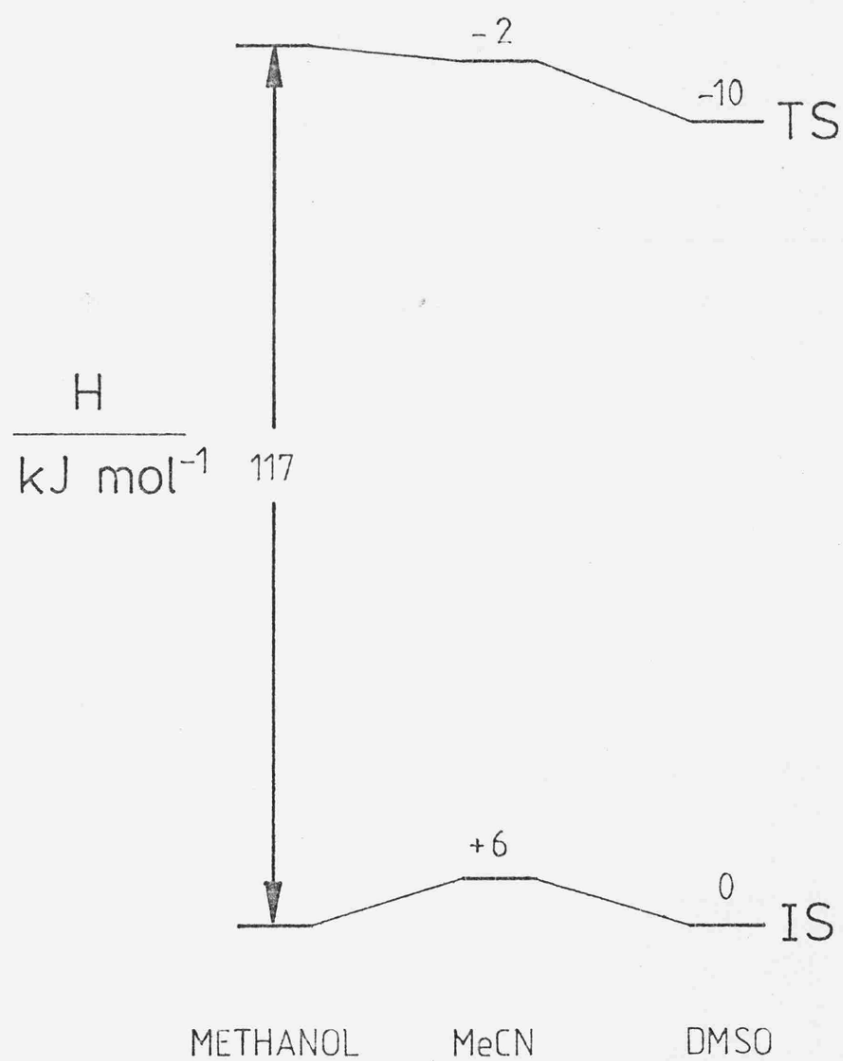


Figure 6 The effect of temperature on the uv/vis spectrum of $\text{Mo}(\text{CO})_4\text{btz}$ in methanol.

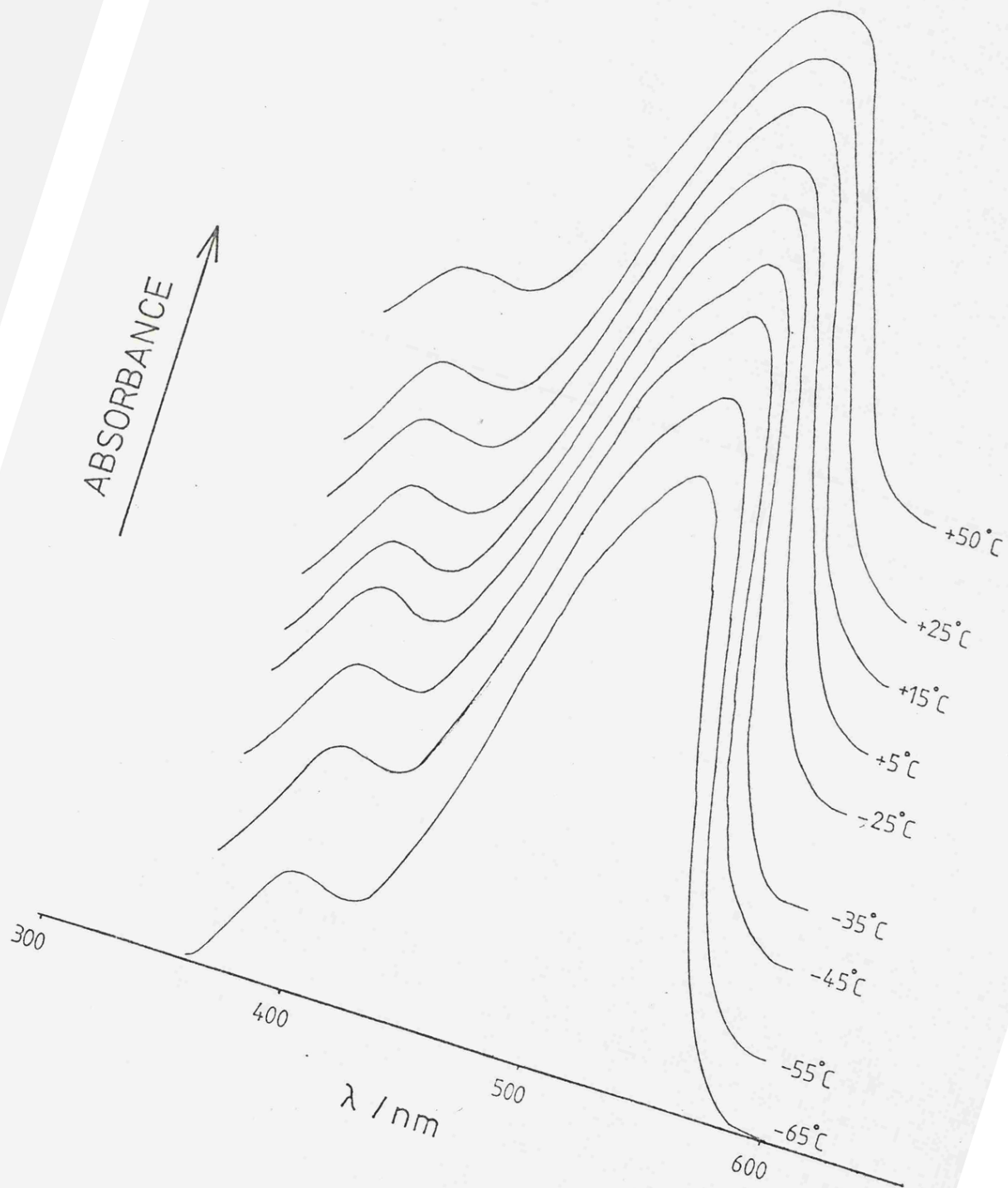


Figure 7 Stereo pair for $\text{Mo}(\text{CO})_4\text{btz}$.

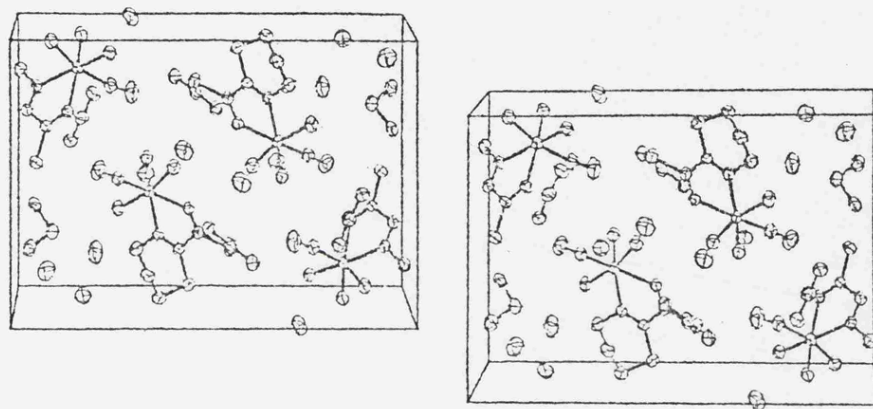


Figure 8(1) The structure of $\text{Mo}(\text{CO})_4\text{btz}$.

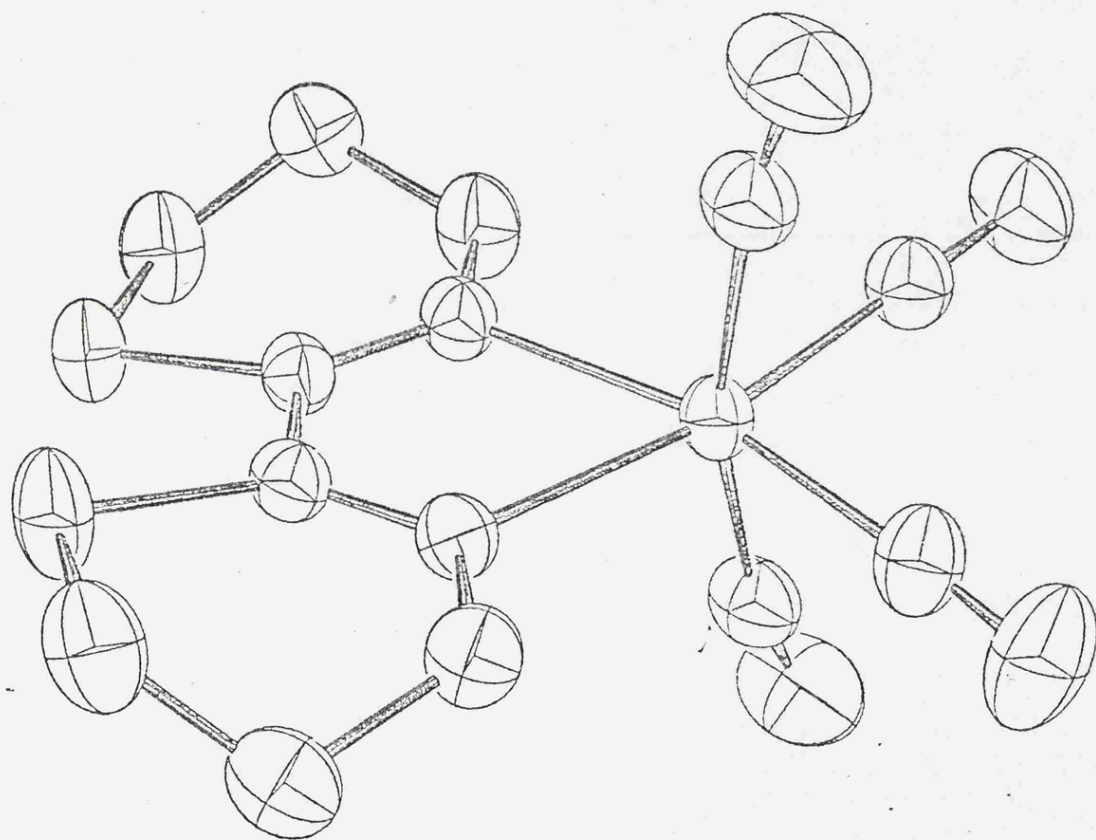


Figure 3(2) The structure of $\text{Mo}(\text{CO})_4\text{btz}$.

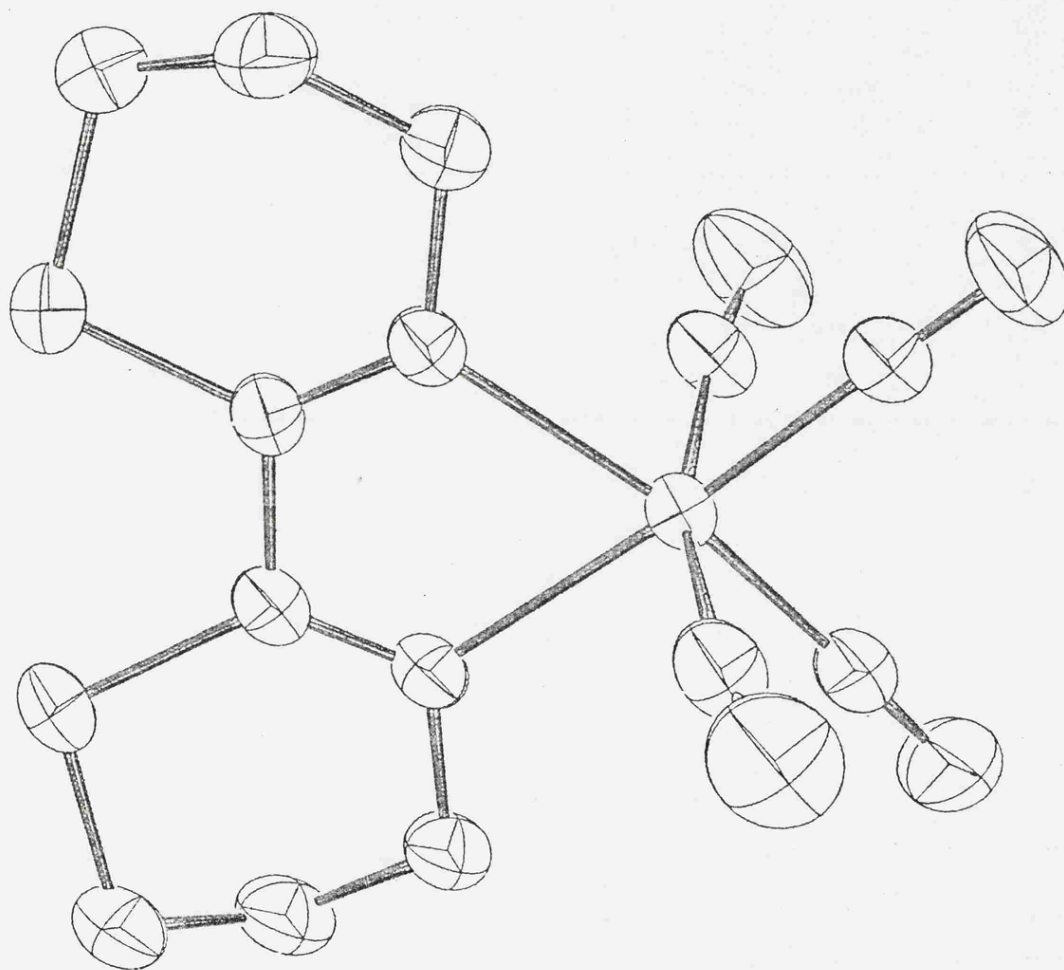


Figure 8(3) The structure of $\text{Mo}(\text{CO})_4\text{btz}$.

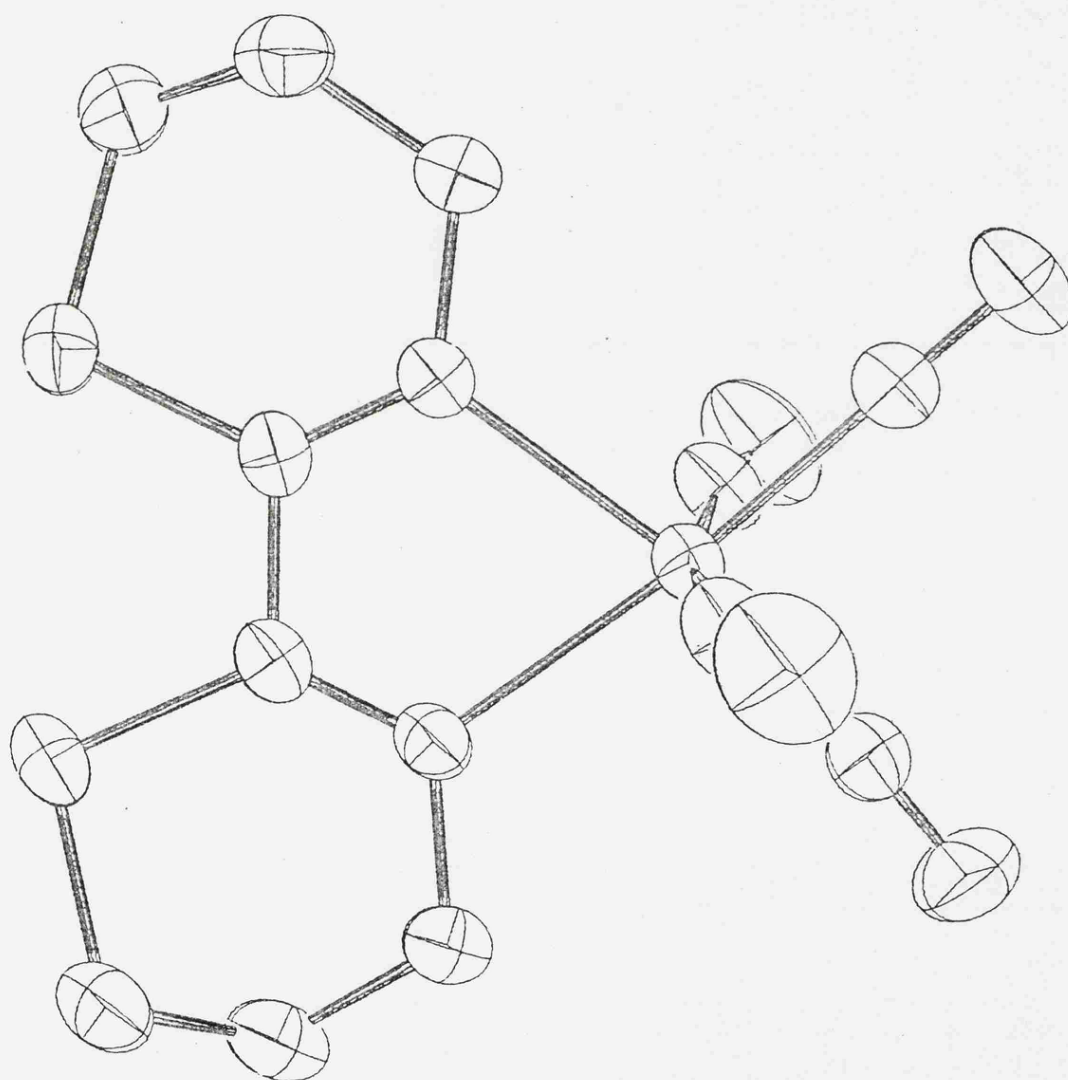


Figure 9 Initial state-transition state analysis (G) for the solvolysis of $\text{Mo}(\text{CO})_4\text{bipy}$.

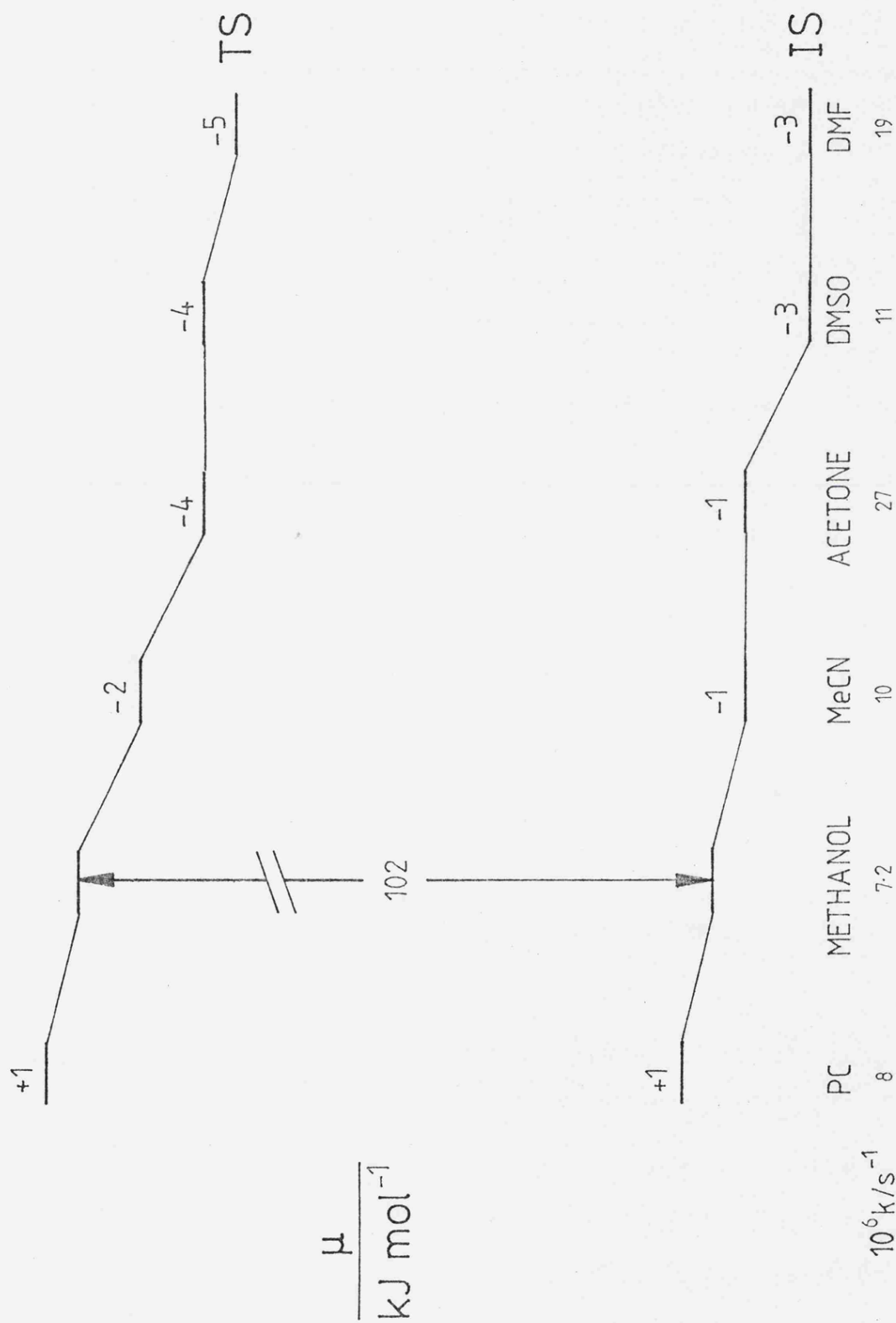


Figure 10 The solvatochromism of $\text{Mo(CO)}_4\text{btz}$.



1

2

3

4

1 ACETONITRILE

2 PHENETOLE

3 CHLOROFORM

4 CARBON TETRACHLORIDE

Figure 11 (see overleaf) Variation in $\tilde{\nu}_{\max}$ (cm^{-1}) for $\text{Mo}(\text{CO})_4\text{btz}$ and solvent $E_{\text{T}}(30)$ values.

The numbers refer to the solvents listed below:

1. DMF
2. Chloroform
3. DMSO
4. Acetone
5. Isopropanol
6. Ethanol
7. Methanol
8. Carbon tetrachloride
9. n-Propanol
10. n-Butanol
11. Diethylether
12. Anisole
13. Phenetole
14. Benzyl alcohol
15. Acetophenone
16. Chlorobenzene
17. Ethyl methyl ketone
18. Cyclohexanone
19. Ethyl bromide

For Figures 13 and 14 the numbers refer to the solvents listed below:

- | | |
|-----------------|--------------------------|
| 1. Methanol | 8. Chlorobenzene |
| 2. Ethanol | 9. Diethylether |
| 3. n-Propanol | 10. Carbon tetrachloride |
| 4. n-Butanol | 11. Nitromethane |
| 5. Isopropanol | 12. Dichloromethane |
| 6. Acetonitrile | 13. Benzene |
| 7. Acetone | 14. t-Butanol |

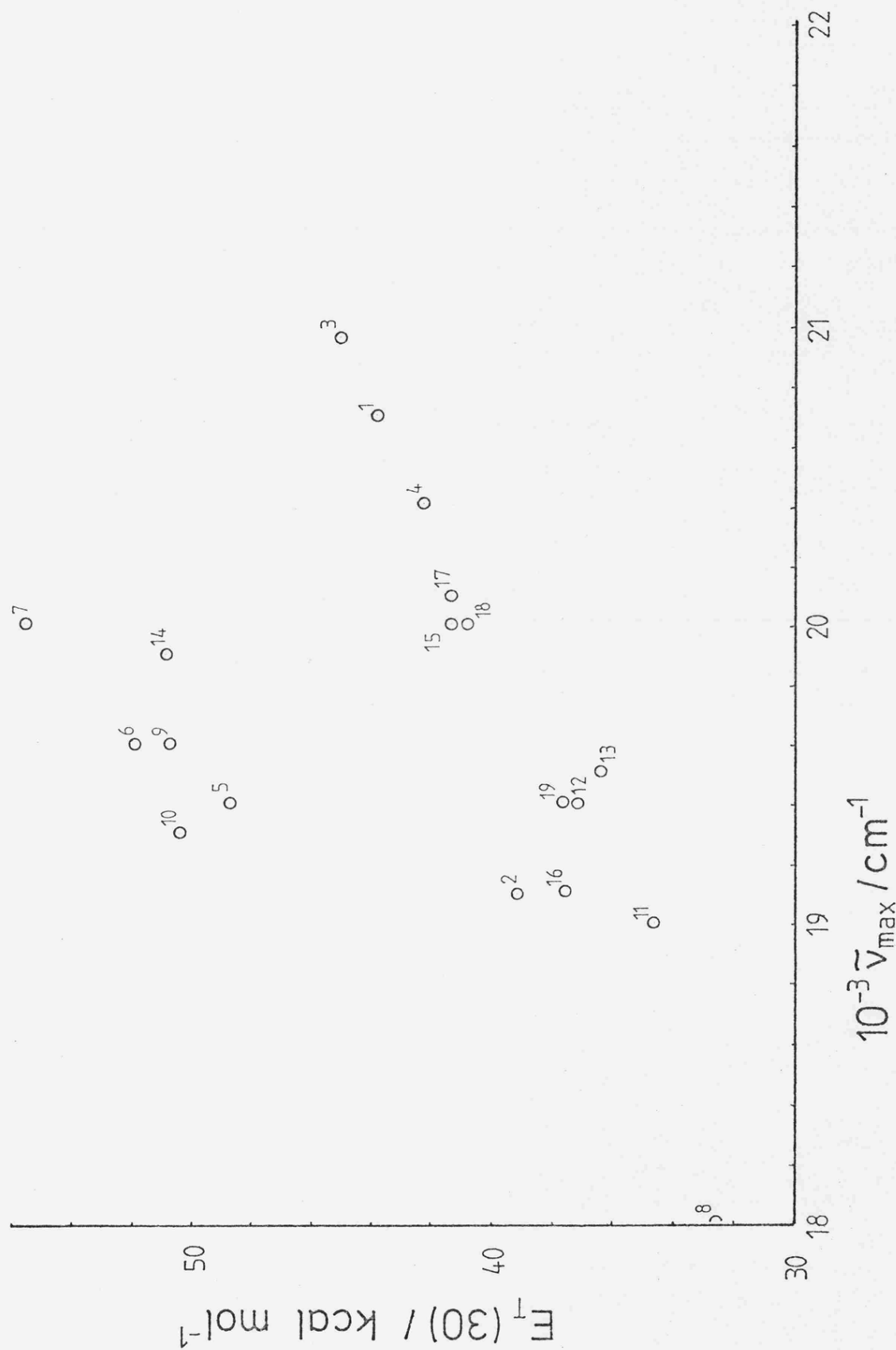
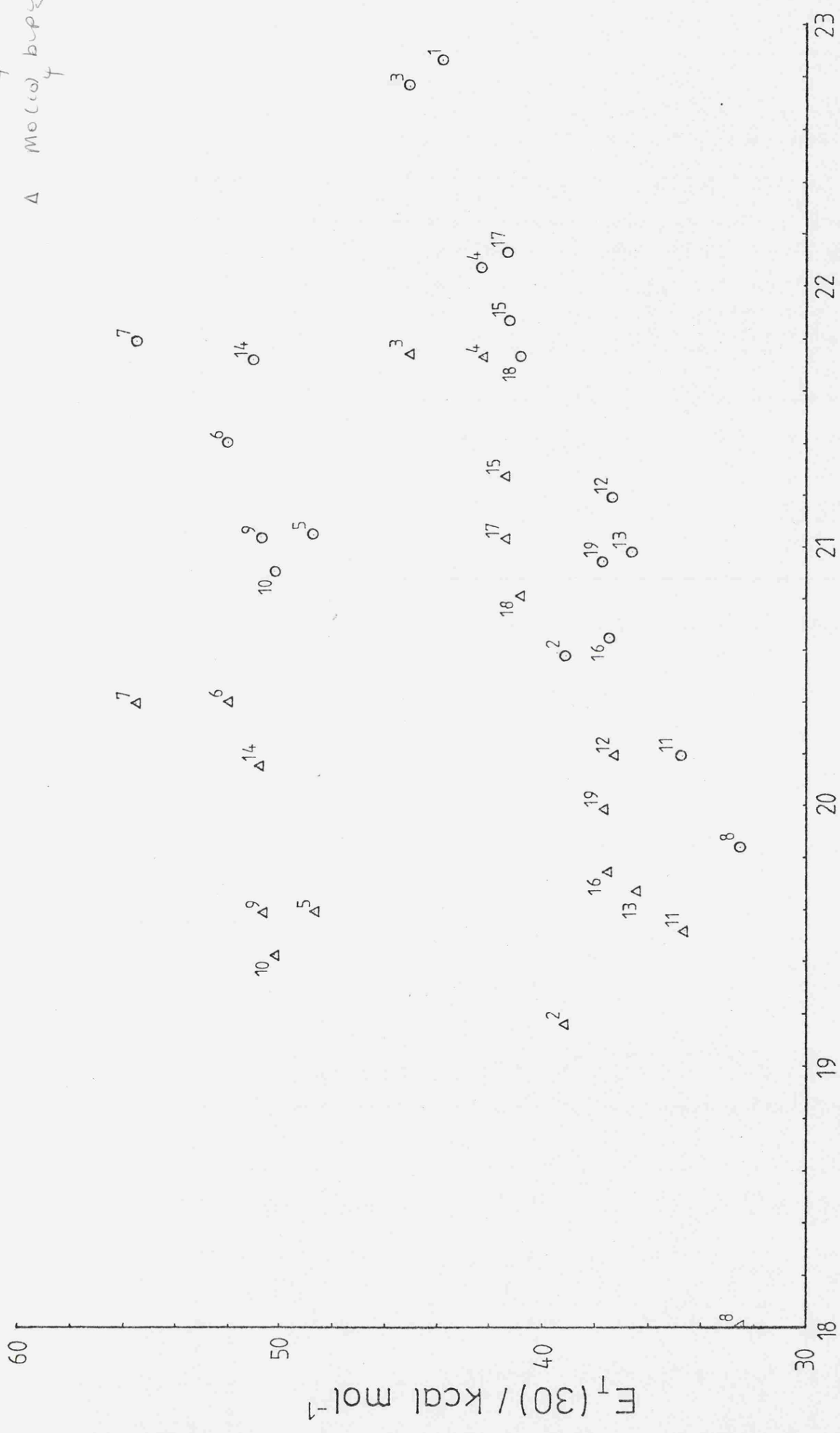


Figure 12 (see overleaf) Variation in ν_{\max} (cm^{-1}) for $\text{Mo}(\text{CO})_4\text{bipy}$ and $\text{Mo}(\text{CO})_4\text{bipym}$ with the solvent parameter $E_T(30)$.

The numbers refer to the solvents listed below:

1. DMF
2. Chloroform
3. DMSO
4. Acetone
5. Isopropanol
6. Ethanol
7. Methanol
8. Carbon tetrachloride
9. n-Propanol
10. n-Butanol
11. Diethylether
12. Anisole
13. Phenetole
14. Benzyl alcohol
15. Acetophenone
16. Chlorobenzene
17. Ethyl methyl ketone
18. Cyclohexanone
19. Ethyl bromide

○ Mol(10) bupg
 △ Mol(10) bupgm



$10^{-3} \tilde{\nu}_{\max} / \text{cm}^{-1}$

$F_1(30) / \text{kcal mol}^{-1}$

Figure 13 Plot of λ_{\max} Mo(CO)₄bipy versus λ_{\max} Mo(CO)₄btz.
 The numbers refer to the solvents as listed on
 page 158

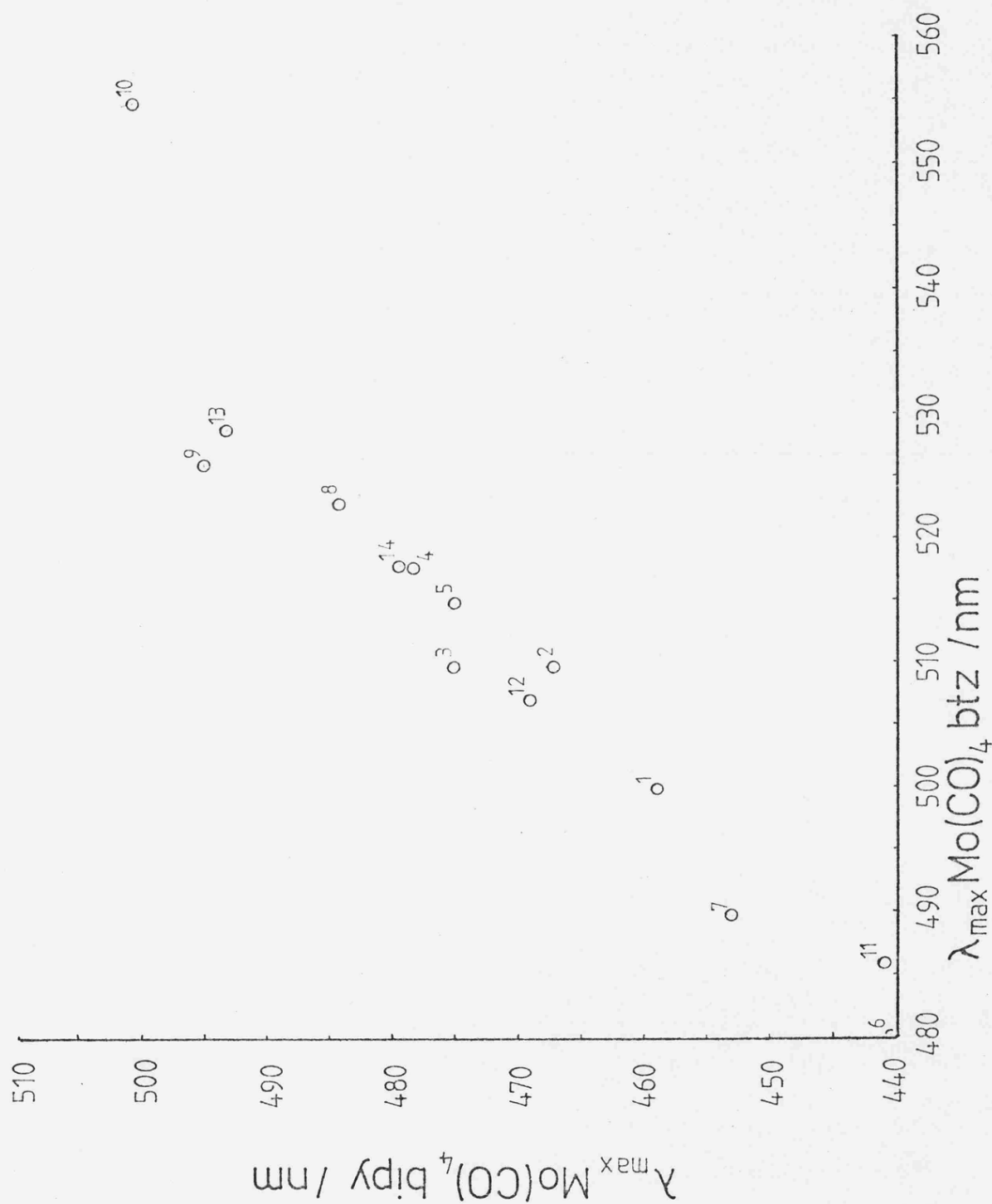


Figure 14 Plot of λ_{\max} Mo(CO)₄bipy versus λ_{\max} Fe(btz)₂(CN)₂.
 The numbers refer to the solvents as listed for Fig.11.

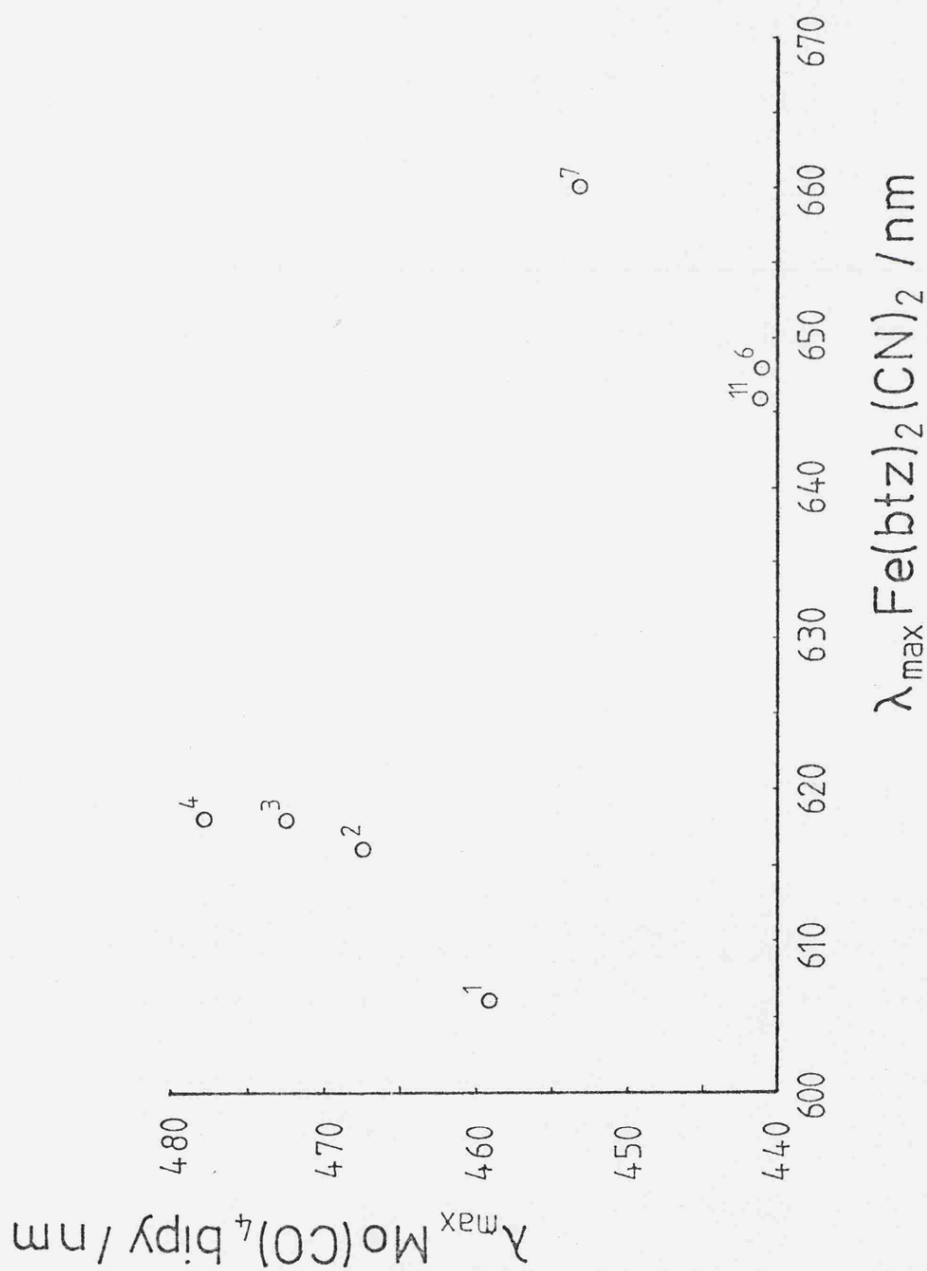
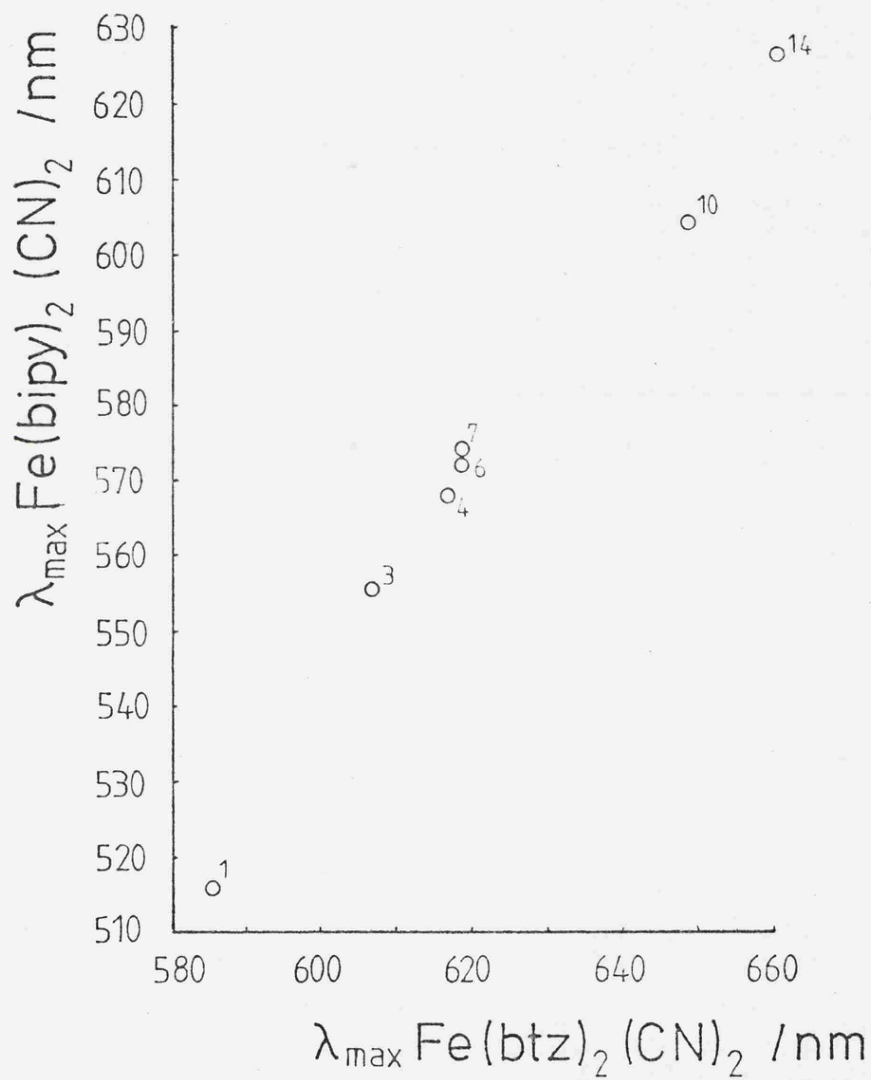


Figure 15 Plot of λ_{\max} $\text{Fe}(\text{bipy})_2(\text{CN})_2$ versus λ_{\max} $\text{Fe}(\text{btz})_2(\text{CN})_2$.

The numbers refer to the solvents listed below.



1. Water
3. Methanol
4. Ethanol
6. n-Propanol
7. n-Butanol
10. Acetonitrile
14. Acetone

Figure 16 Schematic qualitative representation of the solvent effects on the electronic transition energy of dipolar solutes in polar solvents.

a) $\mu_{g.s.} < \mu_{e.s.}$ b) $\mu_{g.s.} > \mu_{e.s.}$

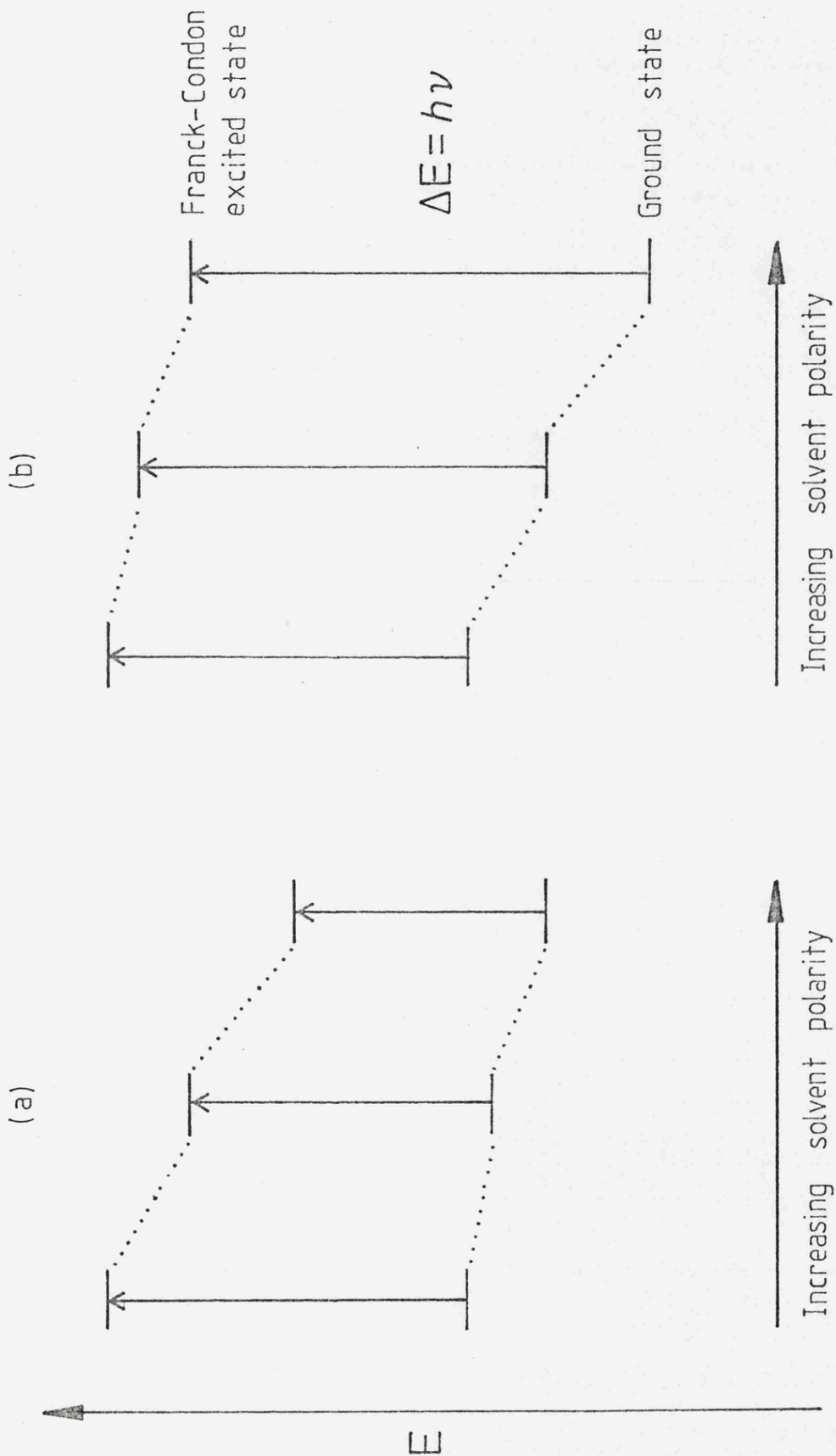
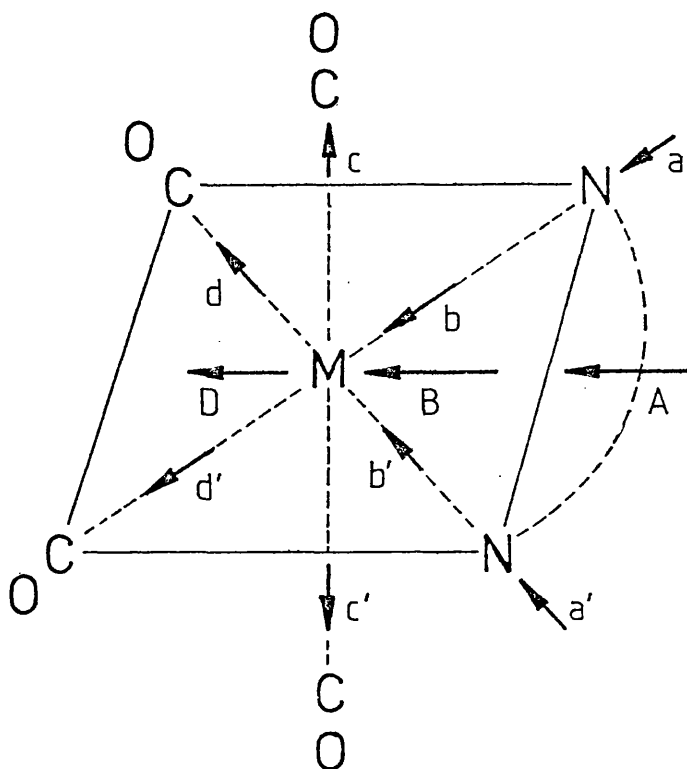


Figure 17. Distribution of dipoles in $M(\text{CO})_4\text{LL}$ complexes
 (M = Cr, Mo, W; LL= diimine).



\vec{a}, \vec{a}' : Dipole moment of the ligand

$\vec{A} = \vec{a} + \vec{a}'$; en, $\approx 6.6 \times 10^{-30}$ Cm; bipy, phen $\approx 1.2 \times 10^{-29}$ Cm

\vec{b}, \vec{b}' : nitrogen to metal ($\overrightarrow{\text{N-M}}$)

$\vec{B} = \vec{b} + \vec{b}'$; $1.7-2.1 \times 10^{-29}$ Cm

\vec{c}, \vec{c}' : metal to carbonyl (trans) ($\overrightarrow{\text{M-CO}}$)

$|\vec{c}| = |\vec{c}'|$; $1.7-2.7 \times 10^{-30}$ Cm

\vec{d}, \vec{d}' : metal to carbonyl (cis) ($\overrightarrow{\text{M-CO}}$)

$\vec{D} = \vec{d} + \vec{d}'$; $2.3-3.7 \times 10^{-30}$ Cm

References Chapter 5

1. See for example M.J.Kamlet and P.W.Taft, *J.Org.Chem.*, 47, 1734 (1982) and refs. therein; B.Eliasson, D.Johnels, S.Wold and V.Edlund, *Acta.Chem.Scand.*, B36, 155 (1982); M.Chastrette and J.Carretto, *Tet.*, 38, 1615 (1982)
2. P.Suppan, *Nouv.J.Chemie*, 6, 285 (1982)
3. D.A.Tomalia and J.N.Paige, *J.Org.Chem.*, 38, 3949 (1973)
4. J.Nelson, S.M.Nelson and W.D.Perry, *J.C.S.Dalton*, 1976, 1282
5. D.J.Darensbourg and R.L.Kump, *Inorg.Chem.*, 17, 2680 (1978)
6. L.W.Houk and G.R.Dobson, *Inorg.Chem.*, 5, 2119 (1966)
7. H.H.Willard, L.L.Merritt, J.A.Dean and F.A.Settle, *Instrumental methods of analysis*, 6ed., Van Nostrand, N.Y. 1981, Chaps, 2 and 3.
8. N.G.M.Pay, Ph.D. thesis (1981) University of Leicester
9. M.H.B.Stiddard, *J.Chem.Soc.*, 1962, 4712
10. M.J.Blandamer, J.Burgess, J.G.Chambers and A.J.Duffield, *Trans.Met.Chem.*, 6, 156 (1981)
11. J.Burgess, J.G.Chambers and R.I.Haines, *Trans.Met.Chem.*, 6, 145 (1981)

12. J.Burgess, Spectrochim.Acta, 26A, 1369 (1969)
13. E.G.McRae, J.Phys.Chem., 61, 562 (1957)
14. H.Saito, J.Fujita and K.Saito, Bull.Chem.Soc.Jap.,
41, 863 (1968)
15. A.J.Parker and D.Brody, J.Chem.Soc., 1963, 4061
16. P.W.Vittum and G.H.Brown, J.Am.Chem.Soc., 68, 2235
(1946)
17. P.Haberfield, J.Am.Chem.Soc., 96, 6526 (1974);
P.Haberfield and M.S.Lux, J.Am.Chem.Soc., 99, 6828
(1977)
18. K.Dimroth, C.Reichardt and A.Schweig, Liebigs.Ann.
Chem. 669, 95 (1963)
19. H.A.Staab, Einführung in die Theoretische Organische
Chemie, Verlag Chemie, Weinheim (1959)
20. See for example Jaffé and Orchin, "Theory and
Applications of Ultraviolet Spectroscopy", John Wiley
and Sons, 1962

CHAPTER SIX:

The reactions between $\text{Mo}(\text{CO})_4\text{btz}$ and L
(L = HgCl_2 , Hg^{2+} , In^{3+} , Cd^{2+} , $\text{Mo}(\text{CO})_4(\text{pip})_2$,
 PtCl_4^{2-} , PtCl_2 , MeI , PPh_3 , $\text{P}(\text{OPh})_3$, bipy).
The reactions between $\text{Mo}(\text{CO})_4(\text{pip})_2$ and R
(R = btz , dt , ($\text{btz} + \text{phen}$), PtCl_2btz). The
reaction between $\text{Mo}(\text{CO})_4(\text{PPh}_3)_2$ and btz .
The preparation of PtCl_2btz . The reaction
between $\text{Mo}(\text{CO})_4\text{dt}$ and btz .

Introduction

In the previous chapter some aspects of the chemistry of $\text{Mo}(\text{CO})_4\text{btz}$ were discussed; this chapter is concerned with developing this chemistry.

There are two broad areas of interest: the possibility of using the aliphatic sulphur atoms of the btz ligand for metalation and methylation reactions; an investigation into various synthetic routes of $\text{Mo}(\text{CO})_4\text{btz}$, making a detailed kinetic analysis where possible.

These compounds have the advantage of being non-electrolytes, thus the problems of single ion values do not arise; this makes them particularly suited for initial state-transition state analysis.

The sulphur atoms on btz can be classified as "soft"¹, and so it is of interest to see whether these react with "soft" metals to form binuclear complexes and to examine the stability, and solvatochromic behaviour of any such complexes. There is also the possibility that these binuclear complexes might decompose to form new btz complexes.

Experimental

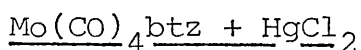
$\text{Mo}(\text{CO})_4\text{btz}$ ², $\text{Mo}(\text{CO})_4(\text{PPh}_3)_2$ ³, $\text{Mo}(\text{CO})_4(\text{dithiane})$ ⁴, $\text{Mo}(\text{CO})_4(\text{pip})_2$ ³ were prepared as described previously. Reaction of $\text{Mo}(\text{CO})_4\text{btz}$ with HgCl_2 , HgClO_4 , PtCl_2 , K_2PtCl_4 , $\text{P}(\text{OPh})_3$, AgNO_3 , PPh_3 , MeI , $\text{In}_2(\text{SO}_4)_3$ and $\text{CdSO}_4 \cdot 8/3\text{H}_2\text{O}$.

Generally these reactions were performed in a suitable solvent, on a 1:1 stoichiometric ratio as summarised in

table 1.

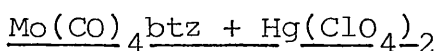
The other reactions were 1:1 stoichiometric ratios in suitable solvents, and are summarised in table 2.

Results

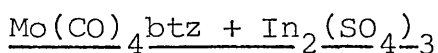


The characteristic colour of a methanolic solution of $\text{Mo(CO)}_4\text{btz}$ changed to a bright, blood red colour. A precipitate was observed and could be isolated as a bright red solid. Its uv/vis spectrum in methanol was different from that of $\text{Mo(CO)}_4\text{btz}$. Addition of toluene to this solution did not alter the uv/vis spectrum appreciably. When toluene is added to a methanol solution of $\text{Mo(CO)}_4\text{btz}$, a spectral change is observed, consistent with its solvatochromic behaviour.

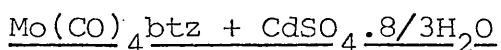
The colour of the blood red solution would fade within thirty minutes, resulting in a brown solution.



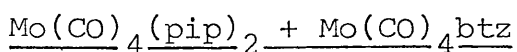
The original red solution became colourless within a few minutes, and a yellow precipitate was observed.



There was no observable change of the solution; uv/vis spectrum remained unchanged.

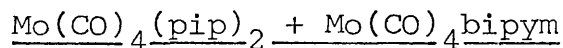


There was no observable change; uv/vis spectrum showed no evidence for complex formation.

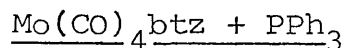


Uv/vis spectrum showed no evidence for complex formation:

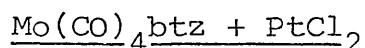
$\text{Mo(CO)}_4\text{btz}$ was still present, and $\text{Mo(CO)}_4(\text{pip})_2$ appeared to have solvolysed.



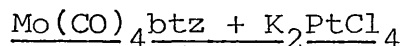
The uv/vis spectrum indicated the presence of $\text{Mo(CO)}_4(\text{pip})_2$ and $\text{Mo(CO)}_4\text{bipym}$ only. There was no evidence for $[\text{Mo(CO)}_4]_2\text{bipym}$.



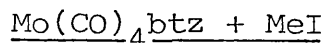
At room temperature no reaction occurred. At reflux temperature $\text{Mo(CO)}_3(\text{PPh}_3)\text{btz}$ was isolated.



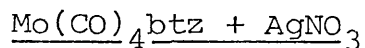
Although a change in the colour of the solution was observed, no spectral changes could be detected.



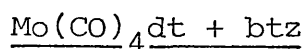
The solution became colourless very quickly, with the formation of a white precipitate.



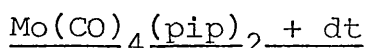
The uv/vis spectrum of a solution of $\text{Mo(CO)}_4\text{btz}$ in methyl iodide showed no change over several days.



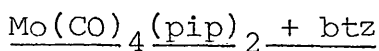
The solution rapidly became colourless with the formation of a brown precipitate.



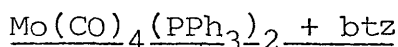
$\text{Mo(CO)}_4\text{btz}$ was formed, as characterised by uv/vis spectroscopy.



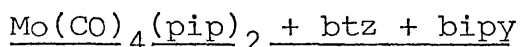
No reaction was observed other than decomposition of starting material; no $\text{Mo(CO)}_4\text{dt}$ was formed.



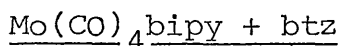
There was rapid formation of $\text{Mo(CO)}_4\text{btz}$.



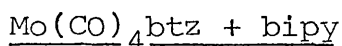
$\text{Mo(CO)}_4\text{btz}$ was formed, but at a slower rate than the above.



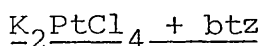
In a reaction mixture of 1:2:2 stoichiometry ($\text{Mo}:\text{btz}:\text{bipy}$), $\text{Mo(CO)}_4\text{btz}$ was the major product with very little $\text{Mo(CO)}_4\text{bipy}$. By increasing the quantity of bipy relative to the other two, then $\text{Mo(CO)}_4\text{bipy}$ was the major product.



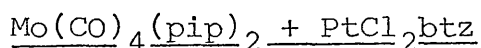
There was no evidence for the formation of $\text{Mo(CO)}_4\text{btz}$.



There was no evidence for the formation of $\text{Mo(CO)}_4\text{bipy}$.



The reaction between K_2PtCl_4 and btz resulted in an olive green solid, PtCl_2btz as confirmed by elemental analysis. The solid was not soluble in the common organic solvents. It was soluble in DMSO but it reacted with the solvent.



No reaction between $\text{Mo(CO)}_4(\text{pip})_2$ and PtCl_2btz could be observed. The uv/vis spectrum indicated $\text{Mo(CO)}_4(\text{pip})_2$ and the slow solvolysis of PtCl_2btz .

Discussion

The reaction between $\text{Mo(CO)}_4\text{btz}$ and HgCl_2 resulted in a complex whose solvatochromic behaviour was different

from that of the parent compound. This complex may have been S-bonded to mercury as shown in Fig.1. The presence of chloride would help to stabilise such a complex.

Tetrahedral complexes of the type $(R_2S)_2HgCl_2$ are known⁵, the formation of a complex as shown in Fig.1 is an attractive possibility. However, $Mo(CO)_4bipy$ reacts with $HgCl_2$ resulting in similar spectral changes (Fig.3). This reaction yields $Mo^{II}(CO)_3bipyCl(HgCl)$ ⁶. Therefore $Mo(CO)_4btz$ would be expected to produce the analogous complex, $Mo^{II}(CO)_3btzCl(HgCl)$.

The similar reaction with $Hg(ClO_4)_2$ did not result in the S-bonded complex (Fig.2). Such a complex appears to be very unstable, and probably decomposes to a mercury btz complex, the fate of the $Mo(CO)_4$ moiety being unknown. Although Nelson has prepared several mercury btz complexes of the type HgX_2btz , the mode of co-ordination was not thoroughly investigated.

Extending these reactions to other soft metals, the reaction with $PtCl_2$ did not result in any observable complex; the main problem being the limited solubility of $PtCl_2$. The reaction between $Mo(CO)_4btz$ and K_2PtCl_4 in aqueous ethanol mixtures resulted in immediate precipitation of a gelatinous white solid.

No complex formation could be observed between $Mo(CO)_4btz$ and Cd^{2+} or In^{3+} ; there was no problem with solubility. There are very few sulphur complexes of indium, and cadmium's affinity for sulphur is less than that for mercury.

The reaction of $\text{Mo}(\text{CO})_4\text{btz}$ with AgNO_3 did not yield any complex, but resulted in decomposition of $\text{Mo}(\text{CO})_4\text{btz}$. Thus Hg^{2+} , PtCl_4^{2-} and Ag^+ react with $\text{Mo}(\text{CO})_4\text{btz}$ with very rapid precipitation. All precipitates were white/pale yellow, and this clearly indicates that $\text{Mo}(\text{CO})_4\text{btz}$ is no longer present. From the kinetic point of view precipitation is undesirable. For this reason the precipitates were not investigated further.

The reaction between $\text{Mo}(\text{CO})_4\text{btz}$ and MeI did not yield any complex. It would have been interesting to isolate a complex of the type shown in Fig.4. However, interaction between methyl groups may make the complex energetically unfavourable. There have been no reports of S-methylated 1,3 thiazines, and this appears to be a reflection of the stability of thiazines⁷.

Reactions between $\text{Mo}(\text{CO})_4\text{LL}$ and phosphines where LL is a bidentate ligand, are well known⁸. At room temperature triphenylphosphine does not react with $\text{Mo}(\text{CO})_4\text{btz}$. Under reflux conditions $\text{Mo}(\text{CO})_3(\text{PPh}_3)\text{btz}$ can be isolated. Using a stronger base, triphenylphosphite, at room temperature the analogous compound can be isolated: $\text{Mo}(\text{CO})_3\text{P}(\text{OPh})_3\text{btz}$. Kinetic studies have been done on the bipy^9 and phen^{10} systems; for the reaction between $\text{Mo}(\text{CO})_4\text{bipy}$ and triphenylphosphine complex kinetic patterns are obtained, and the product of the reaction is not $\text{Mo}(\text{CO})_3(\text{PPh}_3)\text{bipy}^{11}$. Under certain conditions $\text{Mo}(\text{CO})_4(\text{pyridine})_2$ reacts with PPh_3 to produce $\text{Mo}(\text{CO})_4(\text{PPh}_3)_2^{12}$.

$\text{Mo}(\text{CO})_4\text{btz}$ can be prepared very easily from a variety

of $\text{Mo}(\text{CO})_4\text{LL}$ derivatives. A very convenient route involves $\text{Mo}(\text{CO})_4(\text{pip})_2$ where the piperidines are very labile. Preliminary studies¹³ indicate that kinetics of formation of $\text{Mo}(\text{CO})_4\text{LL}$ (LL = bidentate diimine ligand) from $\text{Mo}(\text{CO})_4(\text{pip})_2$ is complex, involving at least two steps, with a fast first step (approx. 1s^{-1}).

$\text{Mo}(\text{CO})_4\text{btz}$ may also be prepared from $\text{Mo}(\text{CO})_4(\text{PPh}_3)_2$ and btz , although reaction rates are very much slower. The reaction between $\text{Mo}(\text{CO})_4(\text{PPh}_3)_2$ and 1,10-phen has been analysed in terms of initial state-transition state contributions¹⁴ (Fig.5). The reactions between $\text{Mo}(\text{CO})_4(\text{PPh}_3)_2$ and bidentate diimine ligands are believed to occur by a dissociative mechanism.

The lability of $\text{Mo}(\text{CO})_4(\text{pip})_2$ prompted attempts to prepare some multinuclear complexes. Thus, from the reaction between $\text{Mo}(\text{CO})_4(\text{pip})_2$ and $\text{Mo}(\text{CO})_4\text{btz}$ it was hoped to produce $\text{Mo}(\text{CO})_4\text{btz}(\text{CO})_4\text{Mo}$ (Fig.6), where the btz is both S and N bonded. No product could be isolated. Attempts to prepare the simple dithiane complex from $\text{Mo}(\text{CO})_4(\text{pip})_2$ were also unsuccessful. This strongly suggests that bidentate sulphur ligands are thermodynamically not very stable. Further evidence was provided from the reaction between $\text{Mo}(\text{CO})_4\text{dt}$ and btz , which under ambient conditions resulted in $\text{Mo}(\text{CO})_4\text{btz}$. At present there is much discussion about relating solution reactivity with solid state structure, especially in $\text{Mo}(\text{CO})_4\text{LL}$ systems, where LL is a bidentate sulphur ligand¹⁵.

K_2PtCl_4 reacts with btz to produce PtCl_2btz . The

method used was that of Morgan and Burstall¹⁶ who prepared PtCl_2bipy . PtCl_2bipy is a red solid which is not soluble in a range of common organic solvents. The i.r. spectrum of PtCl_2btz indicated that btz was N-bonded to Pt: $\nu(\text{C}=\text{N})$ was $1553\text{cm}^{-1}(\text{s})$ compared to $\nu(\text{C}=\text{N})$ of 1614cm^{-1} for the free ligand. The negative reaction between $\text{Mo}(\text{CO})_4(\text{pip})_2$ and PtCl_2btz supports the idea of btz being N-bonded.

PtCl_2btz readily dissolves in DMSO, but a slow solvolysis takes place. Presumably one of the chlorides is being replaced by a DMSO molecule¹⁷.

Phen, bipy and btz are known to react with $\text{Mo}(\text{CO})_4(\text{pip})_2$. In a competition experiment with bipy and btz, $\text{Mo}(\text{CO})_4\text{btz}$ is the major product. The stability of the btz complex over the bipy complex is in direct contrast with the corresponding iron complexes. It was also found that bipym reacts with $\text{Mo}(\text{CO})_4(\text{pip})_2$ to produce $\text{Mo}(\text{CO})_4\text{bipym}$ as expected. Bipym is interesting because there are two pairs of nitrogens available for bonding. However, the reaction between $\text{Mo}(\text{CO})_4(\text{pip})_2$ and $\text{Mo}(\text{CO})_4\text{bipym}$ failed to produce $[\text{Mo}(\text{CO})_4]_2\text{bipym}$ (Fig.7). The uv/vis spectrum clearly indicated $\text{Mo}(\text{CO})_4\text{bipym}$ and $\text{Mo}(\text{CO})_4(\text{pip})_2$, and bands¹⁸ corresponding to $[\text{Mo}(\text{CO})_4]_2\text{bipym}$ could not be found.

Attempts to extend this further were unsuccessful: the reaction between $\text{Fe}(\text{bipym})_3^{2+}$ and $\text{Mo}(\text{CO})_4(\text{pip})_2$ did not produce any multinuclear complexes (Fig.8). One of the problems was that $\text{Fe}(\text{bipym})_3^{2+}$ solutions in water which contained only a small quantity of organic co-solvent

(acetone, methanol) resulted in decomposition of the complex. Thus all preparations had to be done in water, in which $\text{Mo}(\text{CO})_4(\text{pip})_2$ has very limited solubility.

Using a microemulsion comprising 3.93 mls of butoxyethanol, 0.18 mls H_2O and 1.95 mls decane to try and react $\text{Fe}(\text{bipym})_3^{2+}$ with $\text{Mo}(\text{CO})_4(\text{pip})_2$ resulted in decomposition of $\text{Fe}(\text{bipym})_3^{2+}$. $\text{Fe}(\text{bipym})_3^{2+}$ alone in the microemulsion decomposed rapidly.

It was found that $\text{Fe}(\text{bipym})_3^{2+}$ could dissolve in MeNO_2 without decomposition. In this way it was possible to react $\text{Fe}(\text{bipym})_3^{2+}$ with $\text{Mo}(\text{CO})_4(\text{pip})_2$ to produce $\text{Mo}(\text{CO})_4\text{bipym}$ (see Chapter 4).

Table 1

Reaction	Solvent	Temp.	Approx. Time
$\text{Mo}(\text{CO})_4\text{btz} + \text{HgCl}_2$	MeOH	R.T.	10 mins
$\text{Mo}(\text{CO})_4\text{btz} + \text{Hg}(\text{ClO}_4)_2$	acetone/water	R.T. ^a	60s
$\text{Mo}(\text{CO})_4\text{btz} + \text{P}(\text{OPh})_3$	CH_2Cl_2	R.T.	3 days
$\text{Mo}(\text{CO})_4\text{btz} + \text{PPh}_3$	CH_2Cl_2	R.T. & reflux ^b	≈10 mins
$\text{Mo}(\text{CO})_4\text{btz} + \text{PtCl}_2$	MeOH	R.T. ^c	30 mins
$\text{Mo}(\text{CO})_4\text{btz} + \text{MeI}$	MeI	R.T.	1 day
$\text{Mo}(\text{CO})_4\text{btz} + \text{AgNO}_3$	acetone/water	R.T. ^d	60s
$\text{Mo}(\text{CO})_4\text{btz} + \text{In}_2(\text{SO}_4)_3$	MeOH	R.T.	1 day
$\text{Mo}(\text{CO})_4\text{btz} +$ $\text{CdSO}_4 \cdot 8/3\text{H}_2\text{O}$	MeOH	R.T.	1 day
$\text{Mo}(\text{CO})_4\text{btz} + \text{K}_2\text{PtCl}_4$	EtOH/water	R.T.	10 mins

a) $\text{Mo}(\text{CO})_4\text{btz}$ dissolved in acetone added to $\text{Hg}(\text{ClO}_4)_2$ dissolved in water.

b) no reaction at R.T.

c) Heterogenous reaction.

d) $\text{Mo}(\text{CO})_4\text{btz}$ dissolved in acetone added to AgNO_3 dissolved in water.

Table 2

Reaction	Solvent	Temp.	Approx. Time
$\text{Mo}(\text{CO})_4\text{dt} + \text{btz}$	acetone	R.T.	1 min
$\text{Mo}(\text{CO})_4(\text{pip})_2 + \text{dt}$	acetone	R.T.	30 mins
$\text{Mo}(\text{CO})_4(\text{pip})_2 + \text{btz}$	acetone	R.T.	2s
$\text{Mo}(\text{CO})_4(\text{PPh}_3)_2 + \text{btz}$	toluene/MeOH	R.T.	1 hr.
$\text{Mo}(\text{CO})_4(\text{pip})_2 +$ $\text{Fe}(\text{bipym})_3^{2+}$	water	R.T.	3 days
$\text{Mo}(\text{CO})_4(\text{pip})_2 + \text{bipy}$ $+ \text{btz}$	toluene	R.T.	3 days
$\text{Mo}(\text{CO})_4\text{btz} + \text{bipy}$	toluene	R.T.	3 days
$\text{Mo}(\text{CO})_4\text{bipy} + \text{btz}$	toluene	R.T.	3 days
$\text{Mo}(\text{CO})_4(\text{pip})_2 +$ $\text{Mo}(\text{CO})_4\text{btz}$	acetone	R.T.	1 hr.
$\text{K}_2\text{PtCl}_4 + \text{btz}$	EtOH/water	R.T.	1 day
$\text{Mo}(\text{CO})_4\text{bipym} +$ $\text{Mo}(\text{CO})_4(\text{pip})_2$	MeNO_2	R.T.	1 hr.
$\text{PtCl}_2\text{btz} +$ $\text{Mo}(\text{CO})_4(\text{pip})_2$	DMSO	R.T.	1 hr.
$\text{Fe}(\text{bipym})_3^{2+} +$ $\text{Mo}(\text{CO})_4(\text{pip})_2$	NO_2Me	R.T.	
$\text{Fe}(\text{bipym})_3^{2+} +$ $\text{Mo}(\text{CO})_4(\text{pip})_2$	m.e.	R.T.	

Figure 1 Hypothetical mercury chloride adduct of $\text{Mo}(\text{CO})_4\text{btz}$.

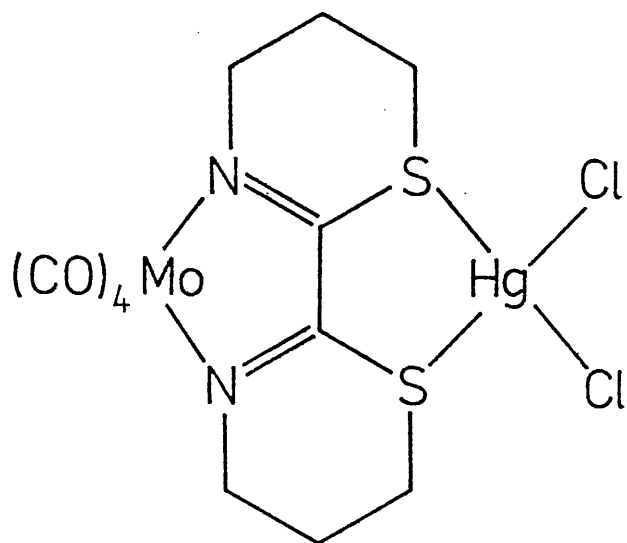


Figure 2 Hypothetical Hg^{2+} adduct of $\text{Mo}(\text{CO})_4\text{btz}$.

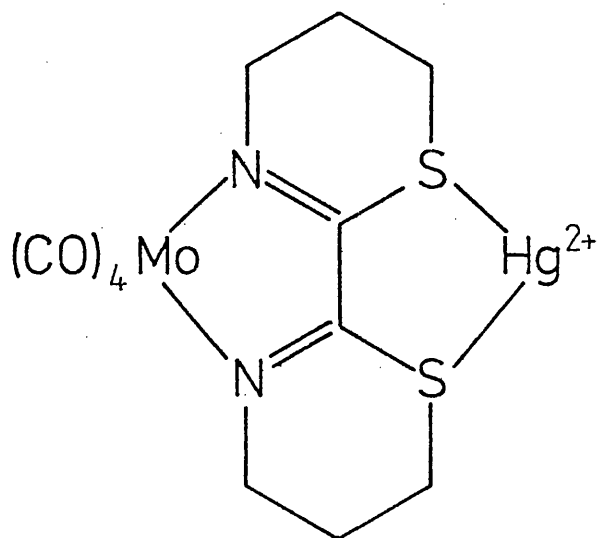


Figure 3(1) Uv/vis spectra of $\text{Mo}(\text{CO})_4\text{btz}$ (i) and the product of the reaction between $\text{Mo}(\text{CO})_4\text{btz}$ and HgCl_2 (ii) in methanol at 298.2 K.

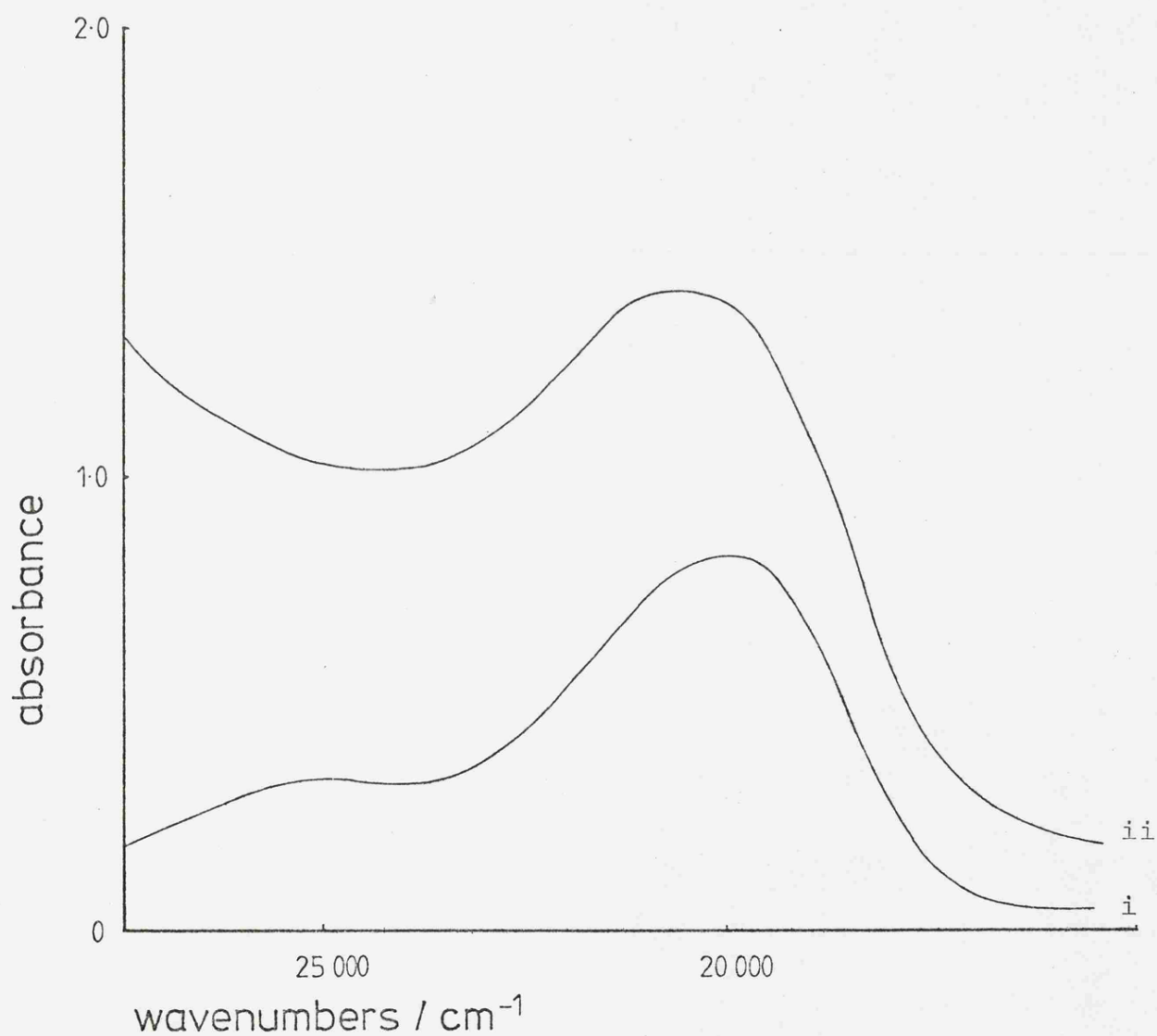


Figure 3(2) Uv/vis spectra of $\text{Mo}(\text{CO})_4\text{bipy}$ (i) and $\text{Mo}(\text{II})(\text{CO})_3\text{bipyCl}(\text{HgCl})$ (ii) in methanol at 298.2 K.

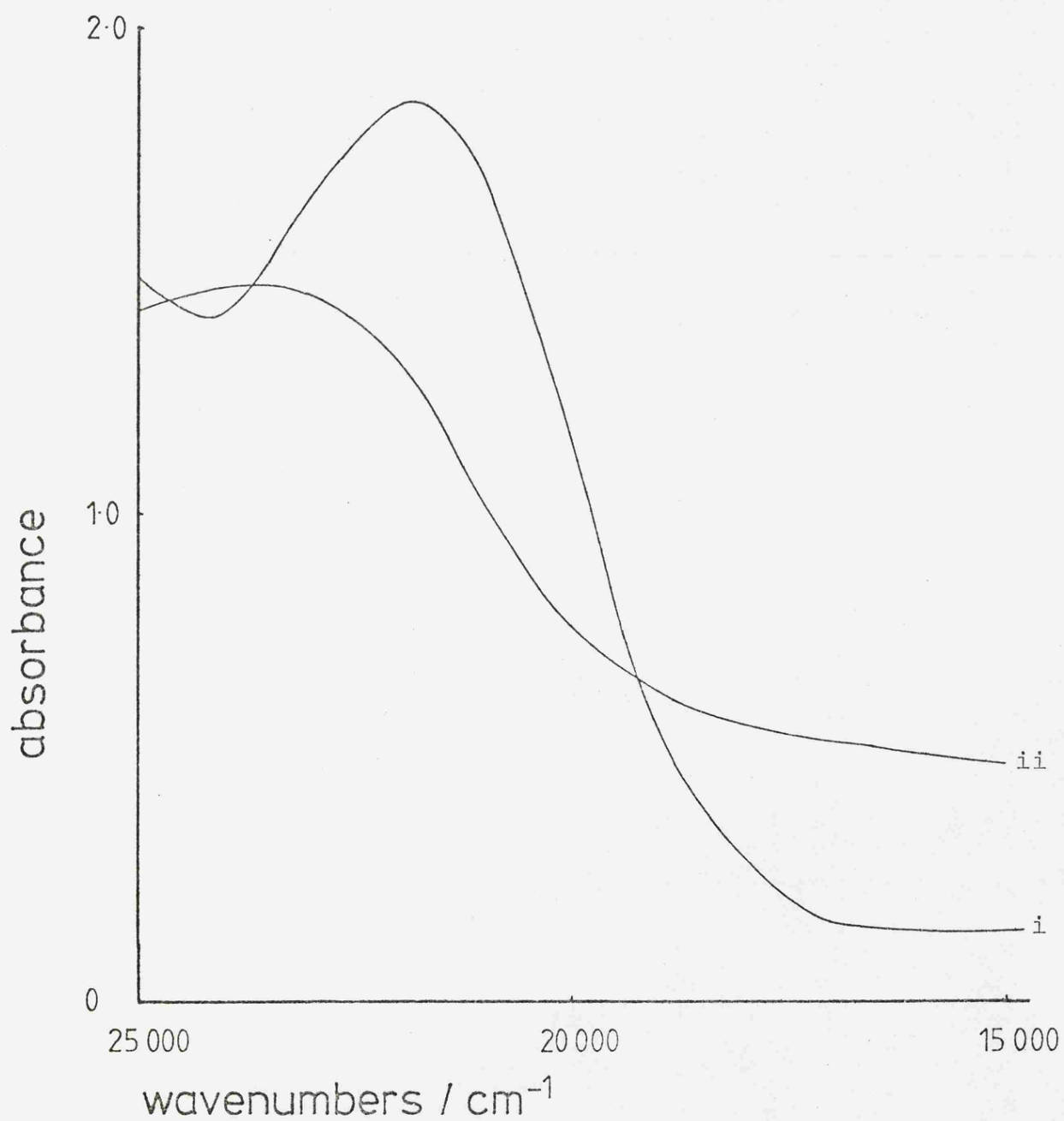


Figure 4 Hypothetical methyl iodide adduct of $\text{Mo}(\text{CO})_4\text{btz}$.

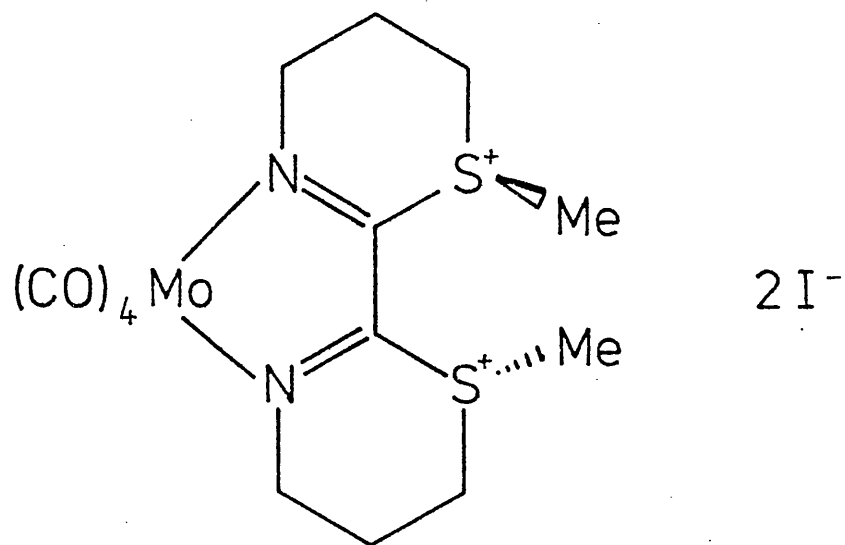


Figure 6 Hypothetical binuclear molybdenum bithiazine complex.

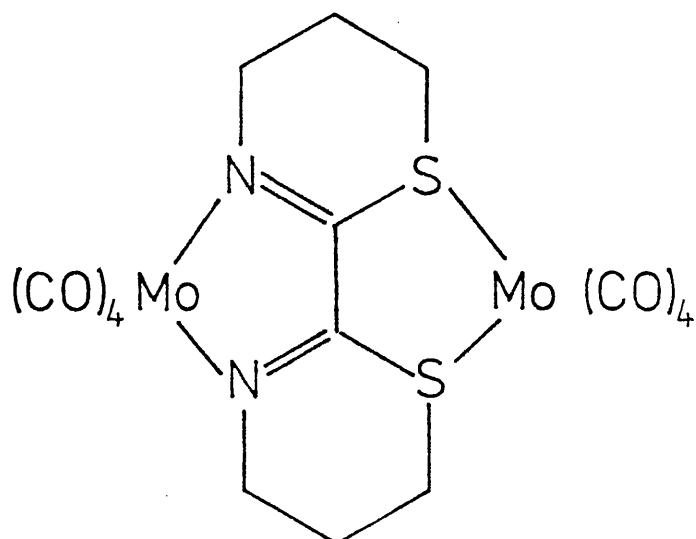


Figure 5 Initial state-transition state analysis for the reaction between $\text{Mo}(\text{CO})_4(\text{PPh}_3)_2 + \text{LL}$ (LL = phen, bipy).

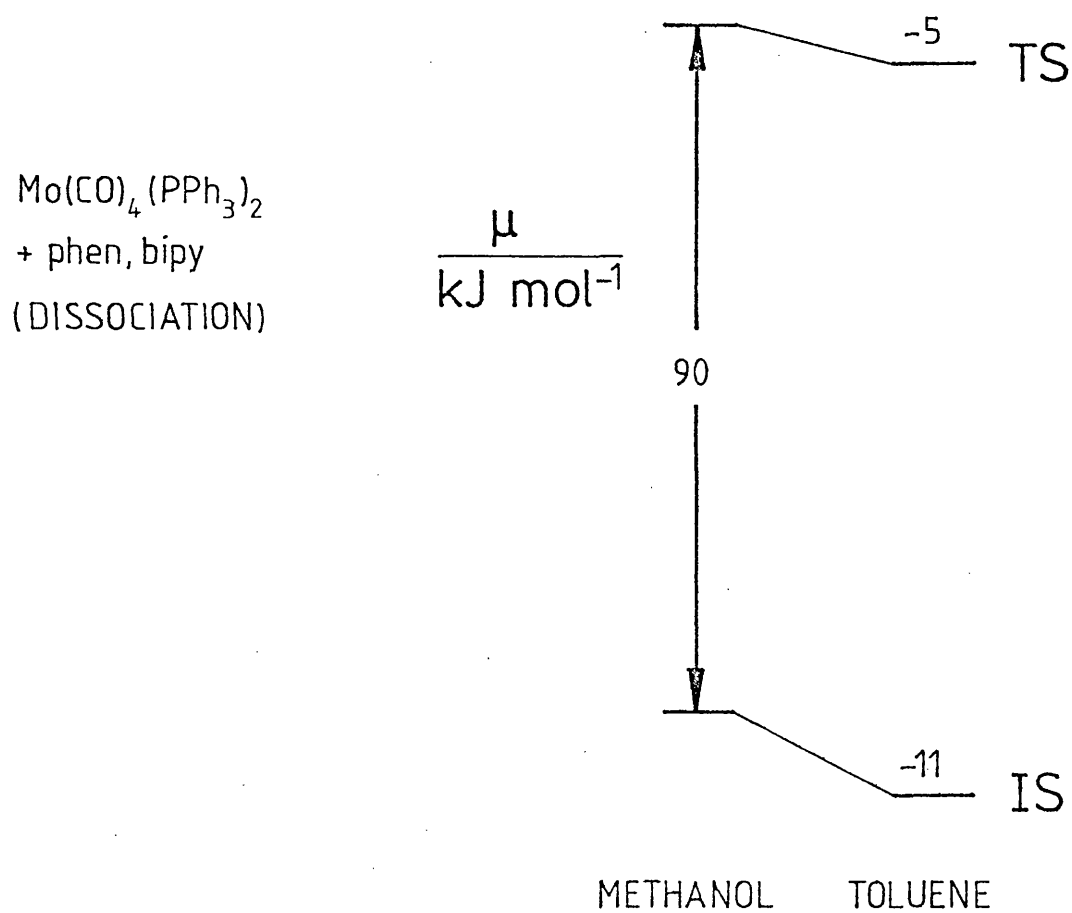


Figure 7 The binuclear molybdenum bipyrimidine complex.

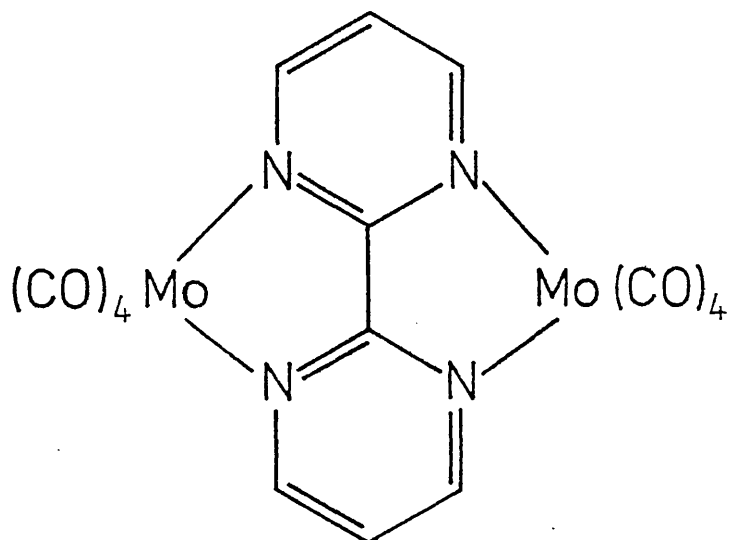
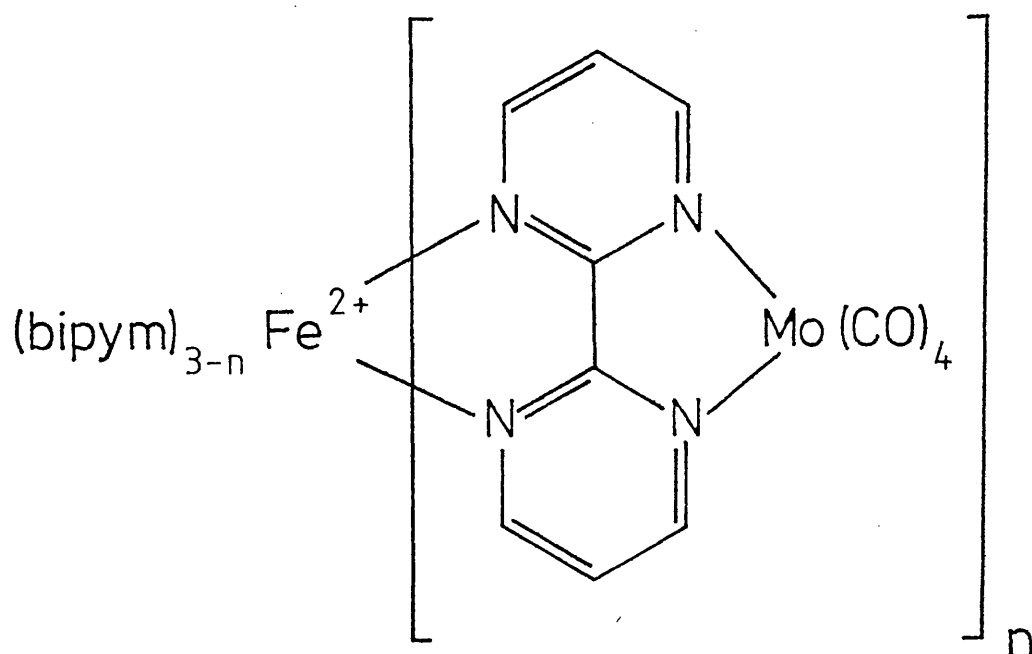


Figure 8 Hypothetical iron-molybdenum bipyrimidine complexes.



References Chapter 6

1. "Hard and Soft Acid and Bases" ed. by R.G.Pearson, Dowden, Hutchinson, and Ross, Stroudsburg, Pennsylvania, 1977
2. J.Nelson, S.M.Nelson and W.D.Perry, J.C.S.Dalton, 1976, 1282; see also Chapter 5
3. D.F.Darensbourg and R.L.Kump, Inorg.Chem., 17, 2680 (1978)
4. M.C.E.Mannerskantz and G.Wilkinson, J.Chem.Soc., 1962, 4455
5. See for example R.S.McEwen and G.A.Sim, J.Chem.Soc.(A), 1967, 271
6. J.W.McDonald and F.Basolo, Inorg.Chem., 10, 492 (1971)
7. "Comprehensive Organic Chemistry", vol. 4, ed. P.G. Sammes, Pergamon Press, 1979
8. G.R.Dobson and L.W.Houk, Inorg.Chem., 5, 2119 (1966)
9. R.J.Angelici and J.R.Graham, J.Am.Chem.Soc., 87, 5586 (1965); *ibid* 5590
10. R.J.Angelici and J.R.Graham, Inorg.Chem., 6, 988 (1967); *ibid* 992

11. M.J.Blandamer, J.Burgess, J.G.Chambers and A.J.Duffield, *Trans.Met.Chem.*, 6, 156 (1981)
12. Tobias Macholdt, personal communication
13. C.D.Hubbard, personal communication
14. M.J.Blandamer and J.Burgess, *Pure.Appl.Chem.*, 54, 2285 (1982)
15. D.E.Halverson, G.M.Reisner, G.R.Dobson, I.Bernal and T.Mulcahy, *Inorg.Chem.*, 21, 4285 (1982)
16. G.T.Morgan and F.H.Burstall, *J.Chem.Soc.*, 1934, 965
17. R.Romeo and M.L.Tobe, *Inorg.Chem.*, 13, 1170 (1974); *ibid* 1991; Yu.N.Kukushkin and V.V.Kirillov, *Rus.J. Inorg.Chem.*, 17, 1351 (1972); *ibid* 20, 1504 (1975)
18. J.A.Connor and C.Overton, *Poly.*, 1, 53 (1982)

Timothy Digman: The Effects of Solvents on Reactivities, Kinetics, and Charge Transfer Spectra of some Transition Metal Diimine Complexes.

The reaction between $\text{Fe}(\text{phen})_3^{2+}$ and Nu (Nu = OH^- , CN^-) in aqueous methanol mixtures was analysed, in terms of H into initial state-transition state contributions.

The racemisation of the $(-)\text{Fe}(\text{phen})_3^{2+}$ cation in aqueous DMSO and aqueous methanol mixtures was analysed, in terms of G, into initial state-transition state contributions. $\text{Fe}(\text{mppm})_3^{2+}$ was resolved, and the kinetics of racemisation were investigated. $\text{Fe}(\text{5NO}_2\text{phen})_3^{2+}$ was resolved and found to racemise very quickly at 25°C. $\text{Ru}(\text{5NO}_2\text{phen})_3^{2+}$ was resolved, and showed no tendency to racemise at 25°C. Attempts to resolve $\text{Fe}(\text{btz})_3^{2+}$ and $\text{Ru}(\text{btz})_3^{2+}$ were unsuccessful.

The reactions between $\text{Fe}(\text{btz})_3^{2+}$ and R (R = OH^- , H^+ , Hg^{2+} , Cd^{2+} , Ag^+ , $\text{S}_2\text{O}_8^{2-}$, phen, bipy) are reported. The stability constants of $\text{Fe}(\text{btz})_3^{2+}$, Agbtz^+ , Cdbtz^{2+} and Hgbtz^{2+} were measured.

The solvatochromism of $\text{Mo}(\text{CO})_4\text{btz}$, $\text{Mo}(\text{CO})_4\text{bipym}$, PNA, DMIA, $\text{Fe}(\text{btz})_2(\text{CN})_2$ are reported. The solvatochromism of $\text{Mo}(\text{CO})_4\text{btz}$, PNA and DMIA were analysed into ground state-excited state contributions.

The structure of $\text{Mo}(\text{CO})_4\text{btz}$ is described. The solvolysis of $\text{Mo}(\text{CO})_4\text{btz}$ was analysed in terms of initial state-transition state contributions. The reactions between $\text{Mo}(\text{CO})_4\text{btz}$ and Q (Q = Hg^{2+} , HgCl_2 , PtCl_4^{2-} , In^{3+} , Cd^{2+} , MeI, PtCl_2 , PPh_3 , $\text{P}(\text{O}Ph)_3$, $\text{Mo}(\text{CO})_4(\text{pip})_2$) are reported. The reactions between $\text{Mo}(\text{CO})_4(\text{pip})_2$ and R (R = btz, dt, (btz + bipy), PtCl_2btz) are reported. The preparation of PtCl_2btz is described.